



Universität Karlsruhe (TH)  
Forschungsuniversität · gegründet 1825



# Andreev bound states in Josephson quantum dot devices

Gebundene Andreev-Zustände in Josephson-Quantenpunkten

Diplomarbeit von  
Tobias Meng

März 2009

Institut Néel - Département Nano  
CNRS Grenoble

Betreuer: Dr. Serge Florens und Prof. Dr. Pascal Simon  
Referent: Prof. Dr. Pascal Simon  
Koreferent: Prof. Dr. Peter Wölfle

**Andreev bound states in Josephson quantum dot devices**  
© Copyright 2009 by Tobias Meng

Institut Néel, CNRS/UJF  
25 rue des Martyrs  
BP 166  
38042 Grenoble cedex 9  
France

## Abstract

In this diploma thesis, the physics of Andreev bound states in quantum dots coupled to superconducting leads is analyzed. At first, we formulate a general perturbative framework based on a *superconducting atomic limit* for the description of Andreev bound states (ABS) in interacting quantum dots. An effective local Hamiltonian for dressed ABS, including both the atomic or molecular levels and the induced proximity effect on the dot is argued to be a natural starting point. Self-consistent expansions in single-particle tunneling events are shown to provide accurate results in regimes where the superconducting gap is larger than the Kondo temperature, as demonstrated by the comparison to recent Numerical Renormalization Group calculations. These analytical results may have bearings for interpreting Andreev spectroscopic measurements with STM on carbon nanotubes coupled to superconducting electrodes.

In the second part, the results of this effective local approach are compared to a perturbation theory around the non-interacting limit, and good agreement is found in an intermediate regime. Furthermore, we point out that this second perturbative calculation is complementary to the effective local Hamiltonian approach, because it describes the low gap regime.

The last section is devoted to the Luttinger-Ward functional of this system. The latter is explicitly given up to second order in the Coulomb interaction and the Luttinger-Ward equation is generalized to superconducting leads.



## Acknowledgments

First of all, I would like to thank everyone in the theory group of the département Nano, CNRS Grenoble. Most of all, I am indebted to my supervisors Serge Florens and Pascal Simon. Their great physical knowledge and intuition guided me throughout this thesis and their explanations and advice taught me a lot. Especially Serge, my main supervisor, has always been there to answer my questions and made me see “the physics behind the equations”. But I also want to thank Denis Feinberg for helpful discussions and sharing his great knowledge, and last but not least Régis Mélin, Sabine Andergassen, Davide Venturelli and Axel Freyn for making our group such a nice place to work. I also want to acknowledge very interesting discussions with C. Winkelmann and thank J. Bauer, A. Oguri and A. Hewson for providing me their NRG data. Finally, I thank Prof. Wölfle for having accepted the duty of “Koreferent”.

But of course I am also very thankful toward my friends and family, who encouraged and supported me throughout this thesis and all of my studies and helped me correcting this work.

## Preliminary remarks

Throughout the text, the definition  $\hbar = 1$  is adapted.

Parts of this thesis have been submitted to Physical Review B for publication. A preprint is available at <http://arxiv.org/abs/0902.1111> .



# Contents

<b>1</b>	<b>Introduction</b>	<b>1</b>
1.1	Motivation . . . . .	1
1.1.1	Quantum dots and superconductivity . . . . .	1
1.1.2	Andreev bound states . . . . .	2
1.2	Some remarks on the relevant physical phenomena . . . . .	2
1.3	Outline . . . . .	4
<b>2</b>	<b>Superconducting quantum dot: generalities</b>	<b>7</b>
2.1	Single dot model . . . . .	7
2.1.1	Hamiltonian . . . . .	7
2.1.2	Gauge transformation . . . . .	8
2.2	The non-interacting limit . . . . .	9
2.2.1	Exact Green's functions . . . . .	9
2.2.2	Density of states . . . . .	11
2.2.3	The Josephson current . . . . .	12
2.3	Weak tunneling limit in the interacting case . . . . .	15
<b>3</b>	<b>Self-consistent description of the ABS</b>	<b>19</b>
3.1	Motivation . . . . .	19
3.2	The effective local Hamiltonian . . . . .	20
3.3	Spectrum of the effective local Hamiltonian . . . . .	22
3.4	Andreev bound states . . . . .	23
3.5	Perturbation expansion around $H_{eff}$ . . . . .	24
3.5.1	Preliminaries . . . . .	24
3.5.2	The corrections of the energy levels . . . . .	25
3.5.3	Self-consistent renormalization of the energies . . . . .	27
3.6	Results . . . . .	29
3.6.1	Phase diagram for the single dot with Coulomb interaction . . . . .	29
3.6.2	Kondo physics . . . . .	30
3.6.3	Energy renormalizations at particle hole symmetry ( $\xi_d = 0$ ) . . . . .	31
3.6.4	Energy renormalizations outside particle hole symmetry ( $\xi_d \neq 0$ ) . . . . .	33
3.6.5	Superconducting correlations on the dot . . . . .	35
3.6.6	Josephson current . . . . .	37
3.7	A first glance at more complex systems . . . . .	38
3.7.1	Effective local Hamiltonian . . . . .	40
3.7.2	Phase diagram for the effective Hamiltonian . . . . .	40
3.8	Summary . . . . .	41

<b>4</b>	<b>Perturbation theory in the Coulomb interaction</b>	<b>43</b>
4.1	Introduction . . . . .	43
4.2	Perturbation expansion . . . . .	44
4.2.1	First order . . . . .	44
4.2.2	Second order . . . . .	45
4.2.3	Skeleton expansion . . . . .	47
4.2.4	Particle hole symmetry . . . . .	50
4.2.5	Explicit calculation of the skeleton self energy . . . . .	52
4.3	Results . . . . .	54
4.3.1	Density of states and Green's functions . . . . .	54
4.3.2	Andreev bound state energies and phase diagram . . . . .	55
4.3.3	Superconducting correlations . . . . .	58
4.4	Summary . . . . .	58
<b>5</b>	<b>Luttinger-Ward functional and Friedel sum rule</b>	<b>61</b>
5.1	Luttinger-Ward functional . . . . .	61
5.1.1	Introduction . . . . .	61
5.1.2	Explicit form up to second order . . . . .	62
5.1.3	Symmetries of the Luttinger-Ward functional . . . . .	63
5.2	Friedel sum rule at particle hole symmetry . . . . .	65
5.2.1	Luttinger-Ward equations . . . . .	65
5.2.2	Some simple limiting cases . . . . .	68
<b>6</b>	<b>Conclusion</b>	<b>75</b>
6.1	Summary and Conclusions . . . . .	75
6.2	Outlook . . . . .	76
6.2.1	Andreev bound state spectroscopy . . . . .	77
<b>A</b>	<b>On Matsubara Green's functions</b>	<b>79</b>
<b>B</b>	<b>Analytic continuation</b>	<b>83</b>
<b>C</b>	<b>Superconducting single dot Green's functions</b>	<b>85</b>
<b>D</b>	<b>The Bogoliubov transformation for <math>H_{eff}</math></b>	<b>89</b>
<b>E</b>	<b>Some basics of quantum field theory</b>	<b>91</b>
E.1	Introduction . . . . .	91
E.2	Grassmann numbers . . . . .	91
E.3	The partition function . . . . .	92
<b>F</b>	<b>Derivation of the effective action</b>	<b>95</b>
<b>G</b>	<b>Derivation of the partition function</b>	<b>97</b>
<b>H</b>	<b>Explicit self consistent expression of <math>\delta a</math></b>	<b>101</b>

<b>I</b>	<b>Perturbation expansion in <math>U</math></b>	<b>103</b>
I.1	First order . . . . .	103
I.2	Explicit calculation of the self-energy . . . . .	104
I.2.1	Deriving the explicit formula . . . . .	104
I.2.2	Evaluation of the self-energies for superconducting leads . . . . .	105
<b>J</b>	<b>List of the most important Symbols</b>	<b>109</b>



# Zusammenfassung

In den letzten Jahren und Jahrzehnten haben sich Quantenpunkte zu einem beliebten Modellsystem der Festkörperphysik entwickelt. Quantenpunkte sind mikroskopisch bis nanoskopische kleine, oftmals halbmetallische Strukturen. Es können jedoch auch Moleküle, zum Beispiel Kohlenstoff-Nanoröhrchen, verwendet werden [1–4].

In solchen Strukturen ist die Beweglichkeit der Leitungselektronen in allen drei Raumrichtungen eingeschränkt, so dass die Energiespektren denen von Atomen ähneln. Allerdings können ihre Eigenschaften (Elektronendichte, Energieniveaus etc.) in situ durch Elektroden verändert werden.

Wird ein Quantenpunkt an supraleitende Elektroden gekoppelt, ändert sich sein Energiespektrum drastisch. Auf Grund des Proximityeffekts induzierter Supraleitung bildet sich um das Fermi-Niveau eine Lücke in der Zustandsdichte aus. Diese Lücke ist mit jener in den Elektroden identisch. Innerhalb der Lücke kommt es zur Bildung diskreter, gebundener Zustände die Andreev-Zustände genannt werden [5, 6].

Diese Andreev-Zustände tragen im Allgemeinen einen großen Teil des Josephson-Stroms und können auch ein hohes spektrales Gewicht aufweisen [7, 8]. Daher ist es wichtig, die Physik dieser Zustände zu analysieren, um das Verhalten eines Quantenpunktes, der an supraleitende Elektroden gekoppelt ist, zu verstehen. Dies gilt insbesondere im Hinblick auf mögliche Anwendungen, zum Beispiel im Quantencomputing [9]. Darüber hinaus gibt es aktuell sowohl von experimenteller als auch theoretischer Seite Bemühungen, die Andreev-Zustände in Kohlenstoff-Nanoröhrchen durch spektroskopische Messungen direkt nachzuweisen [10, 11]; außerdem gibt es Vorschläge, das Rauschen für die Messung der Andreev-Zustände auszunutzen [12]. Eine schon realisierte Anwendung von Quantenpunkten mit supraleitenden Elektroden stellen nano-SQUIDS dar [13].

In dieser Diplomarbeit soll die Physik solcher Systeme mit Hilfe eines allgemeinen Modells (einfacher Quantenpunkt mit nur einem Energieniveau) untersucht werden. Im ersten Kapitel werden grundlegende Phänomene, wie der Josephson-Effekt, der Proximityeffekt oder der  $0 - \pi$  Übergang, näher vorgestellt. Dabei wird nochmals die physikalische Wichtigkeit der Andreev-Zustände begründet. Dies wird der Einfachheit halber in verschiedenen Grenzfällen geschehen, wobei jedoch die Resultate, zumindest qualitativ, allgemein gültig sind.

Das darauf folgende Kapitel handelt von der selbstkonsistenten Beschreibung der Andreev-Zustände in Quantenpunkten mit supraleitenden Elektroden. Dabei ist zu beachten, dass eine exakte theoretische Beschreibung dieses Systems leider nur möglich ist, wenn die Coulomb-Wechselwirkung vernachlässigt wird. Wechselwirkende Quantenpunkte wurden statt dessen bisher entweder durch Molekularfeldnäherungen [14–16], Störungstheorien in der Coulomb-Wechselwirkung [17] oder der Tunnelkopplung [18] oder die Non-Crossing Approximation [19, 20] beschrieben. Darüber hinaus wurden auch numerische Techniken, wie zum Beispiel die funktionelle Renormierungsgruppe (FRG)

und numerische Renormierungsgruppe (NRG) [8, 21–25] oder Quantum Monte Carlo Simulationen [26, 27] verwendet.

Keine der analytischen Methoden kann die Physik eines Quantenpunktes mit supraleitenden Elektroden zur Gänze beschreiben. Störungstheorien in der Tunnel-Kopplung werden zum Beispiel den Proximityeffekt, also die induzierte Supraleitung, zumindest in den niedrigen Ordnungen der Störungstheorie nicht korrekt wiedergeben. Molekularfeldnäherungen wiederum können den Kondoeffekt nicht beschreiben. NRG Simulationen zu guter Letzt sind numerisch sehr anspruchsvoll und können daher nicht direkt auf komplexere Systeme ausgeweitet werden. Zusätzlich fehlt ihnen ein intrinsisches physikalisches Bild, durch welches die Ergebnisse interpretiert werden können.

Das Ziel dieser Arbeit ist es daher, eine neue, analytische und möglichst einfache Beschreibung der Andreev-Zustände zu finden, die die Physik in einem großen Parameterbereich korrekt wiedergibt. Wir erreichen dies durch eine Störungstheorie um den Grenzfall einer großen supraleitenden Bandlücke, die den Proximityeffekt und die Coulomb-Wechselwirkung exakt beschreibt. Für diesen Grenzfall werden analytische Lösungen hergeleitet; dies ist möglich da sich der Hamilton-Operator dann zu einem effektiv lokalen Operator für den Quantenpunkt vereinfacht. Wir verdeutlichen weiterhin wie unser Formalismus die Andreev-Zustände beschreibt. Danach erweitern wir den Gültigkeitsbereich unserer Näherung durch das Implementieren einer Selbstkonsistenzbedingung. So können auch Bandlücken, die sogar deutlich kleiner als die anderen charakteristischen Energieskalen sind, beschrieben werden. Die so gefundenen, renormalisierten Energien stimmen über große Parameterbereiche mit numerische Daten überein. Allerdings wird das Kondoregime auf Grund fehlender Vertex-Korrekturen nur qualitativ beschrieben.

Aufbauend auf den Energiekorrekturen können dann noch weitere Observablen, wie zum Beispiel supraleitende Korrelationen, berechnet werden. Bezüglich des Josephsonstroms kann der Formalismus jedoch nur eine grobe Abschätzung leisten, da dieser auch einen Beitrag des Zustandskontinuums oberhalb der Bandlücke enthält, zu dem wir keinen Zugang haben.

Unser Formalismus sollte auf Grund seiner Einfachkeit auf komplexere Systeme, wie zum Beispiel Doppelquantenpunkte oder Moleküle mit komplexer Orbitalstruktur, übertragbar sein (siehe zum Beispiel [28–31]). Dies stellt, zusammen mit der physikalischen Interpretation supraleitender atomarer Zustände, einen großen Vorteil im Vergleich zu numerischen Rechnungen dar.

Um die Ergebnisse im Grenzfall kleiner supraleitender Bandlücken zu verbessern, betrachten wir im folgenden Kapitel eine Störungstheorie in der Coulomb-Wechselwirkung. Diese wird bis zur zweiten Ordnung ausgeführt, da die Coulomb-Wechselwirkung experimentell oft eine der größten Energien des Quantenpunkts ist. Eine weitere Verbesserung der Ergebnisse wird durch die Verwendung einer so genannten Skelett-Entwicklung erreicht, die an Stelle der einfachen Propagatoren die vollen Greenschen Funktionen, d.h. inklusive der Selbstenergien, verwendet.

Die Ergebnisse dieser Methode stimmen über weite Parameterbereiche mit denen der selbstkonsistenten Beschreibung (die im vorherigen Kapitel entwickelt wurde) überein. Sie verbessern diese aber für kleine Bandlücken deutlich. Dies wird durch Vergleiche der renormalisierten Energien, aber auch der supraleitenden Korrelationen, gezeigt. Darüber hinaus können nun auch Zustandsdichten für den wechselwirkenden Quantenpunkt berechnet werden. Allerdings kann die Störungstheorie in der Coulomb-Wechselwirkung nur in einer der beiden Phasen des Quantenpunktes verwendet werden, wohingegen die

renormierte effektive lokale Rechnung beide Phasen beschreibt.

Das letzte Kapitel ist allgemeineren Betrachtungen über die Invarianzen des zur Störungstheorie in der Coulomb-Wechselwirkung gehörige Luttinger-Ward Funktional gewidmet. Dieses hat verschiedene Symmetrien, welche ausgenutzt werden, um zum ersten Mal überhaupt die Verallgemeinerung der Friedel Summenregel auf Quantenpunkte mit supraleitenden Elektroden zu analysieren. Dabei finden wir zwei Quantisierungsbedingungen, die im Falle normalleitender Elektroden der Quantisierung der Überschlußladung entsprechen. Diese beiden Gleichungen werden für einige einfache Grenzfälle analytisch überprüft.



# Chapter 1

## Introduction

### 1.1 Motivation

#### 1.1.1 Quantum dots and superconductivity

##### Generalities on quantum dots

Quantum dots are small, man-made structures. Typical sizes range from some nanometers to several micrometers. Due to these small sizes, the electrons' movement in quantum dots is restricted in all three spatial dimensions and parallels to atoms arise; in particular, the energy levels are often discrete. A striking advantage of quantum dots, compared to atoms, is that today's microfabrication techniques allow to control their form, size and electron density. In addition, their properties may be tuned in situ via gates voltages. This high degree of controllability has made of quantum dots a widely studied model system. For a more detailed introduction to the rich physics of quantum dots, the reader may be referred to reviews (see for example [1–3] and references therein). Whereas the above described structures are mostly semiconductors, molecules (for example carbon nanotubes [4]) can also be used as quantum dots because they show similar properties.

##### Superconducting quantum dots

Superconductivity is one of the most studied phenomena in condensed matter physics. Pioneer work has been done by Bardeen, Cooper and Schrieffer who proposed a very successful microscopic theory (often referred to as the BCS-theory) [32]. A major ingredient to that theory is that electrons form so-called Cooper pairs, leading to a gap in the density of states.

Connecting a quantum dot to superconducting electrodes instead of normal ones drastically modifies the dot's electronic structure. Due to the tunnel coupling Cooper pairs "leak" into the dot. This phenomenon is known as the proximity effect [5]. It leads to the formation of a gap in the dot's density of states. Furthermore, discrete sub-gap states arise [6]. These states are commonly referred to as Andreev bound states.

Experimentally, superconducting quantum dots can be realized with carbon nanotube junctions. It has been shown that e.g. nanotubes and InAs quantum dots connected to superconducting electrodes can be tuned from a Coulomb blockade regime, to a Kondo regime [33–35], to a weakly interacting Fabry-Perot regime by changing local gate voltages [36]. The Josephson current at zero bias and multiple Andreev reflections at finite

bias voltage have been measured in such devices [5, 36–38]. The transition from a 0-junction to a  $\pi$ -junction, namely a reversal in the sign of the Josephson current [18], has also been observed when a magnetic moment forms on the dot [13, 39–41]. As a possible application of superconducting junctions, nano-SQUID devices have been fabricated [13]. Furthermore, superconducting quantum dots are possible components of spintronics devices.

### 1.1.2 Andreev bound states

The Andreev bound states (ABS) play certainly an important role for the physics of a quantum dot connected to superconducting electrodes as they may contribute a large part of the spectral weight [8] and carry most of the Josephson current [7]. Whereas the ABS have been observed in metal-superconductor hybrid structures [42], no direct spectroscopy has so far been achieved in quantum dot systems. Andreev bound states come in pairs, one state above and one below the Fermi level, forming a two level system. Consequently, recent interest in the spectroscopy of the bound states [10, 43] has also been stimulated by proposals to use the latter as a qubit [9].

This work endeavors to contribute to the understanding of the physics of the Andreev bound states by developing a new perturbative approach based on an effective local Hamiltonian for dressed ABS, that extends the limit of large superconducting gap proposed previously [8, 44–46]. Our approach will illuminate the nature of the ABS in interacting quantum dots, as well as provide a simple and accurate analytical framework in most relevant case, that may be useful for interpreting future spectroscopic experiments. In addition, the formalism developed in this thesis should easily be extended to describe more complex systems, as for instance superconducting double quantum dots or molecules with more complicated orbital structure (see e.g. [28–31]).

## 1.2 Some remarks on the relevant physical phenomena

### Josephson effect

In 1962, Josephson predicted that at zero voltage bias, a constant current

$$J = J_c \sin(\varphi) \quad (1.1)$$

would flow between two superconductors coupled by a tunnel barrier [47]. The driving force should be the phase difference  $\varphi = \varphi_L - \varphi_R$  of the two superconductors' wave functions  $|\Psi_i\rangle = \prod_{\vec{k}} \left( |u_{\vec{k}}| + |v_{\vec{k}}| e^{i\varphi_i} c_{\vec{k},\uparrow,i}^\dagger c_{-\vec{k},\downarrow,i}^\dagger \right) |0\rangle$  ( $i = L, R$ ). The amplitude  $J_c$  is called the critical current.

Josephson predicted furthermore that if a finite voltage bias  $V$  was applied across the junction, the phase difference would evolve with time  $t$  as

$$\varphi(t) = 2eV \cdot t. \quad (1.2)$$

Therefore, the current across the voltage biased junction would be an alternating one. The free energy stored in the junction is then given by the electrical work

$$F = \int J \cdot V dt = \int J \frac{d\varphi}{2e} = -\frac{J_c}{2e} \cos(\varphi) + \text{const.} \quad (1.3)$$

These predictions, today referred to as the AC and DC Josephson effect, respectively, have been fully confirmed in many experiments.

Ambegaokar and Baratoff have shown [48] that the product of the critical current  $J_c$  and the resistance in the normal state  $R_n$  depends only on the temperature  $T$  and superconductors' gap  $\Delta$ :

$$J_c R_n = \frac{\pi \Delta(T)}{2e} \tanh\left(\frac{\Delta(T)}{2kT}\right). \quad (1.4)$$

Probably the most famous application of the Josephson effect are so-called SQUIDs (*Superconducting QUantum Interference Devices*), used for ultra-sensitive magnetic flux measurements. More information on the Josephson effect in general and its applications can be found in textbooks [49].

### Coulomb blockade and Kondo effect

The number of electrons on a quantum dot can experimentally be controlled by a gate electrode. The latter, being capacitively coupled to the dot, determines its electrical potential and is therefore used to shift the energy levels relative to the Fermi energy. If the gate voltage is adjusted such that one of the dot's levels is in resonance, electrons will easily tunnel from the electrodes into the dot. Nevertheless, due to the small size of the dot, Coulomb repulsion opposes the addition of electrons. Therefore, if a finite bias voltage between source and drain contact is applied, the Coulomb interaction leads to a suppression of the conductance for low temperatures (i.e. not thermally activated regime), apart from points of charge degeneracy. This phenomenon is called Coulomb blockade. At the degeneracy points, the gate voltage is such that two states with  $n$  and  $n + 1$  electrons have the same energy. Then, electrons can hop on and off the dot without having to overcome a barrier. This gives rise to a periodic peak pattern in the conduction, known as Coulombs diamonds. The Coulomb blockade for a quantum dot connected to superconducting electrodes is illustrated in figure 1.1 (experimental data by Jørgensen and collaborators [50]). It shows the differential conductance as a function of a bias voltage  $V_{sd}$  across the junction and a gate voltage  $V_{gate}$ . The latter simply shifts the energy level of the dot. The characteristic diamond-shaped conduction pattern is clearly observed. Furthermore, the superconducting gap  $\Delta$  in the electrodes results in a gap in the conduction (visible as a white line for low bias voltages  $V_{sd}$ ).

Due to Coulomb blockade, the occupation of the dot can easily be manipulated. If it is tuned to an even integer, the dot's total spin is  $S = 0$ , whereas it is  $S = \frac{1}{2}$  for odd integer occupation. A quantum dot therefore constitutes a fully controllable localized magnetic moment. It has been known since the 1960's that a magnetic impurity, whilst surrounded by a Fermi sea, can be screened by the latter (i.e. formation of a spin  $S = 0$  state) [51]. This so-called Kondo effect occurs if the dot is strongly coupled to the electrodes, which then hybridize with the dot's level. The hybridization results in an increased conductance [52]. In contrast, the Kondo effect decreases the conductance in the case of a magnetic impurity in a bulk metal because the impurity constitutes a scattering center for the otherwise freely moving electrons.

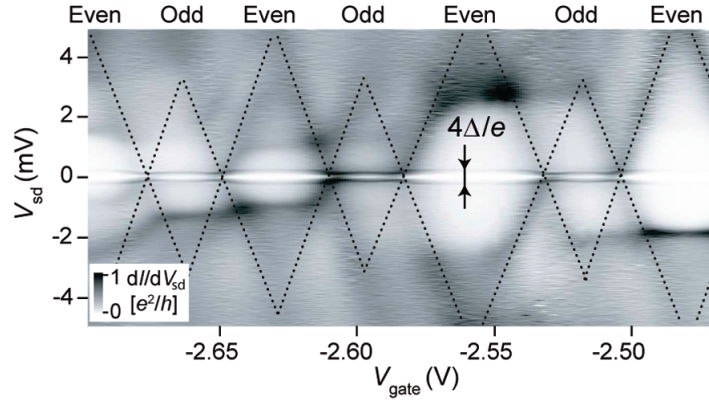


Figure 1.1: Typical differential conductance of a quantum dot connected to superconducting electrodes (experimental data by Jørgensen et al. [50]). The dot's occupancy is given on top.

### Superconductivity and Kondo effect

Both superconductivity and the Kondo effect are characterized by the formation of spin singlets. In a superconductor, Cooper pairs consisting of electrons with opposite spin and momentum are formed. In the Kondo effect, the dot's magnetic moment is screened due to the hybridization with electrons in the conduction band. The interplay of these two effects is physically interesting. It has been shown that the zero-bias conductance of single quantum dots universally scales with  $\Delta/(k_B T_K)$  (where  $\Delta$  is the superconducting gap and  $T_K$  is the Kondo temperature) [34]. It has further been demonstrated that the Kondo effect is not destroyed by the superconducting gap as long as  $k_B T_K \gg \Delta$  [35].

## 1.3 Outline

This thesis is a joint Master 2 recherche and diploma thesis for the Université Joseph Fourier Grenoble, the Ecole Nationale Supérieure de Physique de Grenoble and the Universität Karlsruhe (TH). It endeavors to contribute to the understanding of the physics of a quantum dot coupled to superconducting electrodes, thereby mainly focusing on the Andreev bound states inside the gap.

Although throughout the text only quantum dots will be dealt with, similar considerations may apply to organic molecules, e.g. carbon nanotubes. Thus, this thesis may have an impact on experiments envisioning a direct STM spectroscopy of the Andreev bound states.

In a first introductory chapter, some important physical phenomena in a quantum dot coupled to superconducting electrodes are rederived. Thereby, the importance of the Andreev bound states will be underlined by analyzing the dot's density of states (which is strongly modified by the proximity effect of induced superconductivity) and by calculating the Josephson current in some simple limiting cases. The mechanism of the  $0 - \pi$  transition in such a quantum dot device is explained.

Chapter 3 is devoted to the derivation of a new, simple and analytic description of the Andreev bound states in Josephson quantum dots. This approach is based on a perturbation expansion around an effective local limit Hamiltonian. The latter describes the system in the limiting case of a large superconducting gap. By comparing our results

to numerical data, this approach is proven to be as simple as reliable. As a drawback, some difficulties arise in the Kondo regime.

The 4<sup>th</sup> chapter deals with a perturbation theory around the non-interacting limit. As the Coulomb interaction may be one of the biggest energy scales in a molecular quantum dot, the perturbation series needs to be expanded to the second order. Further improvement of the results is achieved by the use of a skeleton expansion. In the spin singlet phase, this second perturbative approach describes the quantum dot very well, as is shown by comparison to both numerical data and the results of the previous chapter. Nevertheless, and in contrast to the effective local Hamiltonian, it is not valid in the spin doublet phase.

In the last chapter, we derive the Luttinger-Ward functional associated with the perturbation expansion around the non-interacting limit. For the first time, the Friedel sum rule is generalized to a quantum dot coupled to superconducting electrodes. The resulting Luttinger equations are finally checked in some simple limiting cases.



# Chapter 2

## Superconducting quantum dot: generalities

### 2.1 Single dot model

Although quantum dots are relatively small and therefore fairly simple objects (compared to complex macroscopic structures), they bear a wealth of interesting physics. An experimental quantum dot has in general several electronic levels. The latter may be coupled, for instance by spin-spin interactions, or inter-level transitions. Coulomb interaction between the different levels and also between electrons on the same level is generally important. Last but not least, these electronic levels may be coupled to one or several electrodes. These coupling will in general be asymmetric and dependent on the level in question.

An exact theoretical modeling of a quantum dot coupled to superconducting electrodes is therefore impossible. Fortunately, especially molecular junction devices often exhibit a relatively large single electron level spacing. In this sense, and especially for low temperatures, a realistic simplification is to analyze a quantum dot with only one electronic level.

In the following chapter, some important properties of a single level quantum dot system shall be reviewed. Although this reduces the general multilevel dot model drastically, many physically important phenomena will persist, thus giving helpful indications of a more complex system's behavior. The results we will encounter in this section are well-known. Yet, it is worth spending some time on them, not only in order to gain insight into the basic physics of quantum dot systems coupled to superconducting electrodes, but also because the considerations below will serve as a starting point for the subsequent calculations.

#### 2.1.1 Hamiltonian

A simple Hamiltonian able to describe such a quantum dot coupled to superconducting leads (as depicted in figure 2.1) is given by the superconducting Anderson model,

$$H = \sum_{i=L,R} H_i + H_D + \sum_{i=L,R} H_{T_i} + U n_{\uparrow} n_{\downarrow} \quad (2.1)$$

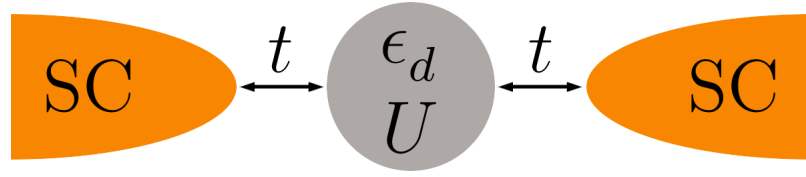


Figure 2.1: Single quantum dot with an energy level  $\epsilon_d$  and Coulomb interaction  $U$ , coupled to superconducting leads (SC) via a tunneling amplitude  $t$ .

with

$$\begin{aligned}
 H_i &= \sum_{\vec{k},\sigma} \epsilon_{\vec{k},i} c_{\vec{k},\sigma,i}^\dagger c_{\vec{k},\sigma,i} - \sum_{\vec{k}} \left( \Delta_i c_{\vec{k},\uparrow,i}^\dagger c_{-\vec{k},\downarrow,i}^\dagger + \text{h.c.} \right), \\
 H_D &= \sum_{\sigma} \epsilon_d d_\sigma^\dagger d_\sigma, \\
 H_{T_i} &= \sum_{\vec{k},\sigma} (t d_\sigma^\dagger c_{\vec{k},\sigma,i} + t^* c_{\vec{k},\sigma,i}^\dagger d_\sigma).
 \end{aligned} \tag{2.2}$$

In the above equations,  $d_\sigma$  is the annihilation operator of an electron with spin  $\sigma$  on the dot,  $c_{\vec{k},\sigma,i}$  that of an electron with spin  $\sigma$  and wave vector  $\vec{k}$  in the lead  $i = L, R$ , and  $n_\sigma = d_\sigma^\dagger d_\sigma$ .

The dot consists of a single electronic level of energy  $\epsilon_d$  and can thus be occupied by up to two electrons. The Coulomb repulsion  $U$  between electrons on the dot is taken into account. This precludes an exact solution to the problem. The leads are assumed to be described by standard s-wave BCS Hamiltonians  $H_i$  with superconducting gaps  $\Delta_i = \Delta e^{i\varphi_i}$ . The phase difference of the latter will be noted  $\varphi = \varphi_L - \varphi_R$ . Furthermore, the leads are assumed to have flat and symmetric conduction bands, i.e. the kinetic energy  $\epsilon_{\vec{k},i}$  measured from the Fermi level ranges in  $[-D, D]$  and the density of states is  $\rho_0 = 1/(2D)$ . We assume  $\vec{k}$ -independent and symmetric tunneling amplitudes  $t$  between the dot and both superconducting leads. Experimentally, the crucial characteristic energy scales, namely Coulomb interaction  $U$ , total hybridization  $\Gamma = 2\pi t^2 \rho_0$  and gap  $\Delta$ , are typically all of the same order of magnitude [13, 50], providing a challenge for analytical methods. Note that the level energy  $\epsilon_d$  and the tunneling amplitude  $t$  can be controlled via gate electrodes.

### 2.1.2 Gauge transformation

In equation (2.1), the superconducting gap is a complex number  $\Delta_i = \Delta e^{i\varphi_i}$  ( $\varphi_i$  denotes the macroscopic phase in the electrode  $i$  and the absolute value of the gap is taken to be  $\Delta$  in both electrodes). It turns out to be useful to perform a gauge transformation that absorbs this phase into the tunnel matrix elements  $t$ . This is a commonly used procedure, described in detail in textbooks [53]. The correct transformation is

$$c_{\vec{k},\sigma,i} \rightarrow c_{\vec{k},\sigma,i} e^{i\frac{1}{2}\varphi_i}. \tag{2.3}$$

By applying this transformation, the gap  $\Delta$  becomes a real number,  $\Delta_i = \Delta e^{i\varphi_i} \rightarrow \Delta$ , and the tunnel matrix elements are transformed according to  $t \rightarrow t e^{i\frac{1}{2}\varphi_i}$ .

## 2.2 The non-interacting limit

At first, the non-interacting single dot is analyzed, which reduces the Hamiltonian (2.1) to

$$H_0 = \sum_{i=L,R} H_i + H_D + \sum_{i=L,R} H_{T_i}. \quad (2.4)$$

This approximation is valid for strong coupling to the electrodes (i.e.  $\Gamma \gg U$ ). The density of states as well as the effect of resonant tunneling on the Josephson current will be analyzed. In contrast to the interacting case, the non-interacting limit can be solved analytically [6, 7, 14].

### 2.2.1 Exact Green's functions

The properties of a quantum mechanical system are described by expectation values. These expectation values can (mostly) be inferred from the calculation of Green's functions. Therefore, the knowledge of the Green's functions of a system is sufficient for the description of its properties. In the context of many-body physics, a generic Green's function has the form of a correlation function  $-\langle \hat{\Psi}(t) \hat{\Psi}^\dagger(t') \rangle$  and can be interpreted as a propagator. It basically indicates the temporal evolution (between  $t$  and  $t'$ ) of a particle put into the system in a certain state  $|\Psi\rangle$ .

In the case of a single dot coupled to (any type of) electrodes, it is mainly the physics of the dot that is interesting. Therefore, the most important Green's functions are  $\langle d_\sigma^\dagger(t) d_\sigma(t') \rangle$ -types (which only involve the dot's operators). Furthermore, if the leads are superconducting, some kind of superconducting correlation should be induced on the dot, i.e. there should be non-zero expectation values of two creation or annihilation operators. Because of this correlation, it turns out to be greatly simplifying to use Nambu notation [53]. The idea is that, as the BCS wave function has a non-defined particle (Cooper pair) number, annihilation and creation operators are very similar objects in a superconductor. Therefore, spinors are introduced to describe both types of operators on equal footing,

$$\Psi_{\vec{k},i} := \begin{pmatrix} c_{\vec{k},\uparrow,i} \\ c_{-\vec{k},\downarrow,i}^\dagger \end{pmatrix} \text{ and } \Psi_D := \begin{pmatrix} d_\uparrow \\ d_\downarrow^\dagger \end{pmatrix}. \quad (2.5)$$

These spinors are now used to calculate the different Green's functions. Entities in Nambu notation will be pointed out by hats. The Hamiltonian in Nambu notation reads

$$\begin{aligned} H_0 &= \sum_{\vec{k},i=L,R} \Psi_{\vec{k},i}^\dagger \hat{H}_{\vec{k},i} \Psi_{\vec{k},i} + \Psi_D^\dagger \hat{H}_D \Psi_D \\ &+ \sum_{\vec{k},i=L,R} (\Psi_D^\dagger \hat{H}_{T_i} \Psi_{\vec{k},i} + \Psi_{\vec{k},i}^\dagger \hat{H}_{T_i}^\dagger \Psi_D) \end{aligned} \quad (2.6)$$

with

$$\hat{H}_{\vec{k},i} = \begin{pmatrix} \epsilon_{\vec{k},i} & -\Delta_{\vec{k},i} \\ -\Delta_{\vec{k},i}^* & -\epsilon_{-\vec{k},i} \end{pmatrix}, \quad \hat{H}_D = \begin{pmatrix} \epsilon_d & 0 \\ 0 & -\epsilon_d \end{pmatrix}, \quad \hat{H}_{T_i} = \begin{pmatrix} t e^{i\frac{1}{2}\varphi_i} & 0 \\ 0 & -t e^{-i\frac{1}{2}\varphi_i} \end{pmatrix}. \quad (2.7)$$

In order to simplify the following calculations as much as possible, the Matsubara imaginary-time formalism is used. In this method, the Green's functions (defined for real times) are "extended" into the complex plane. The "normal" time is then given by the real axis. This analytic continuation does not have a physical meaning, it is just a clever mathematical trick and comparable to the use of the residue theorem for the evaluation of real integrals. Some remarks on the Matsubara imaginary-time formalism can be found in appendices A and B.

In the non-interacting limit, the dot's Green's function in Nambu notation and with Matsubara imaginary-time (noted by  $\tau$ ) is defined as

$$\begin{aligned}\widehat{G}_{d,d}^0(\tau) &= -\langle T_\tau \Psi_D(\tau) \Psi_D^\dagger(0) \rangle \\ &= \begin{pmatrix} -\langle T_\tau d_\uparrow(\tau) d_\uparrow^\dagger(0) \rangle & -\langle T_\tau d_\uparrow(\tau) d_\downarrow(0) \rangle \\ -\langle T_\tau d_\downarrow^\dagger(\tau) d_\uparrow^\dagger(0) \rangle & -\langle T_\tau d_\downarrow^\dagger(\tau) d_\downarrow(0) \rangle \end{pmatrix}.\end{aligned}\quad (2.8)$$

It is evaluated with the equation of motion technique. Thereby, the Green's function is derived with respect to  $\tau$ . The resulting differential equation is simplified using the Schrödinger equation. It is solved via Fourier transformation, yielding the frequency dependent Green's function.

In order to obtain the final expression of the Green's function, sums over wave vectors  $\vec{k}$  in the leads are transformed into integrals, i.e.

$$\sum_{\vec{k}} \rightarrow \int_{\text{band}} d\epsilon \rho(\epsilon).$$

The density of states in the leads  $\rho(\epsilon)$  is thereby assumed to be  $\rho_0 = \text{const.}$ , i.e. the conduction band is taken to be flat. Furthermore, the band shall for now be assumed to be infinite, i.e. the integration ranges from  $-\infty$  to  $+\infty$ . This simplification is motivated by the fact that the Fermi energy of the leads is normally much bigger than any other energy scale of the system, but the generalization to finite bandwidth is straightforward, as will be shown in chapter 3.

For the sake of clarity, only the final expression of  $\widehat{G}_{d,d}^0(i\omega_n)$  shall be stated here. A more complete derivation can be found in appendix C. In Matsubara frequency space and Nambu notation, the Green's function of the dot is

$$\widehat{G}_{d,d}^0(i\omega_n) = \frac{1}{\text{Det}(i\omega_n)} \begin{pmatrix} i\omega_n + \epsilon_d - \sum_i t^2 G_{i,22}^0 & -\sum_i t^2 e^{i\varphi_i} G_{i,12}^0 \\ -\sum_i t^2 e^{-i\varphi_i} G_{i,21}^0 & i\omega_n - \epsilon_d - \sum_i t^2 G_{i,11}^0 \end{pmatrix}, \quad (2.9)$$

where  $G_{i,\alpha\beta}^0$  denotes the matrix element  $\widehat{G}_i^0|_{\alpha,\beta}$  of the bare lead  $i$  Green's function

$$\widehat{G}_i^0 = \frac{\pi\rho_0}{\sqrt{\Delta^2 - (i\omega_n)^2}} \begin{pmatrix} -i\omega_n & \Delta \\ \Delta & -i\omega_n \end{pmatrix}. \quad (2.10)$$

Thereby, "bare leads" means decoupled from the quantum dot and

$$\begin{aligned}\text{Det}(i\omega_n) &= \left| \widehat{G}_{d,d}^0(i\omega_n)^{-1} \right| \\ &= -(\omega_n(1 + \alpha(i\omega_n)))^2 - \epsilon_d^2 - \left( \alpha(i\omega_n)\Delta \cos\left(\frac{\varphi}{2}\right) \right)^2.\end{aligned}\quad (2.11)$$

In the above equation,  $\varphi = \varphi_L - \varphi_R$  is the phase difference of the two superconducting electrodes and

$$\alpha(i\omega_n) = \frac{2\pi\rho_0 t^2}{\sqrt{\Delta^2 - (i\omega_n)^2}} = \frac{\Gamma}{\sqrt{\Delta^2 - (i\omega_n)^2}}. \quad (2.12)$$

### 2.2.2 Density of states

Before trying to analyze more subtle phenomena like the Josephson effect it is necessary to understand how the coupling to the electrodes changes the electronic structure on the dot. For this purpose, the electrons' density of states on the dot is calculated. In general, the latter is defined as the imaginary part of the retarded Green's function  $\rho_{\uparrow}^0(\omega) = -\frac{1}{\pi} \text{Im}\{G_{d\uparrow, d\uparrow}^{0,R}(\omega)\}$  (here only considering spin up; the total density of states is the sum of  $\rho_{\uparrow}^0(\omega)$  and  $\rho_{\downarrow}^0(\omega)$ , which are equal by symmetry). As explained in appendix A, the retarded Green's function can be found by the analytic continuation  $i\omega_n \rightarrow \omega + i\eta$  (with  $\eta \rightarrow 0^+$ ) once the Matsubara Green's function  $\widehat{G}_{d\uparrow, d\uparrow}^0(i\omega_n)$  has been obtained. Nevertheless, as explained in appendix B, this analytic continuation is not trivial. Using (2.9) and (B.11) yields

$$G_{d\uparrow, d\uparrow}^{0,R}(\omega) = \frac{1}{\text{Det}(\omega + i\eta)} ((\omega + i\eta)(1 + \alpha(\omega)) + \epsilon_d) \quad (2.13)$$

with

$$\text{Det}(\omega) = (\omega(1 + \alpha(\omega)))^2 - \epsilon_d^2 - \left(\alpha(\omega)\Delta \cos\left(\frac{\varphi}{2}\right)\right)^2 \quad (2.14)$$

and

$$\alpha(\omega) = \begin{cases} \frac{\Gamma}{\sqrt{\Delta^2 - \omega^2}} & , |\omega| < \Delta \\ \frac{i\Gamma \text{sgn}(\omega)}{\sqrt{\omega^2 - \Delta^2}} & , |\omega| > \Delta . \end{cases} \quad (2.15)$$

For  $\omega < \Delta$ ,  $G_{d\uparrow, d\uparrow}^{0,R}(\omega)$  is entirely real as long as  $\text{Det}(\omega) \neq 0$ . In contrast,  $G_{d\uparrow, d\uparrow}^{0,R}(\omega)$  is purely imaginary if  $\text{Det}(\omega) = 0$ . This means that the density of states  $\rho_{\uparrow}^0(\omega)$  vanishes for  $\omega < \Delta$  ("inside the gap") except for certain values. These energetically discrete states are called Andreev bound states (ABS). The formation of Andreev bound states inside a gap is the signature of the so-called proximity effect: as a consequence of the tunnel coupling to the superconducting leads, the dot hybridizes with the latter. This induces a BCS-like correlation on the dot, causing the described BCS-like gap in the density of states.

For  $\omega > \Delta$ ,  $\alpha(\omega)$  is a purely imaginary number. Therefore, the density of states becomes a continuum for energies outside the gap.  $\rho_{\uparrow}^0(\omega)$  is thus given by

$$\rho_{\uparrow}^0(\omega) = \begin{cases} W^+ \delta(\omega - \omega_0) + W^- \delta(\omega + \omega_0) & , |\omega| < \Delta , \\ 0 & , |\omega| = \Delta , \\ \frac{1}{\pi} \frac{\frac{|\omega|\Gamma}{\sqrt{\omega^2 - \Delta^2}} \left( (\omega^2 + \epsilon_1^2) + \frac{\Gamma^2}{\omega^2 - \Delta^2} (\omega^2 - \Delta^2 \cos^2(\frac{\varphi}{2})) \right)}{\left( \omega^2 - \epsilon_1^2 + \frac{\Gamma^2}{\omega^2 - \Delta^2} (\Delta^2 \cos(\frac{\varphi}{2}) - \omega^2) \right)^2 + \frac{4\Gamma^2 \omega^4}{\omega^2 - \Delta^2}} & , |\omega| > \Delta . \end{cases} \quad (2.16)$$

As implied by (2.16), it can be shown that  $\text{Det}(\omega)$  has two roots of multiplicity 1 at  $\pm\omega_0$  with  $|\omega_0| < \Delta$  (i.e. there are two bound states at  $\pm\omega_0$ ). Obviously the exact values of

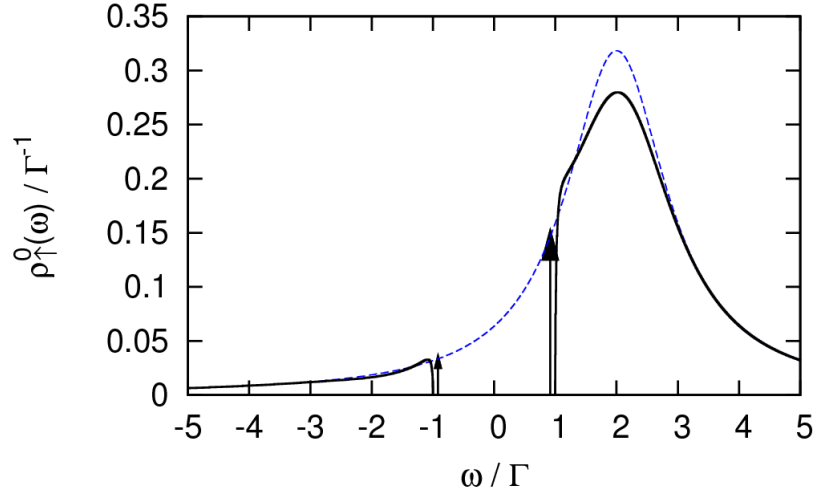


Figure 2.2: Density of states of a single quantum dot connected to electrodes via tunnel coupling, leading to a hybridization  $\Gamma$ . The dot's energy level is  $\epsilon_d = 2\Gamma$  (i.e. not in resonance). The solid curve corresponds to tunnel coupling to superconducting electrodes with  $\Delta = \Gamma$  (arrows indicate the Andreev states, their weight corresponds to their height). The dashed curve indicates the density of states if the dot is connected to normal electrodes.

$\omega_0$  and  $W^\pm$  depend on the parameters  $\Gamma$ ,  $\Delta$ ,  $\epsilon_d$  and  $\varphi$ . As an example, the case  $\Gamma = \Delta$ ,  $\varphi = 0$  shall illustrate the density of states. For  $\epsilon_d = 2\Gamma$ ,

$$\omega_0 \approx 0.915 \text{ and } \begin{cases} W^+ = 0.151 \\ W^- = 0.035 \end{cases} .$$

The corresponding density of states is shown in figure 2.2. Similar to a system with normal electrodes (dashed curve in figure 2.2), the tunneling induces a level broadening of the order of  $\Gamma$  around the initially discrete level (here supposed to be at  $\epsilon_d = 2\Gamma$ ). Furthermore, the density of states strikingly reveals the induced superconductivity:  $\rho_1^0(\omega)$  is cut at  $\omega = \pm\Delta$  and the discrete Andreev bound states arise inside the gap (marked by arrows in figure 2.2). As a conclusion, the hybridization with superconducting leads drastically changes the dot's density of states due to the proximity effect of induced superconductivity.

### 2.2.3 The Josephson current

Similar to the case of a simple tunnel junction between two superconductors (as described in section 1.2), the two leads can exchange Cooper pairs by tunneling via the dot. This exchange is driven by the phase difference  $\varphi = \varphi_L - \varphi_R$  of the wave functions in the leads. The definition of the current is

$$J(t) = e \left\langle \frac{d}{dt} N_L(t) \right\rangle = e \sum_{\vec{k}, \sigma} \left\langle \frac{d}{dt} n_{\vec{k}, \sigma, L}(t) \right\rangle = e \sum_{\vec{k}, \sigma} \left\langle \frac{d}{dt} c_{\vec{k}, \sigma, L}^\dagger(t) c_{\vec{k}, \sigma, L}(t) \right\rangle . \quad (2.17)$$

It might be useful at this point to insist on the fact that all time-dependent operators in the above expression are given in the Heisenberg picture. As a system at equilibrium

is investigated, the operators have no intrinsic time dependence (therefore being time-independent in the Schrödinger picture). Equation (2.17) can thus be further evaluated using the Heisenberg equation of motion, namely

$$\frac{d}{dt}N_L(t) = i[H_0(t), N_L(t)] .$$

It can be shown that the only non-zero contribution to  $\frac{d}{dt}N_L(t)$  is

$$[H_{T_L}(t), N_L(t)] = \sum_{\vec{k}, \sigma} (t e^{i\frac{1}{2}\varphi_L} d_{\sigma}^{\dagger} c_{\vec{k}, \sigma, L} - t e^{-i\frac{1}{2}\varphi_L} c_{\vec{k}, \sigma, L}^{\dagger} d_{\sigma}) .$$

The system's Josephson current is thus given by

$$\begin{aligned} J(t) &= e i \sum_{\vec{k}, \sigma} \langle t e^{i\frac{1}{2}\varphi_L} d_{\sigma}^{\dagger} c_{\vec{k}, \sigma, L} - t e^{-i\frac{1}{2}\varphi_L} c_{\vec{k}, \sigma, L}^{\dagger} d_{\sigma} \rangle \\ &= 2e \langle \frac{\partial}{\partial \varphi} H_{T_L} \rangle . \end{aligned} \quad (2.18)$$

Note that, a priori, the phase derivation can not simply be pulled out of the expectation value because the wave function depends on the phase difference.

It is often convenient to rewrite equation (2.19) as

$$\begin{aligned} J &= 2e \frac{1}{Z} \text{tr} \{ e^{-\beta H} \frac{\partial}{\partial \varphi} H_{T_L} \} \\ &= 2e \frac{1}{Z} \text{tr} \{ \frac{\partial}{\partial \varphi} e^{-\beta H} \} \frac{1}{-\beta} = 2e \frac{1}{-\beta} \frac{1}{Z} \frac{\partial}{\partial \varphi} Z = 2e \frac{-1}{\beta} \frac{\partial}{\partial \varphi} \ln(Z) \\ &= 2e \frac{\partial}{\partial \varphi} F , \end{aligned} \quad (2.19)$$

with the partition function  $Z = \text{tr} \{ e^{-\beta H} \}$  and the free energy  $F = -\frac{1}{\beta} \ln(Z)$ . Indeed, the above equations are nothing but a more general derivation of equation (1.3) and maybe the most common definition of the Josephson current. Unlike above, the phase derivation could be pulled out of the trace because the latter is taken with the Hamiltonian's eigenstates. These are also eigenstates of  $e^{-\beta H}$ , but not of  $H_{T_L}$ . Using the normalization of the latter readily yields equation (2.19).

Equation (2.19) implies that correlations of the type  $\langle c_{\vec{k}, \sigma, L} d_{\sigma}^{\dagger} \rangle$  (i.e. the Green's function of the leads coupled to the non-interacting dot,  $\widehat{G}_{\vec{k}\sigma L, d\sigma}^{U=0}$ ) need to be calculated. A direct calculation of  $\widehat{G}_{\vec{k}\sigma L, d\sigma}^{U=0}$  necessitates the calculation of the hybridized system's eigenstates, which is not trivial. This laborious task can be bypassed using a Dyson's equation. The latter expresses  $\widehat{G}_{\vec{k}\sigma L, d\sigma}^{U=0}$  in terms of  $\widehat{G}_{d,d}^0(i\omega_n)$  and  $\widehat{G}_{\vec{k}L, \vec{k}L}^0(i\omega_n)$ ,  $\widehat{G}_{\vec{k}L, \vec{k}L}^0(i\omega_n)$  being the bare leads' Green's functions (i.e. for leads decoupled from the dot):

$$\widehat{G}_{\vec{k}L, d}^{U=0}(i\omega_n) = \widehat{G}_{\vec{k}L, \vec{k}L}^0(i\omega_n) \widehat{H}_{T_L}^{\dagger} \widehat{G}_{d,d}^0(i\omega_n) . \quad (2.20)$$

$\widehat{G}_{\vec{k}L, \vec{k}L}^0(i\omega_n)$  can be derived similarly  $\widehat{G}_{d,d}^0(i\omega_n)$  (see section 2.2.1), which yields

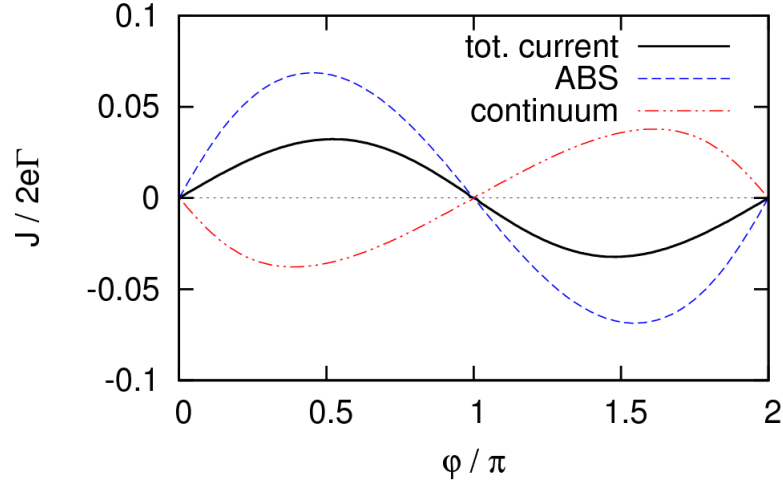


Figure 2.3: Dependence of the different contributions to the Josephson current of the superconducting phase difference  $\varphi$  for  $\Delta = \Gamma$ ,  $\epsilon_d = 2\Gamma$ . The black solid curve corresponds to the total Josephson current  $J$ , the blue dashed curve is the Andreev bound states contribution and the red dash-dotted curve is the continuum contribution.

$$\hat{G}_{\vec{k}L, \vec{k}L}^0(i\omega_n) = \frac{1}{(i\omega_n)^2 - \epsilon_{\vec{k},L}^2 - \Delta^2} \begin{pmatrix} i\omega_n + \epsilon_{\vec{k},L} & -\Delta \\ -\Delta & i\omega_n - \epsilon_{\vec{k},L} \end{pmatrix}. \quad (2.21)$$

Plugging (2.20) into (2.19) yields the Josephson current [54]. The zero temperature limit is

$$J = 2e\Gamma \sin(\varphi) \left( \int_{-\infty}^{-\Delta} \frac{d\omega}{2\pi} \frac{\Delta}{\sqrt{\omega^2 - \Delta^2}} 2 \operatorname{Re}\{\tilde{G}_{d,d;21}^{0,R}(\omega)\} + \int_{-\Delta}^0 \frac{d\omega}{2\pi} \frac{\Delta}{\sqrt{\Delta^2 - \omega^2}} 2 \operatorname{Im}\{\tilde{G}_{d,d;21}^{0,R}(\omega)\} \right) \quad (2.22)$$

(where  $\tilde{G}_{d,d;21}^{0,R}(\omega)$  is  $G_{d,d;21}^{0,R}(\omega)$  without  $e^{-i\varphi}$ , the latter having been pulled out into the  $\sin(\varphi)$  for clarity).

Equation (2.22) points out that both the continuum (first term) and the bound states (second term) contribute to the total Josephson current, as shown in figure 2.3 for the case  $\Delta = \Gamma$  and  $\epsilon_d = 2\Gamma$ . Quite surprisingly, the two contributions to  $J$  have different signs. Also, the current carried by the Andreev bound states is significantly more important than the one carried by the continuum.

The phase dependence is roughly sinusoidal,  $J$  being 0 for  $\varphi = 0$  and  $\pi$ . According to equation (2.19), the system's energy is just the  $\varphi$ -primitive of  $J$ , therefore being approximately proportional to  $-\cos(\varphi)$ . The ground state of such a system is  $\varphi = 0$ , which is why it is called a 0-junction. By contrast, a second type of system, whose ground state is  $\varphi = \pi$  and which arises if the Coulomb interaction on the dot is important [14], is called a  $\pi$ -junction. These two types of junction will be discussed in more detail in section 2.3. The transition between the two ground states is called the 0 –  $\pi$  transition.

The results concord with other work [7, 55]. Note that the total Josephson current could also have been calculated using quantum field theory [14] or the scattering matrix formalism [6]. Nonetheless, the use of Green's functions has the striking advantage of revealing the different contributions.

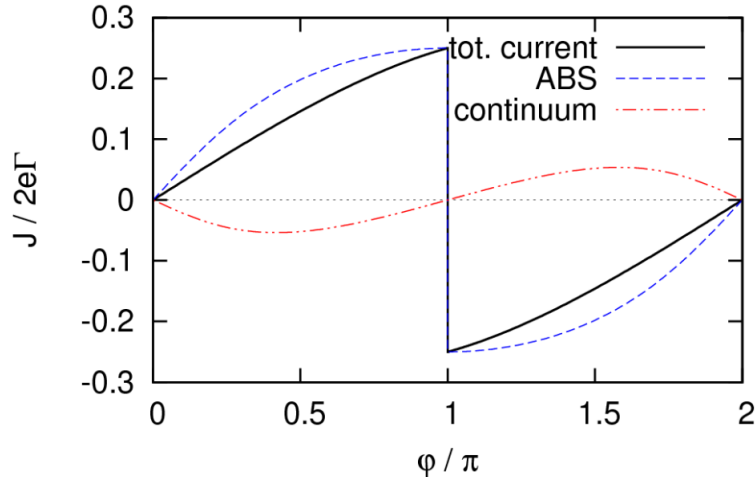


Figure 2.4: Josephson current for  $\Delta = \Gamma$ ,  $\epsilon_d = 0$ . The black solid curve corresponds to the total Josephson current  $J$ , the blue dashed curve is the Andreev states contribution and the red dash-dotted curve is the continuum contribution.

The effect of the dot's energy level can be estimated with equation (2.9). If the level is high (i.e.  $|\epsilon_d| \gg \Gamma$ ), the denominator  $\text{Det}(i\omega_n)$  is basically given by  $\epsilon_d$ . In particular, the  $\cos(\varphi/2)$ -term is not very important. Thus, the current's overall  $\varphi$ -dependence will be more and more purely sinusoidal (due to the global  $\sin(\varphi)$ -factor in (2.22)). Furthermore, as the denominator increases, the critical current will decrease [6]. In other words, as the dot is weakly coupled to the leads in this non-resonant case, Josephson's result [47] is recovered.

If on the other hand the dot is tuned into resonance, i.e.  $\epsilon_d \rightarrow 0$ , the amplitude of the current will increase: the critical current becomes of the order of  $\Gamma$  while it is of the order  $\Gamma^2/\epsilon_d$  outside the resonance. Also, the  $\cos(\varphi/2)$ -term, now being important, will cause the  $\varphi$ -dependence to not be purely sinusoidal. The extreme case of a resonant level (i.e.  $\epsilon_d = 0$ ) is shown in figure 2.4. The total current  $J$  still has the two contributions (Andreev states and continuum) of different signs; again, the bound states carry the most important part of the Josephson current. The current's global "shape" stays somewhat familiar to a sinus and the junction still is a 0-junction. Nevertheless, the  $\varphi$ -dependence is clearly not purely sinusoidal.

## 2.3 Weak tunneling limit in the interacting case

If the Coulomb interaction  $U$  on the dot is taken into account, the dot's behavior changes in general importantly. Obviously, the ground state of the dot will depend crucially on the strength of  $U$ . If the Coulomb interaction is small compared to other energies in the system, the dot should behave as described in section 2.2. In contrast, if the interaction is strong, the total charge on the dot should be limited to 1 by the Coulomb blockade. This opposes the induction of superconducting features (which are linked to the existence of Cooper pairs).

Unfortunately, the presence of interactions precludes an exact, analytic solution to the problem. Fairly often, a perturbative approach around the weak tunneling limit  $\Gamma \rightarrow 0$  is considered in this case [18, 56]. In the limit  $\Gamma \rightarrow 0$ , the Hamiltonian is decomposed as

$$H_0 = \tilde{H}_0 + \tilde{H}_1 \quad (2.23)$$

with

$$\begin{aligned} \tilde{H}_0 &= \sum_{i=L,R} H_i + H_D + U n_\uparrow n_\downarrow, \\ \tilde{H}_1 &= \sum_{i=L,R} H_{T_i}, \end{aligned} \quad (2.24)$$

such that  $\tilde{H}_0$  only contains atomic states.

The explicit calculation of the Josephson current  $J$  (here done following [56]) is similar to the one in section 2.2.3. In particular, equation (2.19) remains valid. The perturbation expansion for expectation values is given by

$$\langle d_{\sigma}^\dagger c_{\vec{k},\sigma,L} \rangle = \sum_{n=0}^{\infty} \frac{1}{n!} \int_0^\beta d\tau_1 \cdots \int_0^\beta d\tau_n \langle T_\tau \tilde{H}_1(\tau_1) \cdots \tilde{H}_1(\tau_n) d_{\sigma,1}^\dagger c_{\vec{k},\sigma,L} \rangle_{\tilde{0}}$$

(where  $\langle \cdot \rangle_{\tilde{0}}$  denotes an expectation value taken with respect to the eigenstates of  $\tilde{H}_0$ ).

The first terms of this expansion vanish:

- the zero order terms vanish because the  $\tilde{H}_0$  eigenstates have a fixed particle number on the dot and because of the pairing in the electrodes,
- the first order terms vanish because there is no BCS-like pairing on the unperturbed dot,
- the second order terms vanish again because of the defined particle number on the dot and the Cooper pairing in the electrodes.

The first non-zero contributions are the third order terms in the tunneling amplitude  $t$ . They involve 8 operators, 4 dot and 4 electrode, and correspond to the tunneling of a Cooper pair from one side to the other.

In order to calculate the Josephson current, the discrete sums over lead states  $|\vec{k}, i\rangle$  are replaced by integrals over a constant and infinitely large density of states  $\rho_0$ . Furthermore, the expectation values involving the lead operators (which can be separated from the dot operators' expectation value) are calculated by Fourier transformation of  $\hat{G}_{\vec{k}i\vec{k}i;12}^0(i\omega_n) = \hat{G}_{\vec{k}i\vec{k}i;21}^0(i\omega_n)$  ( $\hat{G}_{i,j;\alpha\beta}^0$  denotes the matrix element  $\hat{G}_{i,j|\alpha,\beta}^0(i\omega_n)$ ). This yields

$$\begin{aligned} G_{\vec{k}i\vec{k}i;12}^0(\tau) &= \frac{\Delta}{2E_{\vec{k}}} (e^{-E_{\vec{k}}|\tau|} - 2 \cosh(E_{\vec{k}}|\tau|) n_F(E_{\vec{k}})) \\ &\xrightarrow{T \rightarrow 0\text{K}} \frac{\Delta}{2E_{\vec{k}}} (e^{-E_{\vec{k}}|\tau|} - e^{-E_{\vec{k}}(\beta-|\tau|)}) , \end{aligned}$$

where the quasiparticle energy in the leads has been written as  $E_{\vec{k}} = \sqrt{\epsilon_{\vec{k}}^2 + \Delta^2}$  and assumed to be identical for both leads. As the Coulomb interaction on the dot is taken into account, Wick's theorem can not be applied to evaluate the  $\langle T_\tau d_{\downarrow,1}^\dagger(\tau_1) d_{\uparrow,1}^\dagger(\tau_2) d_{\downarrow,1}(\tau_3) d_{\uparrow,1}(0) \rangle_0$ -type terms. Instead, Lehmann representation needs to be used.

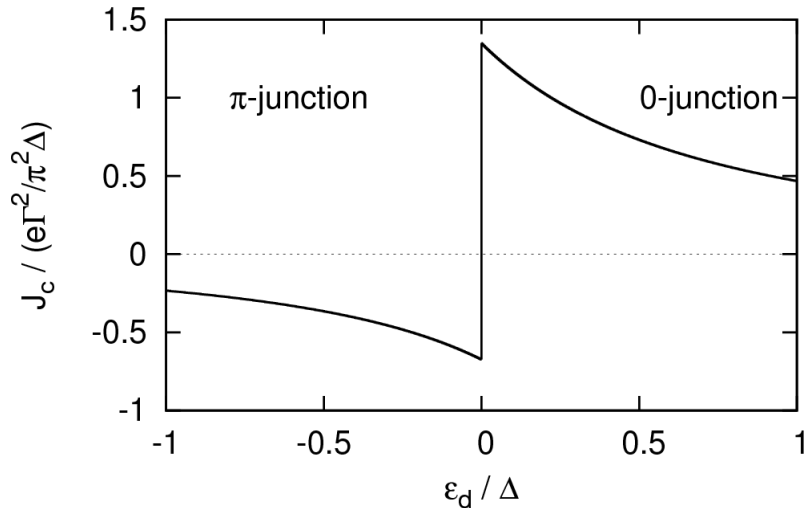


Figure 2.5: Critical Josephson current  $J_c$  as a function of the dot's energy level  $\epsilon_d$  in the limit  $U \rightarrow \infty$  and small  $\Gamma$ .

For the sake of simplicity, only the limit  $U \rightarrow \infty$  and temperature  $T \rightarrow 0$  K shall be analyzed. Nonetheless, the results can easily be generalized to finite Coulomb interaction [56]. For  $U \rightarrow \infty$ , the dot is either empty (if its energy level  $\epsilon_d$  is positive) or singly occupied (if  $\epsilon_d < 0$ ). In the following, the empty state is noted  $|0\rangle$ , its energy is set to be 0, the spin  $\sigma$  state is referred to as  $|\sigma\rangle$  and its energy is given by  $\epsilon_d$ . Due to the strong Coulomb interaction, the dot can not access the doubly occupied state. The Josephson current is

$$J = J_c \sin(\varphi) \quad (2.25)$$

with

$$J_c = \frac{-e\Gamma^2\Delta^2}{\pi^2} \int_{\Delta}^{\infty} \frac{dE}{\sqrt{E^2 - \Delta^2}} \int_{\Delta}^{\infty} \frac{dE'}{\sqrt{E'^2 - \Delta^2}} \quad (2.26)$$

$$\times \frac{2e^{-\beta\epsilon_d}}{1 + 2e^{-\beta\epsilon_d}} \left( \frac{1}{(E + E')(E - \epsilon_d)(E' - \epsilon_d)} - \frac{e^{\beta\epsilon_d}}{(E + E')(E + \epsilon_d)(E' + \epsilon_d)} \right).$$

Equation (2.25) concurs with reference [56]. Figure 2.5 shows the critical current calculated using equation (2.25). If  $\epsilon_d < 0$ , the ground state is a singly occupied dot (double occupation is precluded by  $U \rightarrow \infty$ ). The critical current being negative, the free energy  $F = \frac{1}{2e} \int d\varphi J = -\frac{J_c}{2e} \cos \varphi + \text{const.}$  is minimized for  $\varphi = \pi$ . The system is therefore called a  $\pi$ -junction. If  $\epsilon_d > 0$ , the ground state is an empty dot. Furthermore, as  $J_c > 0$ ,  $F$  is now minimized for  $\varphi = 0$ , i.e. for a 0-junction. Finally, the two shoulders of  $J_c$  around the Fermi level have a height ratio of 2.

The  $\epsilon_d$ -dependence of  $J_c$  has been interpreted intuitively by Spivak and Kivelson [57]. For  $\epsilon_d > 0$ , a Cooper pair can be transferred directly from one electrode to the other. If on the other hand the dot is singly occupied, it can be shown that every possible transfer process of a Cooper pair yields a minus sign due to the interchange of two electrons. This minus sign corresponds to a phase shift of  $\pi$ . Therefore, the most natural phase difference is 0 for  $\epsilon_d > 0$  and  $\pi$  for  $\epsilon_d < 0$ . Figure 2.6 illustrates different transfer processes. The

step interchanging two electrons is black-boxed. The  $\pi$ -junction behavior has been noted in several papers (e.g. [7, 13, 14, 50, 54, 56–58]).

The ratio 2 between the two shoulders is linked to the fact that there are twice as many transfer processes for an empty dot as for a singly occupied one (for  $U \rightarrow \infty$ ): if the dot is empty, the system can choose the order in which the two electrons are transferred. The presence of an electron (and thus a defined spin) and Coulomb interaction on the dot revokes this spin degeneracy [59].

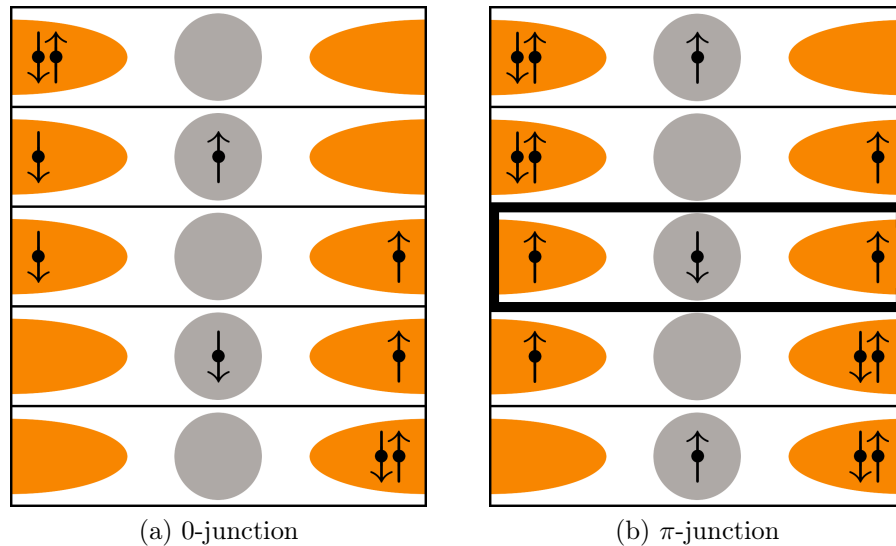


Figure 2.6: Generic tunnel processes of a Cooper pair in a  $0 - \pi$  junction (the boxed step involves the interchange of 2 electrons).

As an example for the numerous experimental evidences for the  $0 - \pi$  transition, figure 2.7 shows the absolute value of the critical current. The results fit very well to the theoretical curve derived above, compare for instance the rightmost part of the curve to the absolute value of figure 2.5. Because the sample does not have infinite Coulomb interaction and more than one electronic level, several  $0 - \pi$  transitions are observed.

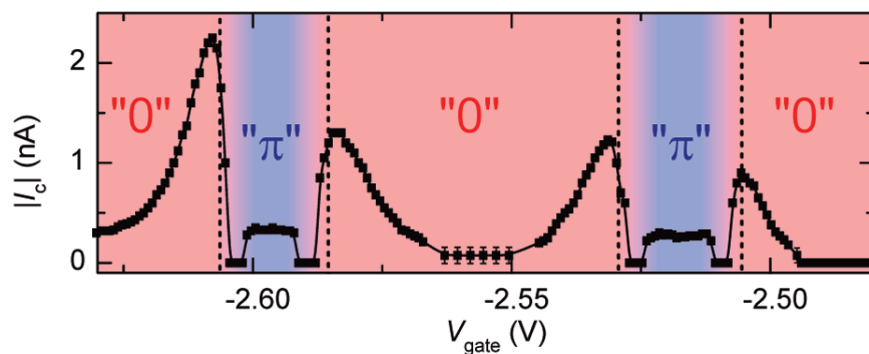


Figure 2.7: Experimental evidence for the  $0 - \pi$  transition in a carbon nanotube (data by Jørgensen et al. [50]). The experimental data fits very well to the theoretical curve in Fig. 2.5.

# Chapter 3

## Self-consistent description of the Andreev bound states

### 3.1 Motivation

As mentioned in the introduction, the Andreev bound states play an important role for the behavior of a quantum dot coupled to superconducting leads. Indeed, section 2.2.2 suggests that the Andreev bound states may carry an important spectral weight. Detailed numerical studies by Bauer et al. [8] substantiate that especially in the 0-phase, the bound states can even carry the biggest part of the total spectral weight.

It is therefore not surprising that the largest contribution to the supercurrent through the quantum dot is also carried by the Andreev bound states, as has been shown in section 2.2.3 as well as in other works (see for example references [7, 55]).

A physical understanding of the ABS requires to characterize how these states are connected to the atomic or molecular levels of the uncoupled quantum dot, and to describe quantitatively their evolution as a function of several parameters, such as gate voltage, Coulomb interaction, tunnel couplings, and superconducting gap.

However, an exact theoretical description of a quantum dot coupled to superconducting leads is only possible when the Coulomb interaction is fully neglected. Hence, the interacting single dot system, as described by the Anderson model with superconducting electrodes, has been so far analyzed by treating the Coulomb interaction with various analytical schemes, such as the mean field theory [14–16], the perturbation expansion in the Coulomb interaction [17] or in the tunnel coupling [18]. Non-perturbative calculations like the Non-Crossing Approximation (NCA) [19, 20], but also numerical simulations based on the numerical renormalization group (NRG) [8, 21–25], the functional renormalization group (FRG) (see [24] and references therein), and Quantum Monte Carlo [26, 27] have been developed.

None of the analytical approaches mentioned above is able to describe entirely the physics of a quantum dot coupled to superconducting leads. Whereas lowest order perturbation expansions in the tunnel coupling will hardly capture the proximity effect induced by the electrodes [60], mean field and weak-interaction approaches will miss the Kondo effect. NRG calculations on the other hand can capture the physics of such a system over a wide range of parameters, but are numerically demanding and not easily portable to more complex molecular systems. More importantly, in the view of describing the ABS alone, none of these techniques provides a simple physical picture. Henceforth we will

develop a new perturbative approach based on an effective local Hamiltonian for dressed ABS, that extends the limit of large superconducting gap proposed previously [44, 61] and used by many authors [8, 43, 45, 46, 62–64]. This approach will illuminate the nature of the ABS in interacting quantum dots, as well as provide a simple and accurate analytical framework in cases where the gap is not smaller than the Kondo temperature, that may be useful for interpreting future spectroscopic experiments. In addition, our formalism, which incorporates the atomic or molecular levels from the outset, should easily be extended to describe more complex systems, as for instance superconducting double quantum dots or molecules with more complicated orbital structure (see e.g. Refs. [28–31] and section 3.7).

## 3.2 The effective local Hamiltonian

As discussed in section 2.1, the total Hamiltonian

$$H = \sum_{i=L,R} H_i + H_D + \sum_{i=L,R} H_{T_i} + U n_{\uparrow} n_{\downarrow} \quad (3.1)$$

is not exactly solvable due to the quartic term in the Coulomb interaction. Therefore, some approximations must be made and a perturbation theory will be set up.

Among the physical ingredients that will be included in a non-perturbative way is the local pairing on the dot that is crucial for the evolution of the Andreev bound states. Furthermore, the Coulomb interaction shall be taken into account in an exact manner in order to describe the atomic states reliably, and to highlight how these are adiabatically connected to the Andreev bound states. However, the usual expansion in a weak tunnel coupling  $t$  around the atomic limit [18] is not sufficient to describe the proximity effect at lowest order. Therefore, we shall consider in what follows an expansion around a *superconducting atomic limit*.

This simple solvable limiting case of the model (3.1) is often referred to as the limit of large gap  $\Delta \rightarrow \infty$ , and has been discussed previously [8, 44–46]. Expansions for finite gaps  $\Delta$  have however not been discussed to our knowledge, and are the topic of this chapter. We emphasize from the outset (see equation (3.3) below), that the superconducting atomic limit as used normally in the literature corresponds to the limit  $D \rightarrow \infty$  (i.e. infinite electronic bandwidth), taken before  $\Delta \rightarrow \infty$ . As will be demonstrated, the order of the two limits is crucial: if the limit  $\Delta \rightarrow \infty$  was to be taken first, the dot would be completely decoupled from the leads and the proximity effect would be lost, so that the limit of infinite gap would reduce to the usual atomic limit.

In this section, it will be shown that the superconducting atomic limit should rather be interpreted as a low frequency expansion, i.e. a limit where the gap is much larger than the characteristic frequencies of the dot. During the derivation of an effective local Hamiltonian, the Coulomb interaction  $U$  will at first be omitted for the sake of clarity. Note that in the end,  $U$  will simply give an extra contribution that adds to the effective Hamiltonian.

Because the physics of the system are entirely described by its Green's function, it is sufficient to derive the effective local Hamiltonian by working the dot's Green's function. As shown in section 2.2.1, the latter is given (in the imaginary time formalism and in Nambu notation) by

$$\widehat{G}_{d,d}^0(i\omega_n) = i\omega_n \mathbb{1} - \widehat{H}_d - \sum_{\vec{k},i} \widehat{H}_{T_i} \widehat{G}_{\vec{k}i,\vec{k}i}^0(i\omega_n) \widehat{H}_{T_i}^\dagger. \quad (3.2)$$

In Eq. (3.2),  $\omega_n$  is a fermionic Matsubara frequency and  $\widehat{G}_{\vec{k}i,\vec{k}i}^0(i\omega_n)$  the bare Green's function of electrons with a wave vector  $\vec{k}$  in the lead  $i$ . As the Coulomb interaction (disregarded for the moment) only enters the dot's Hamiltonian, the latter is still given by equation (2.21). Transforming the sum over wave vectors  $\vec{k}$  into an integral over energies yields

$$\begin{aligned} \sum_{\vec{k}} \widehat{G}_{\vec{k}i,\vec{k}i}^0(i\omega_n) &= 2\rho_0 \int_0^D d\epsilon \frac{1}{\omega_n^2 + \epsilon^2 + \Delta^2} \begin{pmatrix} -i\omega_n - \epsilon & \Delta \\ \Delta & -i\omega_n + \epsilon \end{pmatrix} \\ &= 2\rho_0 \arctan\left(\frac{D}{\sqrt{\omega_n^2 + \Delta^2}}\right) \frac{1}{\sqrt{\omega_n^2 + \Delta^2}} \begin{pmatrix} -i\omega_n & \Delta \\ \Delta & -i\omega_n \end{pmatrix}. \end{aligned} \quad (3.3)$$

Note that the Green's function (3.3) depends on the finite bandwidth  $D$ . As mentioned in the outset of this section, the limit  $\Delta \rightarrow \infty$  should only be taken after a limit  $D \rightarrow \infty$  for the proximity effect to survive. In what follows, both  $D$  and  $\Delta$  will be kept finite, and a low frequency limit  $\omega_n \ll \Delta$  will be taken rather than the limit  $D \rightarrow \infty$ ,  $\Delta \rightarrow \infty$  used in the literature [8, 44–46]. We emphasize that this way, the limit of large gap is extended to finite bandwidths  $D$ .

In the low frequency limit, the Green's function (3.3) becomes

$$\sum_{\vec{k}} \widehat{G}_{\vec{k}i,\vec{k}i}^0(i\omega_n) = 2\rho_0 \arctan\left(\frac{D}{\Delta}\right) \begin{pmatrix} 0 & 1 \\ 1 & 0 \end{pmatrix}. \quad (3.4)$$

Plugging Eq. (3.4) into the Green's function  $\widehat{G}_{d,d}^0(i\omega_n)$  leads to the same result as would have been obtained with the effective local Hamiltonian

$$H_{\text{eff}}^0 = \sum_{\sigma} \epsilon_d d_{\sigma}^{\dagger} d_{\sigma} - \left( \Gamma_{\varphi} e^{i\frac{\varphi_L + \varphi_R}{2}} d_{\uparrow}^{\dagger} d_{\downarrow}^{\dagger} + \text{h.c.} \right), \quad (3.5)$$

where the local pairing amplitude induced by the leads on the dot

$$\Gamma_{\varphi} = \Gamma \frac{2}{\pi} \arctan\left(\frac{D}{\Delta}\right) \cos\left(\frac{\varphi}{2}\right) \quad (3.6)$$

explicitly depends on the ratio  $D/\Delta$ . By an appropriate gauge transformation for the operators  $d_{\sigma}$ , it is always possible to choose  $\Gamma_{\varphi} e^{i\frac{\varphi_L + \varphi_R}{2}} = |\Gamma_{\varphi}|$ , as shall be done from now on.

The complete local effective Hamiltonian is obtained when the Coulomb interaction is taken into account again. Defining  $\xi_d = \epsilon_d + \frac{U}{2}$ , the energy level of the dot is shifted such that the Hamiltonian clearly exhibits particle-hole symmetry for  $\xi_d = 0$ . Omitting an irrelevant global energy shift of  $-\frac{U}{2}$  the final Hamiltonian reads

$$H_{\text{eff}} = \sum_{\sigma} \xi_d d_{\sigma}^{\dagger} d_{\sigma} - |\Gamma_{\varphi}| \left( d_{\uparrow}^{\dagger} d_{\downarrow}^{\dagger} + \text{h.c.} \right) + \frac{U}{2} \left( \sum_{\sigma} d_{\sigma}^{\dagger} d_{\sigma} - 1 \right)^2. \quad (3.7)$$

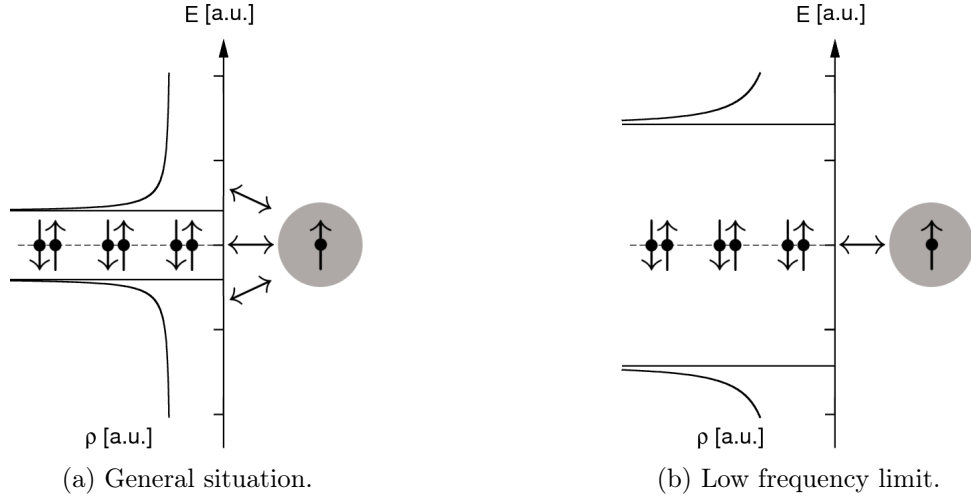


Figure 3.1: In the low frequency limit, the quasiparticle excitations are far in energy and the coupling of the quantum dot to the latter vanishes.

The physical interpretation of this effective local Hamiltonian is simple. For finite gap, the quantum dot is coupled to both the Cooper pairs and the quasiparticles in the leads. The Cooper pairs, which lie at the Fermi level, are responsible for the proximity effect. The quasiparticles give rise to conduction electrons excitations with energies higher than the gap  $\Delta$ . In the limit  $\omega_n \ll \Delta$ , the quasiparticles are far in energy and the coupling between them and the dot vanishes, which greatly simplifies the physics and makes an exact solution possible. Yet, as the dot is still coupled to the Cooper pairs at the Fermi level, the proximity effect survives with a local pairing term proportional to the hybridization  $\Gamma$  between dot and leads. Figure 3.1 illustrates how the coupling to the quasiparticle continuum vanishes in the low frequency limit.

### 3.3 Spectrum of the effective local Hamiltonian

The Hilbert space associated with the quantum dot system is spanned by  $\{|0\rangle, |\uparrow\rangle, |\downarrow\rangle, |\uparrow\downarrow\rangle\}$ . However, these four states are not an eigenbasis of the effective local Hamiltonian (3.7). The latter has the structure of a standard BCS Hamiltonian with  $|\Gamma_\varphi|$  as an effective gap. As furthermore the Coulomb interaction simply yields an extra energy shift of  $U/2$  for both empty and doubly occupied dot, the eigenvectors and eigenvalues of the effective local Hamiltonian (3.7) are readily obtained by a Bogoliubov transformation (see appendix D and [8]), in perfect analogy with solution of the BCS Hamiltonian. The eigenstates of  $H_{\text{eff}}$  are thus the singly occupied spin 1/2 states

$$|\uparrow\rangle \quad \text{and} \quad |\downarrow\rangle \quad (3.8)$$

with energies  $E_{\uparrow}^0 = E_{\downarrow}^0 = \xi_d$ , and two BCS-like states given by

$$\begin{aligned} |+\rangle &= u|\uparrow\downarrow\rangle + v|0\rangle \\ |-\rangle &= -v|\uparrow\downarrow\rangle + u|0\rangle \end{aligned} \quad (3.9)$$

with  $u^2 = \frac{1}{2} \left( 1 + \frac{\xi_d}{\sqrt{\xi_d^2 + \Gamma_\varphi^2}} \right)$  and  $v^2 = \frac{1}{2} \left( 1 - \frac{\xi_d}{\sqrt{\xi_d^2 + \Gamma_\varphi^2}} \right)$ . The energies corresponding to the BCS-like states read

$$E_\pm^0 = \frac{U}{2} \pm \sqrt{\xi_d^2 + \Gamma_\varphi^2} + \xi_d. \quad (3.10)$$

These results are identical to considerations in reference [8].

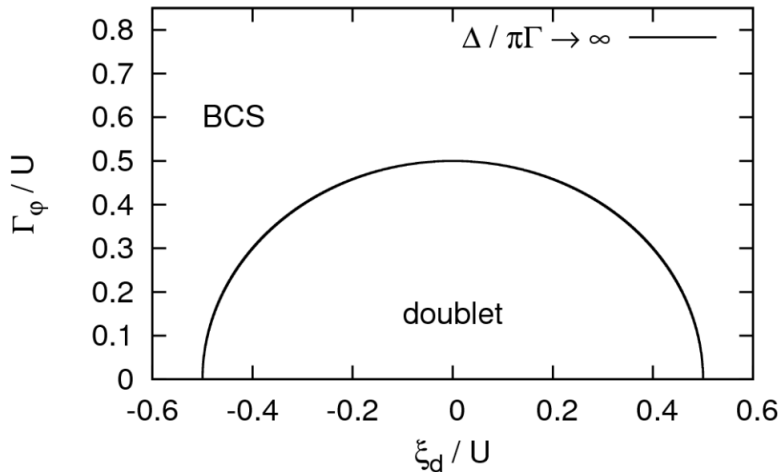


Figure 3.2: Phase diagram of a simple dot with Coulomb interaction  $U$ , energy level  $\xi_d$  and hybridization  $\Gamma$  to superconducting electrodes in the effective local limit. The transition line corresponds to  $E_\sigma^0 = E_-^0$ .

As  $E_+^0$  is always larger than  $E_-^0$ , the effective local Hamiltonian has two possible ground states: the low energy BCS-like state  $|-\rangle$  or the degenerate spin 1/2 doublet  $\{|\uparrow\rangle, |\downarrow\rangle\}$ . In the  $|-\rangle$  state, the energy is minimized for  $\varphi = 0$ . Thus, the spin singlet phase corresponds to a 0-junction (a result well known from the weak coupling limit [18]). The transition between the singlet phase and the spin- $\frac{1}{2}$ -doublet takes place at

$$\xi_d^2 + \Gamma_\varphi^2 = \frac{U^2}{4}.$$

Figure 3.2 shows the corresponding phase diagram for variable  $\xi_d$ ,  $\Gamma$  and  $U$ . In the case of small Coulomb interaction  $U$  and strong hybridization  $\Gamma$ , the system will be in a BCS-like state. This is due to the pairing energy induced by the proximity effect. On the contrary, strong Coulomb interaction opposes the BCS-like state (which is the superposition of the empty dot and the doubly occupied one and therefore affected by Coulomb repulsion). The transition from the BCS-like phase to the singly occupied one thus results in the large gap limit from a competition between the local pairing (induced by the proximity effect and characterized by the hybridization  $\Gamma$ ) and the Coulomb interaction.

### 3.4 Andreev bound states

As outlined in the introduction, the coupling to superconducting leads induces a gap in the spectral function of the dot, inside which discrete Andreev bound states can form. As a result, the spectral function of the dot shows sharp peaks, which could be measured

by STM or microwave experiments as proposed recently in references [10, 43]. Noise measurements have been suggested in reference [12]. The peaks in the spectral function indicate addition energies at which an electron may enter (or leave) the dot, and correspond thus to transitions between states with  $n$  and  $n \pm 1$  electrons. Hence, the ABS peaks in the spectral function may be interpreted as transitions between the superconducting atomic levels of the dot  $\{|\sigma\rangle, |+\rangle, |-\rangle\}$ , possibly renormalized by single-particle tunneling events neglected in  $H_{\text{eff}}$  (to be included in the next section).

Because the gap is taken to be bigger than the characteristic energy scales of the dot, these transitions will indeed result in discrete sub-gap peaks. Furthermore, transitions from a spin 1/2 doublet to a spin singlet necessarily involve an electron exchange between the dot and the superconducting leads. As the states  $|-\rangle$  and  $|+\rangle$  correspond to the superposition of an empty and doubly occupied dot, this electron exchange is in fact a coherent addition of an electron *and* a hole and the final singlet states can be understood within the Andreev reflection picture.

Putting everything together, the effective local Hamiltonian in Eq. (3.7) describes the energies of the Andreev bound states as transition energies from the spin 1/2 doublet to the spin singlet states [8, 45]. There are thus four Andreev bound states in the large gap limit for the model (3.1), with energy  $\pm a_0$  and  $\pm b_0$  which read

$$a_0 = E_-^0 - E_\sigma^0 = \frac{U}{2} - \sqrt{\xi_d^2 + \Gamma_\varphi^2}, \quad (3.11)$$

$$b_0 = E_+^0 - E_\sigma^0 = \frac{U}{2} + \sqrt{\xi_d^2 + \Gamma_\varphi^2}. \quad (3.12)$$

The  $0/\pi$  transition corresponds to the crossing of the  $|-\rangle$  and  $|\sigma\rangle$  states, which occurs for  $a_0 = 0$ .

## 3.5 Incorporating fluctuations: perturbation expansion around the effective local Hamiltonian

### 3.5.1 Preliminaries

The effective Hamiltonian (3.7) is not sufficient to obtain satisfying results for all regimes of parameters. First,  $H_{\text{eff}}$  only describes the  $0 - \pi$  transition due to the competition between a local moment state (stabilized by the Coulomb blockade) and a spin singlet (induced by the proximity effect). However, if the Coulomb interaction is strong (i.e.  $U \gg \Gamma, |\xi_d|$  and below the Kondo temperature), the local moment can be screened by the Kondo effect, which will compete with the superconducting gap for the  $0 - \pi$  transition. Consequently, a typical scaling in the ratio of the Kondo temperature to the gap  $\Delta$  will appear. Also, the Josephson current in the  $\pi$ -phase identically vanishes from  $H_{\text{eff}}$ , as the spin doublet does not disperse with the superconducting phase difference. This is a limitation of the large gap limit, as can be inferred e.g. from experiments and the low hybridization limit (see section 2.3 and refs. [13, 50]). On a more quantitative basis, the experimental gap  $\Delta$  is usually of the order of a few kelvins, which is also the typical scale for both  $\Gamma$  and  $U$  in carbon nanotube quantum dot devices.

In order to extend the description of the quantum dot's physics, energy corrections shall be calculated with a perturbation theory around the effective Hamiltonian (3.7).

Once these corrections have been obtained, physical observables like the Josephson current may be computed via the free energy  $F = -\frac{1}{\beta} \ln(Z)$ , with  $\beta$  the inverse temperature. Therefore, it is most convenient to work in an action based description, which directly yields the partition function  $Z$ .

The action corresponding to the total Hamiltonian (3.1) is derived following the lines of reference [14]. At first, we integrate over the fermions in the leads. Omitting the resulting irrelevant constant, the partition function reads

$$Z = \int \mathcal{D}(\bar{\Psi}_d, \Psi_d) e^{-S_{\text{dot}}} \text{ with} \quad (3.13)$$

$$\begin{aligned} S_{\text{dot}} = & \sum_{\vec{k}, i, \omega_n} \bar{\Psi}_{d,n} \hat{H}_{T_i} \hat{G}_{\vec{k}i, \vec{k}i}^0(i\omega_n) \hat{H}_{T_i}^\dagger \Psi_{d,n} + \sum_{\omega_n} \bar{\Psi}_{d,n} \begin{pmatrix} -i\omega_n + \epsilon_d & 0 \\ 0 & -i\omega_n - \epsilon_d \end{pmatrix} \Psi_{d,n} \\ & + \int_0^\beta d\tau U \bar{d}_\uparrow(\tau) \bar{d}_\downarrow(\tau) d_\downarrow(\tau) d_\uparrow(\tau) \end{aligned} \quad (3.14)$$

(the derivation of the latter can be found in appendix F).

The perturbation consists of the terms in Eq. (3.13) that are not contained in the action  $S_{\text{eff}}$  corresponding to the effective local Hamiltonian, i.e. the low frequency limit of the total action (3.14). This yields

$$\begin{aligned} S_{\text{eff}} = & \int_0^\beta d\tau \left( \sum_{\sigma} \bar{d}_\sigma(\tau) \left( \frac{\partial}{\partial \tau} + \epsilon_d \right) d_\sigma(\tau) - |\Gamma_\varphi| \bar{d}_\uparrow(\tau) \bar{d}_\downarrow(\tau) - |\Gamma_\varphi| d_\downarrow(\tau) d_\uparrow(\tau) \right. \\ & \left. + U \bar{d}_\uparrow(\tau) \bar{d}_\downarrow(\tau) d_\downarrow(\tau) d_\uparrow(\tau) \right), \end{aligned} \quad (3.15)$$

$$\begin{aligned} S_{\text{pert}} = & \int_0^\beta d\tau \int_0^\beta d\tau' \sum_{\vec{k}, i} \bar{\Psi}_d(\tau) \hat{H}_{T_i} \hat{G}_{\vec{k}i, \vec{k}i}^0(\tau - \tau') \hat{H}_{T_i}^\dagger \Psi_d(\tau') \\ & + \int_0^\beta d\tau (|\Gamma_\varphi| \bar{d}_\uparrow(\tau) \bar{d}_\downarrow(\tau) + |\Gamma_\varphi| d_\downarrow(\tau) d_\uparrow(\tau)). \end{aligned} \quad (3.16)$$

Note that  $S_{\text{eff}}$  contains the local pairing term derived in section 3.2. The proximity effect is thus treated non-perturbatively (just like the Coulomb interaction), which is the crucial ingredient of our analytic approach. The perturbation  $S_{\text{pert}}$  simply corresponds to the tunnel coupling between the dot and the electrodes other than the lowest order proximity effect.

### 3.5.2 The corrections of the energy levels

Now that the effective local Hamiltonian and its perturbation have been transposed into the quantum field theory language, one may readily derive the action's perturbation expansion to be

$$Z = \int \mathcal{D}(\bar{\Psi}, \Psi) e^{-S_{\text{eff}} - S_{\text{pert}}} \approx \int \mathcal{D}(\bar{\Psi}, \Psi) e^{-S_{\text{eff}}} \left( 1 - S_{\text{pert}} + \frac{1}{2} S_{\text{pert}} S_{\text{pert}} + \dots \right). \quad (3.17)$$

Observables like the Josephson current may then be computed according to

$$\begin{aligned} J &= 2e \frac{\partial F}{\partial \varphi} = -\frac{2e}{\beta} \frac{1}{Z} \frac{\partial Z}{\partial \varphi} \\ &= \frac{2e}{\beta} \frac{\int \mathcal{D}(\bar{\Psi}, \Psi) e^{-S_{\text{eff}}} \left(1 - S_{\text{pert}} + \frac{1}{2} S_{\text{pert}} S_{\text{pert}} + \dots\right) \left(\frac{\partial S_{\text{eff}}}{\partial \varphi} + \frac{\partial S_{\text{pert}}}{\partial \varphi}\right)}{\int \mathcal{D}(\bar{\Psi}, \Psi) e^{-S_{\text{eff}}} \left(1 - S_{\text{pert}} + \frac{1}{2} S_{\text{pert}} S_{\text{pert}} + \dots\right)}. \end{aligned} \quad (3.18)$$

To the first order,

$$Z \approx Z_{\text{eff}} - \int \mathcal{D}(\bar{\Psi}, \Psi) e^{-S_{\text{eff}}} S_{\text{pert}} \quad (3.19)$$

with  $Z_{\text{eff}} = \int \mathcal{D}(\bar{\Psi}, \Psi) e^{-S_{\text{eff}}}$ . The explicit evaluation of these integrals is done in the standard operator formalism. The passage into this formalism

- replaces the Grassmann fields by the corresponding operators,
- replaces the  $\int e^{-S_{\text{eff}}}(\cdot)$  by  $Z_{\text{eff}} \langle (\cdot) \rangle_0$  (the subscript 0 indicating the evaluation of the expectation value in the effective local limit),
- introduces time-ordering.

The partition function takes the intermediate form

$$\begin{aligned} Z &= Z_{\text{eff}} - Z_{\text{eff}} t^2 \beta \sum_{\vec{k}, i} \int d\tau \left( G_{\vec{k}i\vec{k}i;11}^0(\tau) \langle T_{\tau} d_{\uparrow}^{\dagger}(\tau) d_{\uparrow}(0) \rangle_0 - G_{\vec{k}i\vec{k}i;12}^0(\tau) e^{i\varphi_i} \langle T_{\tau} d_{\uparrow}^{\dagger}(\tau) d_{\downarrow}^{\dagger}(0) \rangle_0 \right. \\ &\quad \left. - G_{\vec{k}i\vec{k}i;21}^0(\tau) e^{-i\varphi_i} \langle T_{\tau} d_{\downarrow}(\tau) d_{\uparrow}(0) \rangle_0 + G_{\vec{k}i\vec{k}i;22}^0(\tau) \langle T_{\tau} d_{\downarrow}(\tau) d_{\downarrow}^{\dagger}(0) \rangle_0 \right) \\ &\quad - 2\beta |\Gamma_{\varphi}| \left( \langle T_{\tau} d_{\uparrow}^{\dagger}(0) d_{\uparrow}^{\dagger}(0) \rangle_0 + \langle T_{\tau} d_{\downarrow}(\tau) d_{\uparrow}(0) \rangle_0 \right). \end{aligned} \quad (3.20)$$

The actual energy corrections are found by identification with

$$Z = \sum_{\sigma} e^{-\beta E_{\sigma}} + e^{-\beta E_{+}} + e^{-\beta E_{-}}, \quad (3.21)$$

where the renormalized superconducting atomic levels  $E_{\sigma} = E_{\sigma}^0 + \delta E_{\sigma}$  and  $E_{\pm} = E_{\pm}^0 + \delta E_{\pm}$  are obtained from

$$e^{-\beta E_{\sigma}} \approx e^{-\beta E_{\sigma}^0} (1 - \beta \delta E_{\sigma}), \quad (3.22)$$

$$e^{-\beta E_{\pm}} \approx e^{-\beta E_{\pm}^0} (1 - \beta \delta E_{\pm}). \quad (3.23)$$

Because the Coulomb interaction is taken into account, Wick's theorem cannot be used to calculate  $Z$ . Instead, expectation values are calculated via Lehmann representation. Explicit calculations may be found in appendix G. In the zero temperature limit  $\beta \rightarrow \infty$ , the energy corrections are

$$\begin{aligned} \delta E_\sigma = & -t^2 \sum_{\vec{k}} \left( \frac{1}{E_{\vec{k}} + (E_+^0 - E_\sigma^0)} + \frac{1}{E_{\vec{k}} + (E_-^0 - E_\sigma^0)} \right. \\ & \left. + \frac{2\Delta}{E_{\vec{k}}} uv \left| \cos\left(\frac{\varphi}{2}\right) \right| \left( \frac{1}{E_{\vec{k}} + (E_+^0 - E_\sigma^0)} - \frac{1}{E_{\vec{k}} + (E_-^0 - E_\sigma^0)} \right) \right), \end{aligned} \quad (3.24)$$

$$\begin{aligned} \delta E_+ = & -t^2 \sum_{\vec{k}, \sigma} \left( \frac{1}{E_{\vec{k}} - (E_+^0 - E_\sigma^0)} - \frac{2\Delta}{E_{\vec{k}}} uv \left| \cos\left(\frac{\varphi}{2}\right) \right| \frac{1}{E_{\vec{k}} - (E_+^0 - E_\sigma^0)} \right) - 2|\Gamma_\varphi| uv \\ & , \end{aligned} \quad (3.25)$$

$$\begin{aligned} \delta E_- = & -t^2 \sum_{\vec{k}, \sigma} \left( \frac{1}{E_{\vec{k}} - (E_-^0 - E_\sigma^0)} + \frac{2\Delta}{E_{\vec{k}}} uv \left| \cos\left(\frac{\varphi}{2}\right) \right| \frac{1}{E_{\vec{k}} - (E_-^0 - E_\sigma^0)} \right) + 2|\Gamma_\varphi| uv, \end{aligned} \quad (3.26)$$

with the quasiparticle energy  $E_{\vec{k}} = \sqrt{\epsilon_{\vec{k}}^2 + \Delta^2}$ .

### 3.5.3 Self-consistent renormalization of the energies

Eqs. (3.24)-(3.26) yield the first order corrections to the energy levels, so that the bound states energies are simply shifted by  $\delta a = \delta E_- - \delta E_\sigma$  and  $\delta b = \delta E_+ - \delta E_\sigma$  with

$$\begin{aligned} \delta a = & -\frac{\Gamma}{\pi} \int_0^D d\epsilon \left( \frac{2}{E - a_0} - \frac{1}{E + b_0} - \frac{1}{E + a_0} \right. \\ & + \frac{\Delta}{E} uv \left| \cos\left(\frac{\varphi}{2}\right) \right| \left( \frac{2}{E - a_0} - \frac{1}{E + b_0} + \frac{1}{E + a_0} \right) \\ & + 2|\Gamma_\varphi| uv \end{aligned} \quad (3.27)$$

and

$$\begin{aligned} \delta b = & -\frac{\Gamma}{\pi} \int_0^D d\epsilon \left( \frac{2}{E - b_0} - \frac{1}{E + b_0} - \frac{1}{E + a_0} \right. \\ & + \frac{\Delta}{E} uv \left| \cos\left(\frac{\varphi}{2}\right) \right| \left( \frac{-2}{E - b_0} - \frac{1}{E + b_0} + \frac{1}{E + a_0} \right) \\ & - 2|\Gamma_\varphi| uv \end{aligned} \quad (3.28)$$

(with  $a_0, b_0$  as defined in Eqs. 3.11 and 3.12 and  $E = \sqrt{\epsilon^2 + \Delta^2}$ ).

Nevertheless, these expressions are only valid in the perturbative regime, i.e. as long as  $\Delta \gg U, \Gamma, \xi_d$ . They diverge logarithmically when the bound states energies  $a_0$  and  $b_0$  approach the gap edge, and are therefore only reliable if e.g.  $a_0 \gg \Gamma \log[(D+\Delta)/(\Delta-a_0)]$ .

In the limit of large gap  $\Delta \gg a_0$ , the above corrections to  $a_0$  are thus of the order  $\Gamma a_0/\Delta$ , so that  $\Gamma/\Delta$  is indeed the small dimensionless parameter controlling the perturbation expansion. However, the peculiar logarithmic dependence of the Andreev bound state energy renormalizations shows that doing a straightforward  $1/\Delta$  expansion around



Figure 3.3: Diagrammatic illustration of the resummation achieved by the self-consistency condition, that “plugs the correction into the correction”.

the effective local Hamiltonian will be rapidly uncontrolled, and will have a hard time reproducing the logarithmic singularities at  $\Delta$  close to  $a_0$ . For this reason, and also because the very large gap limit becomes trivial for a finite electronic bandwidth (as discussed in section 3.2), it was indeed more appropriate to single out all terms in the total action that correspond to the effective local Hamiltonian, and to perform the perturbation expansion around these (see equations (3.15) and (3.16)).

Because our lowest-order expansion obviously still breaks down when the gap becomes comparable to the bound state energy, one would naturally seek to resum the leading logarithmic divergences in equations (3.24)-(3.26). Indeed, the renormalization group (RG) framework allows to extend the regime of validity greatly.

The idea behind the renormalization group is that a small change of the physically interesting scales (in the present case the energy gap  $\Delta$ ) will not change the physics of the system dramatically. In fact, the “new” system can be described similarly to the old one by simply renormalizing its parameters (e.g. energy levels, coupling strengths, etc.). This renormalization is also called the “flow” of the parameters. It has been shown by works of Wilson [65] and others that this is equivalent to summing up the most important terms of the perturbation expansion to infinite order. In the present case, the renormalization group allows to sum up the logarithmically divergent contributions to  $\delta a$  and  $\delta b$ . This gives access to a regime where  $\Delta$  is not the largest energy scale anymore.

In a standard RG approach, one would calculate the modified energies for a slightly lowered gap  $\Delta$ . These renormalized energy levels would then be used to perform another perturbation expansion and to calculate another energy correction and so on. Instead of such a classical renormalization group approach, we will derive self-consistent equation inspired by Brillouin-Wigner perturbation theory [66]. Similarly to a standard RG procedure, the latter resums the logarithmic divergences by plugging the renormalized energies into the energy corrections. As illustrated in figure 3.3, diagrams with the first order correction plugged into the first order correction are summed up to infinite order.

In order to derive the self-consistency condition, one must thus identify the logarithmically divergent contributions to  $\delta a$  and  $\delta b$ , here given by the terms  $2/(E - a_0)$  and  $2/(E - b_0)$ . They are regularized by using the renormalized energies, which yields

$$\begin{aligned}
\delta a &= -\frac{\Gamma}{\pi} \int_0^D d\epsilon \left( \frac{2}{E - a(\Delta)} - \frac{1}{E + b_0} - \frac{1}{E + a_0} \right. \\
&+ \frac{\Delta}{E} uv \left| \cos\left(\frac{\varphi}{2}\right) \right| \left( \frac{2}{E - a(\Delta)} - \frac{1}{E + b_0} + \frac{1}{E + a_0} \right) \right) \\
&+ 2|\Gamma_\varphi| uv
\end{aligned} \tag{3.29}$$

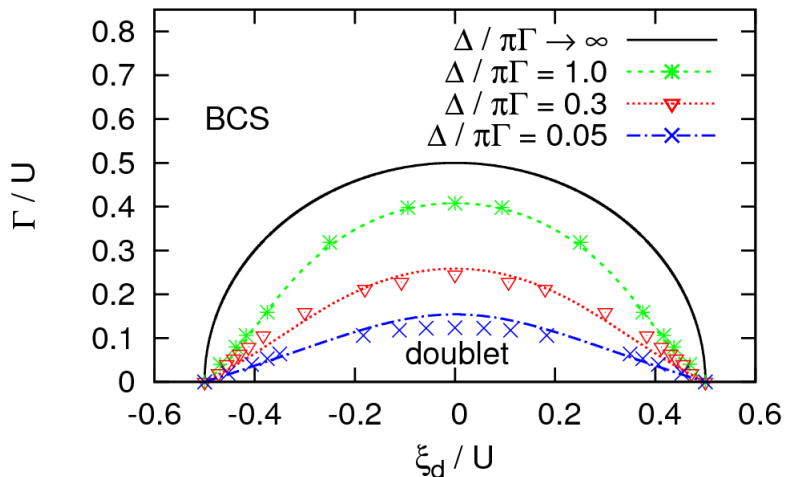


Figure 3.4: Phase diagram of a simple dot with Coulomb interaction  $U$ , tunnel coupling  $\Gamma$  to superconducting electrodes with gap  $\Delta$  for  $\varphi = 0$  and  $\pi\Gamma = 0.2D$ . The symbols indicate NRG data from Ref. [8] and the various lines our results.

and

$$\begin{aligned}
 \delta b &= -\frac{\Gamma}{\pi} \int_0^D d\epsilon \left( \frac{2}{E - b(\Delta)} - \frac{1}{E + b_0} - \frac{1}{E + a_0} \right. \\
 &+ \frac{\Delta}{E} uv \left| \cos\left(\frac{\varphi}{2}\right) \right| \left( \frac{-2}{E - b(\Delta)} - \frac{1}{E + b_0} + \frac{1}{E + a_0} \right) \\
 &- 2|\Gamma_\varphi| uv,
 \end{aligned} \tag{3.30}$$

where  $a(\Delta) = a_0 + \delta a$ ,  $b(\Delta) = b_0 + \delta b$  and again  $E = \sqrt{\epsilon^2 + \Delta^2}$ . Note that terms like  $1/(E+a_0)$  have no self-consistency because there are no associated divergences. Eq. (3.29) and (3.30) now clearly hold as long as the *renormalized* energies  $a(\Delta)$  and  $b(\Delta)$  are not too close to the gap edge,  $\pm\Delta$  respectively.

## 3.6 Results

### 3.6.1 Phase diagram for the single dot with Coulomb interaction

We start by discussing the  $0 - \pi$  transition line, by comparison to the numerical renormalization group (NRG) data by Bauer et al. [8]. This transition, being nothing but the crossing of the states  $|-\rangle$  and  $|\sigma\rangle$ , also corresponds to the crossing of the low energy Andreev bound state and the Fermi level, i.e.  $a(\Delta) = E_-(\Delta) - E_\sigma(\Delta) = 0$ .

Fig. 3.4 shows the extension of the phase diagram to finite values of the gap  $\Delta$ . As a general rule, the global shape of the phase diagram remains fairly similar to the large gap case shown in figure 3.2 and discussed in section 3.3. Nevertheless, the phase diagram now depends on the ratio of gap and hybridization. If this ratio  $\Delta/(\pi\Gamma)$  decreases, i.e. the energy scale  $\Gamma$  associated with the dot-electrode-hybridization increases, the pairing induced by the coupling to the electrodes becomes stronger and the BCS-like phase extends.

Even though our perturbative approach is fairly simple, the results reproduce nicely the NRG data of Refs. [8] and [24]. The analytically obtained phase diagram is indeed

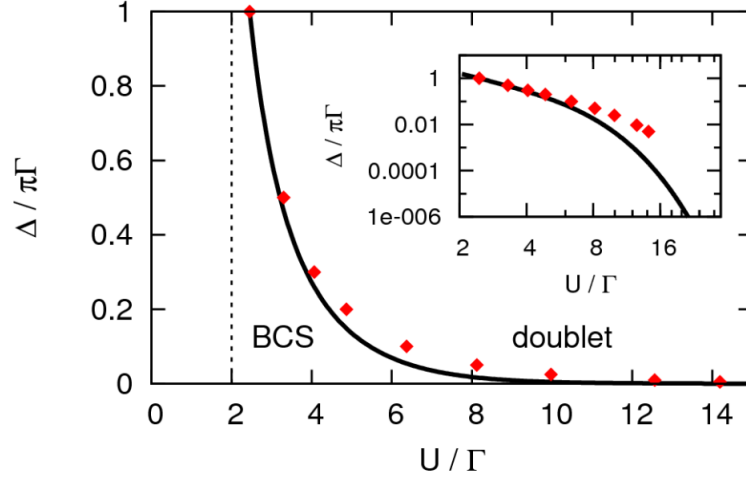


Figure 3.5: Transition line between the spin 1/2 doublet and the BCS-like state at particle hole symmetry  $\xi_d = 0$  (solid curve) for  $\varphi = 0$  and  $\pi\Gamma = 0.2D$ . The vertical dotted line corresponds to the transition asymptote in the effective local limit at  $\Delta \rightarrow \infty$ . The dots indicate NRG data from Ref. [8] and the solid line our result. The inset displays the same data on a logarithmic scale.

identical to the NRG data for  $\Delta \gtrsim \Gamma$ .

### 3.6.2 Kondo physics

For smaller  $\Delta/\Gamma$ , the Kondo effect sets in, but the transition lines remain quantitatively correct for  $\xi_d$  near  $\pm U/2$ , with increasing deviations from the NRG calculations close to the particle-hole symmetric point  $\xi_d = 0$  at large Coulomb interaction  $U$ . In this regime, the 0-phase possesses a Kondo singlet ground state. As the leads are superconductors, the formation of a Kondo resonance involves the breaking of Cooper pairs. Therefore, the transition is now due to the competition between  $T_K$  and the superconducting gap  $\Delta$ , and should occur at  $k_B T_K \propto \Delta$ .

Fig. 3.5 shows a plot of the transition line for  $\xi_d = 0$  as obtained with Eq. (3.29) (solid curve). The vertical, dotted line depicts the asymptote in the effective local limit. The symbols again correspond to NRG data [8]. For the particle hole symmetric case  $\xi_d = 0$ , the Kondo temperature is given by

$$T_K = 0.182 U \sqrt{\frac{8\Gamma}{\pi U}} e^{-\frac{\pi U}{8\Gamma}} \quad (3.31)$$

(see for example Ref. [8]). The inset shows on a log-log scale that our approach captures an exponential decay of the transition line with the Coulomb interaction. Nonetheless, the suppression of the BCS-like phase appears quantitatively stronger than expected: a factor 4 instead of 8 is found in the exponential factor of  $T_K$ . The reason for this is that the vertex renormalizations have not been taken into account, as discussed in the context of U-NCA [67]. Far away from the particle-hole symmetric limit, our results for the Kondo temperature reproduce the lowest-order scaling theory for the infinite- $U$  Anderson model [59], and are in relatively good agreement with NRG data for all  $\Delta/\Gamma$  values.

### 3.6.3 Energy renormalizations at particle hole symmetry ( $\xi_d = 0$ )

While Fig. 3.4 only indicates the transition line between the spin 1/2 doublet and the lowest BCS spin singlet, it is also instructive to look at the actual renormalization of the energy levels while varying the gap  $\Delta$  from large values to smaller ones beyond the critical point. Fig. 3.6 indicates the renormalized energies of the two Andreev bound states (i.e. the difference between the spin 1/2 doublet and the two spin singlets energies) for different hybridizations  $\Gamma$ . We note that our results are in quantitative agreement with the NRG calculations of Yoshioka and Ohashi [23]. Several regions need to be distinguished. If the gap  $\Delta$  is much larger than the bandwidth  $D$ , all curves collapse at the value  $U/2$  (left hand side of Fig. 3.6), since there is no hybridization with both quasiparticles and Cooper pairs anymore, and one recovers the bare atomic levels. When the gap starts to decrease, the proximity effect simply splits the two Andreev bound states according to equations (3.11)-(3.12). When the gap becomes of the same order than the typical energy scales of the dot  $a_0$  and  $b_0$ , the superconducting atomic levels start to mix with each other and the electrodes, so that the energies renormalize in a non trivial way. The high energy Andreev bound states end up touching the gap edge for  $\Delta \approx U/2$ , so that half of the ABS are absorbed into the continuum above  $\Delta$ , as can be seen in Fig. 3.7. The lowest Andreev bound state follows however a downward renormalization, until the Fermi level is crossed and the 0-state becomes the ground state. The difference in behavior between the low and high energy bound states (the former being never allowed to leave the superconducting gap) can be tracked into equations (3.29)-(3.30), where level repulsion effects from the gap edge occur for the low energy level  $|-\rangle$  but are canceled for the high energy level  $|+\rangle$ , which is hence allowed to penetrate into the continuum. These considerations unveil how the ABS may be adiabatically connected to the atomic or molecular levels in a complicated fashion.

Again, our simple analytic approach reproduces the NRG results [23] over a vast regime of parameters. Yet, some deviations are observed in the Kondo regime: we find (for the highest hybridization  $\pi\Gamma = 0.005D$ ) that the high energy BCS-like state is not absorbed anymore into the continuum of states - an artifact of the limits of our perturbative approach. Notice also that the energy corrections are too important if the gap becomes very small, an effect actually due to our underestimation of the Kondo temperature at particle-symmetry, as discussed previously. Finally Fig. 3.7 shows that, in the limit of vanishing gap, our approach is only valid as long as  $a(\Delta) \geq -\Delta$  (as has been mentioned in section 3.5.3), because the lowest bound state artificially escapes from the gap.

The expected saturation of  $a(\Delta)$  near  $-\Delta$  can be partly restored by adding a further self-consistency for the term  $1/(E + a_0)$  in the equation (3.29) for  $\delta a$  and  $1/(E + b_0)$  in the equation (3.30) for  $\delta b$ . Figure 3.8 shows the resulting curves, still for the same parameters. The results fit qualitatively somewhat better, especially for  $\pi\Gamma = 0.005D$  (green curves): the high energy Andreev bound state now escapes from the gap.

Nevertheless, the Kondo temperature is overestimated even more dramatically in the case of two flows. Compared to section 3.6.2 where a factor 4 instead of 8 was found in the exponential of  $T_K$  (see equation (3.31)), we now even find a factor of 2 instead of 8. This results in the clearly visible distortion of our curves to the right.

Strictly speaking, equations (3.29) and (3.30) will always have difficulties for small gaps  $\Delta$ , no matter if one uses one or two flows. First of all, this regime corresponds to the limit of a perturbation expansion around a large gap limit. At the same time, it

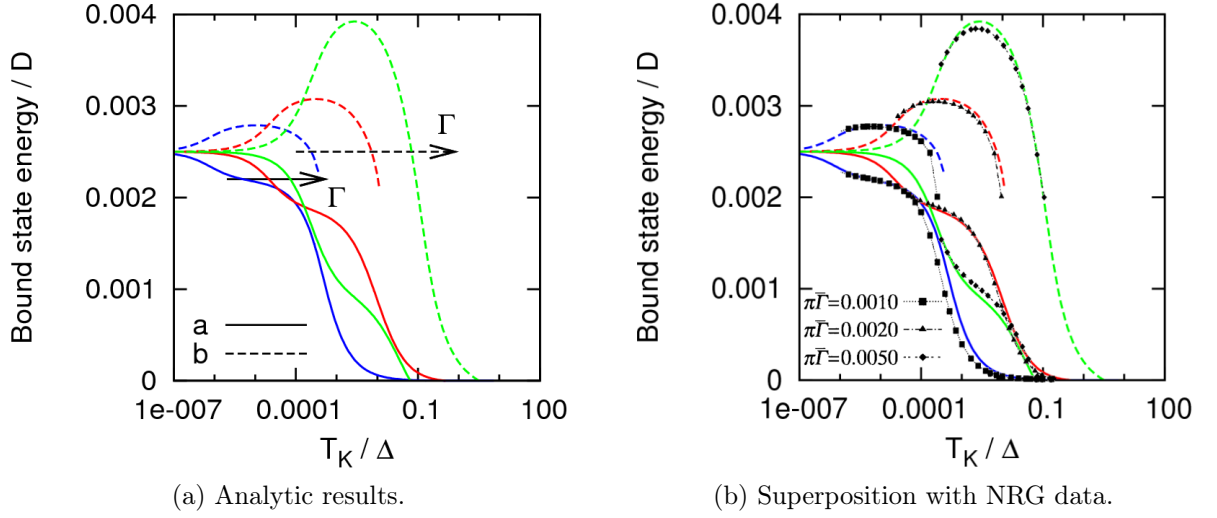


Figure 3.6: Renormalization of the Andreev bound state energies as a function of  $T_K/\Delta$  (the Kondo temperature is given in the text). Figure (a) shows our analytic results. The dashed curves correspond to the high energy bound state  $b(\Delta)$ , the solid curves correspond to  $a(\Delta)$ . All curves have been calculated for  $U = 0.005 D$  and  $\xi_d = 0$ , with several hybridization values  $\pi\bar{\Gamma}/D = 0.001, 0.002, 0.005$  (from left to right). Quantitatively similar results were obtained by the NRG in Ref. [23]. The superposition of the NRG data and our results is given in figure (b), with  $\bar{\Gamma} = \Gamma/D$ .

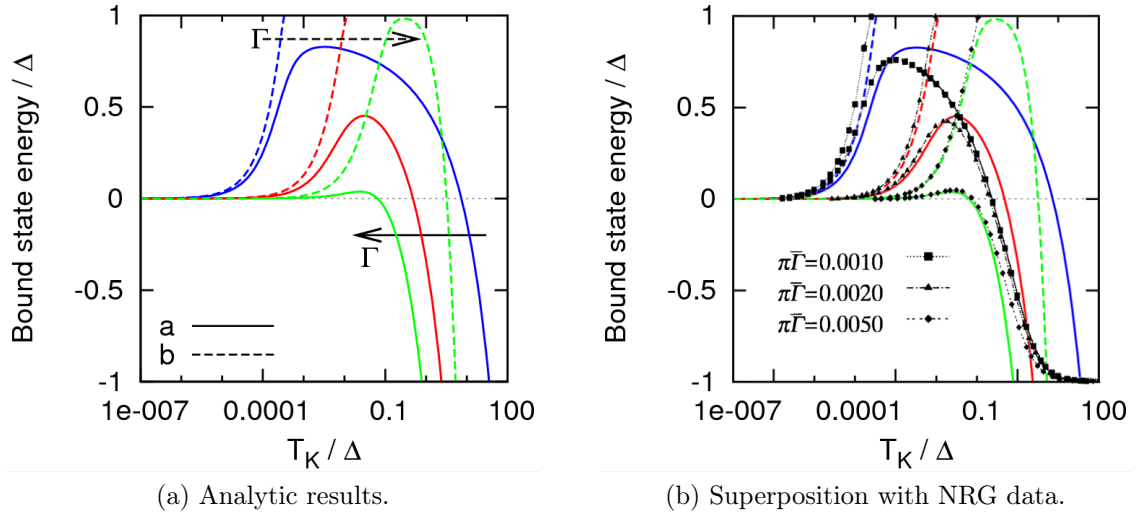


Figure 3.7: Same data as in Fig. 3.6, but normalized by the gap. The numerical data is again taken from Ref. [23] and  $\bar{\Gamma} = \Gamma/D$ .

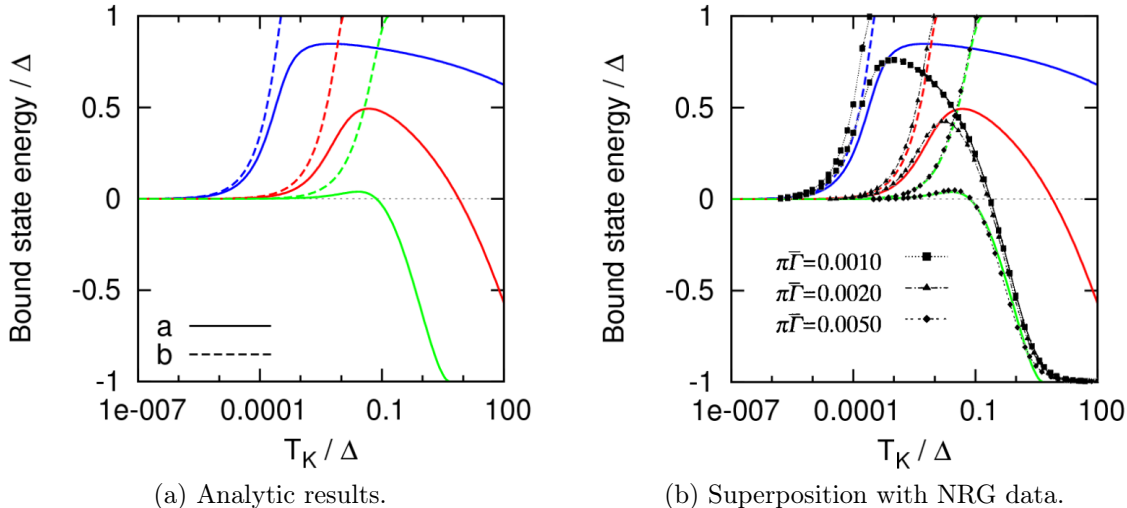


Figure 3.8: Renormalization of the Andreev bound state energies as a function of  $T_K/\Delta$  (the Kondo temperature is given in the text), calculated for 2 flows in equations (3.29) and (3.30) (see text). Figure (a) shows our analytic results. The dashed curves correspond to the high energy bound state  $b(\Delta)$ , the solid curves correspond to  $a(\Delta)$ . All curves have been calculated for  $U = 0.005D$  and  $\xi_d = 0$ , with several hybridization values  $\pi\Gamma/D = 0.001$  (blue curves),  $0.002$  (red curves),  $0.005$  (green curves). The superposition of the NRG data from Ref. [23] and our results is given in figure (b), with  $\bar{\Gamma} = \Gamma/D$ .

corresponds also to the Kondo regime (that we cannot capture quantitatively due to the missing vertex corrections). Finally, equations (3.29) and (3.30) describe a perturbation theory around a limit with 4 Andreev bound states. Nevertheless, we found that the high energy ABS escape from the gap for  $\Delta \approx U/2$ .

It would thus be exaggerated to hope that our simple approach is able to describe the very low gap regime. We therefore prefer to use only the one flow equations (3.29) and (3.30) derived above, that describe the Kondo temperature better than their two-flow correspondents.

### 3.6.4 Energy renormalizations outside particle hole symmetry ( $\xi_d \neq 0$ )

From an experimental point of view, the position of the energy level of the quantum dot is the most controllable parameter of the system (by a simple gate voltage). Therefore, it is important to analyze the evolution of the Andreev bound states for different values of  $\xi_d$ .

Fig. 3.9 illustrates how the energies of the bound states scale with  $\Delta$  for  $\xi_d \neq 0$  and can be favorably compared to the NRG data by Yoshioka and Ohashi [23]. The more the particle-hole symmetry is broken, the more the low energy bound state moves away from the gap edge, ensuring even better convergence of our expansion for a given value of the hybridization  $\Gamma$ . Outside particle-hole symmetry, the dot either seeks to be as empty as possible (for  $\xi_d > 0$ ) or as occupied as possible (for  $\xi_d < 0$ ). Thus, a BCS-like wave function will be favored. As a consequence, the Kondo effect (that necessitates a singly occupied dot) is less important. This corresponds to a regime where our approximation scheme works at best.

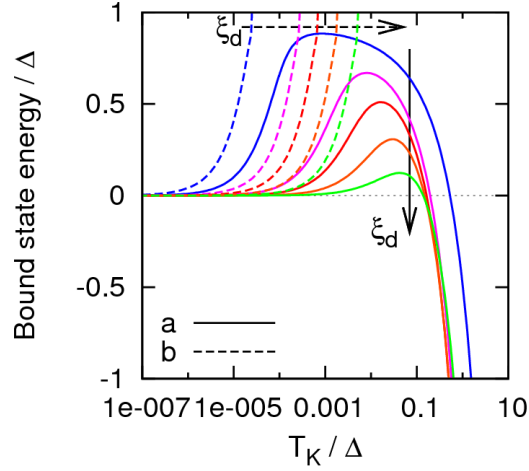


Figure 3.9: Renormalization of the Andreev bound state energies outside particle-hole symmetry. The dotted curves correspond to the high energy bound state  $b(\Delta)$ , the solid curves correspond to  $a(\Delta)$ . All curves have been calculated for  $U = 0.5 D$  and  $\pi\Gamma = 0.05 D$ , with several level shifts  $\xi_d/U = 0.3, 0.375, 0.4, 0.425, 0.45$ .

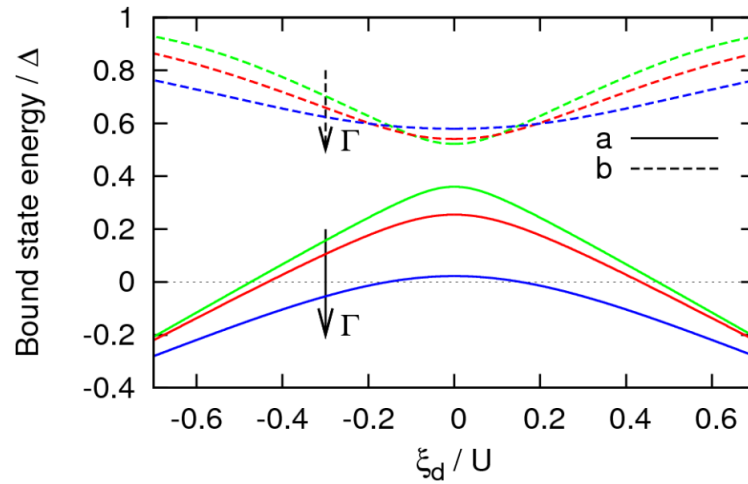


Figure 3.10: Evolution of the Andreev bound state energies as a function of the dot's energy level for  $U = 0.005 D$  and  $\Delta = U$ . The hybridization takes several values  $\pi\Gamma/D = 0.001, 0.002, 0.005$ .

Further understanding can be gained by looking at the energies of the Andreev bound states as a function of  $\xi_d$  in Fig. 3.10. We recover the fact that the high energy bound states increase in energy by breaking particle-hole symmetry, whereas the low energy bound state has a decreasing energy, which is already known from the analytic expressions in the large gap limit. In addition, Fig. 3.10 shows that the dispersion of both ABS weakens for increasing hybridization. Indeed, the more the dot is hybridized with the leads, the less the Andreev bound state energy is sensitive to the bare values of the dot parameters.

### 3.6.5 Superconducting correlations on the dot

In order to further analyze the evolution of the states in the dot as a function of the different parameters, we investigate now the superconducting correlations  $\langle d_{\uparrow}^{\dagger} d_{\downarrow}^{\dagger} \rangle$  on the dot. For the effective local Hamiltonian, these correlations are zero in the spin doublet phase. In the BCS-like phase, the correlations are maximal if the two states  $|0\rangle$  and  $|\uparrow\downarrow\rangle$  are equivalent, i.e. at particle hole symmetry. If the dot level is far from  $\xi_d = 0$ , the wave function will be predominantly  $|0\rangle$  (if  $\xi_d$  is positive) or  $|\uparrow\downarrow\rangle$  (if  $\xi_d$  is negative). This kills the superconducting correlations.

Within the self-consistent energy renormalization scheme derived above, the superconducting correlations can readily be obtained from the renormalized energies. For the effective local limit Hamiltonian

$$H_{\text{eff}} = \sum_{\sigma} \xi_d d_{\sigma}^{\dagger} d_{\sigma} - |\Gamma_{\varphi}| \left( d_{\uparrow}^{\dagger} d_{\downarrow}^{\dagger} + \text{h.c.} \right) + \frac{U}{2} \left( \sum_{\sigma} d_{\sigma}^{\dagger} d_{\sigma} - 1 \right)^2,$$

the expectation value of the energy of the ground state at zero temperature is proportional to

$$E_{GS}^0 = \langle H_{\text{eff}} \rangle_0 \sim -|\Gamma_{\varphi}| \langle d_{\uparrow}^{\dagger} d_{\downarrow}^{\dagger} + d_{\downarrow} d_{\uparrow} \rangle_0$$

(with the bare ground state energy  $E_{GS}^0$ ). Note the amplitudes  $u$  and  $v$  in the states  $|\pm\rangle$  have been chosen to be real (see section 3.3). Equivalently, one might state the physical argument that the superconducting correlations should be a real number in equilibrium. This yields

$$E_{GS}^0 \sim -2|\Gamma_{\varphi}| \langle d_{\uparrow}^{\dagger} d_{\downarrow}^{\dagger} \rangle_0.$$

In the effective local limit, the superconducting correlations can thus be computed by simply deriving the ground state energy with respect to the hybridization. However, the renormalized correlations cannot be calculated by such a simple derivation of the total energy with respect to the hybridization, because the latter also enters several terms of the energy corrections. One thus has to artificially add a hybridization  $\gamma$  only in the effective local limit Hamiltonian that will tend to zero in the end of the calculation,

$$E_{GS}^0 \sim \lim_{\gamma \rightarrow 0} -2(|\Gamma_{\varphi}| + \gamma) \langle d_{\uparrow}^{\dagger} d_{\downarrow}^{\dagger} \rangle_0.$$

Then, superconducting correlations can be written as

$$\langle d_{\uparrow}^{\dagger} d_{\downarrow}^{\dagger} \rangle = \lim_{\gamma \rightarrow 0} -\frac{1}{2} \frac{dE_{GS}^0}{d\gamma}. \quad (3.32)$$

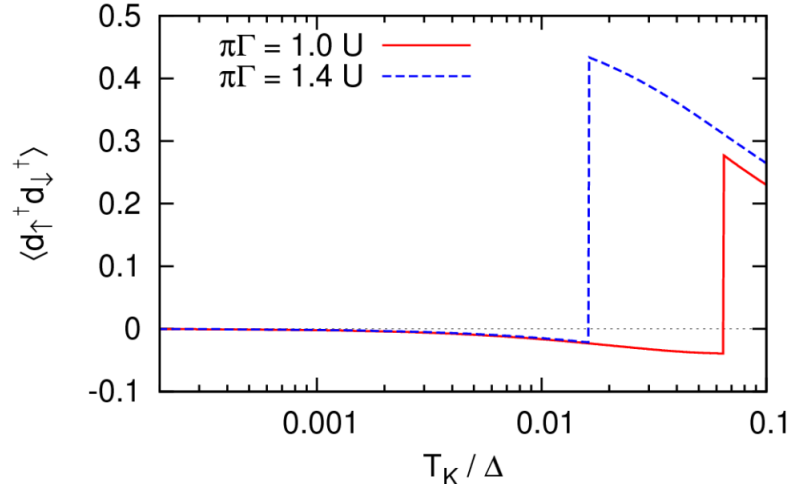


Figure 3.11: Superconducting correlations as a function of the gap  $\Delta$  (for  $D = 200 U$  and  $\xi_d = 0$ ).

For finite gaps  $\Delta$ , the correlations can analogously be computed via

$$\langle d_{\uparrow}^{\dagger} d_{\downarrow}^{\dagger} \rangle = \lim_{\gamma \rightarrow 0} -\frac{1}{2} \frac{dE_{GS}}{d\gamma}. \quad (3.33)$$

In equation (3.33),  $E_{GS}$  denotes the renormalized energy of the respective ground state (i.e. spin doublet or low energy BCS-like state).

As the gap decreases from infinity, the (formerly) singly occupied state will start having a BCS-like admixture and therefore a non zero superconducting correlation. In contrast, the mixing will result in a decreased correlation in the BCS-like phase. Nevertheless, if the gap tends to zero, one would expect the correlations to vanish as well. This is indeed what Fig. 3.11 shows. For large gaps, the dot is in the spin 1/2 phase; the correlations are small, but increase as the states mix. The transition to the BCS-like phase results in a discontinuous jump in the correlations, before they finally vanish for very small gaps. It can thus be concluded that the correlations should be normalized by the gap if one is interested in measuring only the mixing effect. Finally, the two different curves show how the hybridization stabilizes the BCS-like state with respect to the spin doublet.

As the Coulomb interaction opposes the formation of a Cooper pair wave function, the transition between the BCS-like phase and the spin doublet can also be achieved if the Coulomb interaction is tuned, as shown in Fig. 3.12. The effect of the mixing is clearly visible by an increase of the correlation  $\langle d_{\uparrow}^{\dagger} d_{\downarrow}^{\dagger} \rangle$  (now normalized by the gap) while  $U$  is lowered. We also find that the correlations relative to the gap decrease for higher gaps, which is a simple saturation effect (the highest possible correlations are  $\langle d_{\uparrow}^{\dagger} d_{\downarrow}^{\dagger} \rangle = 0.5$ ). Furthermore, our results match reasonably the NRG data from Ref. [8], the mismatch originating probably from the low value of the gap used in this calculation. We also recover the fact that for a given value of the hybridization, a higher gap reduces the proximity effect (see section 3.6.3).

Finally, we analyze how the correlations evolve outside particle hole symmetry. As mentioned above, one expects the correlations to decrease because the dot evolves from a superconducting atomic limit toward the usual atomic limit (i.e. from the states  $|\pm\rangle$  toward the states  $|0\rangle$  and  $|\uparrow\downarrow\rangle$ ). On the other hand, there will be a transition from the spin

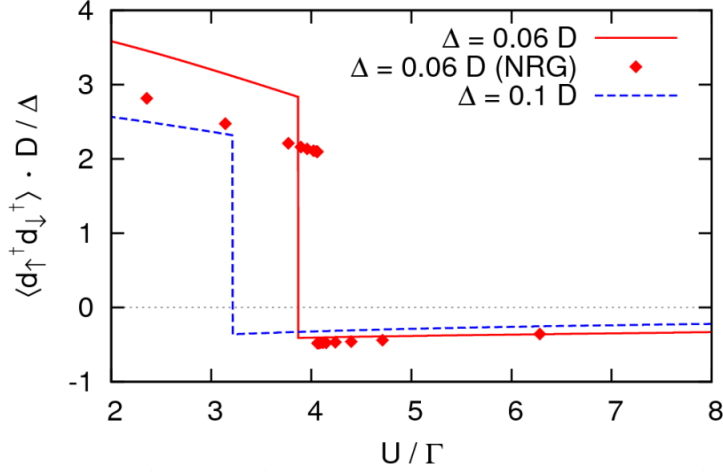


Figure 3.12: Superconducting correlations as a function of the Coulomb interaction  $U$  (for  $\pi\Gamma = 0.2 D$  and  $\xi_d = 0$ ). The diamonds correspond to NRG data from Ref. [8].

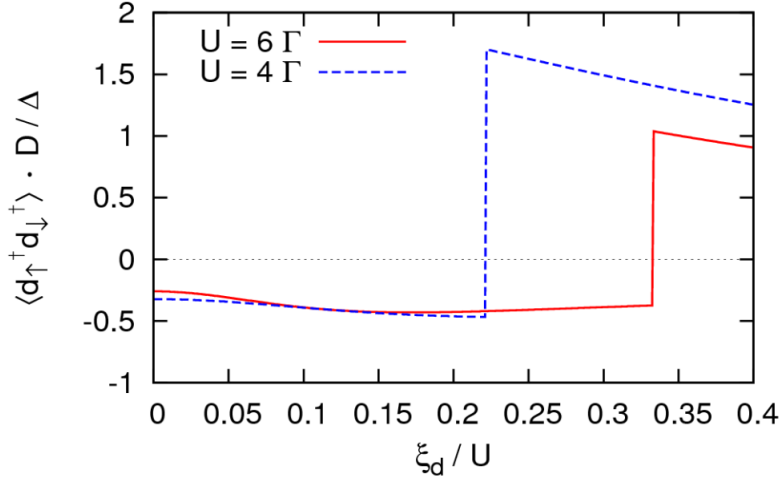


Figure 3.13: Superconducting correlations outside particle hole symmetry (for  $\pi\Gamma = 0.2 D$ ,  $U = 6 \Gamma$  and  $\Delta = 0.1 D$ ).

doublet to the singlet phase and therefore a mixing effect. Fig. 3.13 shows the competition between the mixing effect (that increases the correlations outside particle hole symmetry) and the evolution toward the normal atomic limit (that lowers the correlations) if  $\xi_d$  is increased. The effect of the Coulomb interaction is once more found to favor the single occupancy.

### 3.6.6 Josephson current

We now turn to the Josephson current through the quantum dot. The latter is given by  $J = 2edF/d\varphi$  (where  $F$  is the free energy). At zero temperature, the free energy is the same than the level energies, so that the Josephson current can readily be obtained once the renormalized energy levels have been calculated.

Nevertheless, our analytical approach only describes the effective local limit atomic states, and we can therefore only determine the current through the Andreev bound states. Yet, it is known that the Josephson current also contains a contribution of the

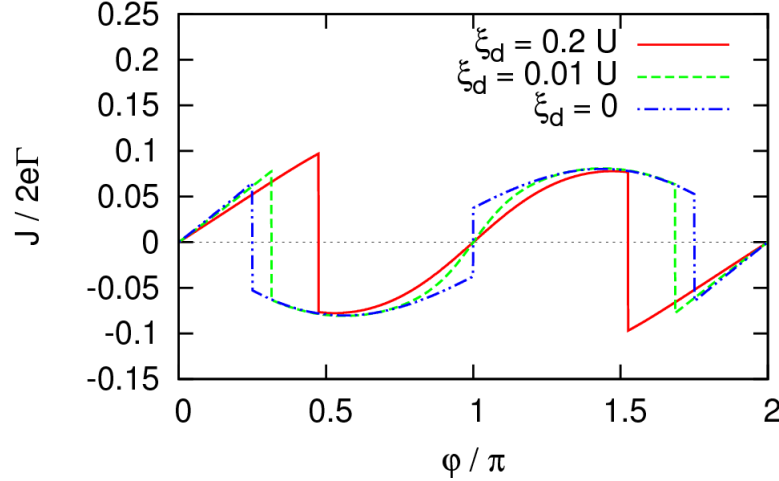


Figure 3.14: Josephson current through the bound states for  $U = 3\Gamma$ ,  $\Delta = 0.1D$ .

continuum of states (see for example Ref. [7] or section 2.2.3). The latter can be of the same order and opposite sign as the bound state contribution. Furthermore, Bauer et al. [8] have shown that the spectral weight of the bound states may vary importantly as a function of the different parameters (like the Coulomb interaction  $U$ ), especially in the spin doublet phase. As we exclusively investigate the effective local limit states, we do not keep track of this effect either. Therefore, the Josephson currents obtained in our approach will only provide a rather rough and qualitative idea of the actual total Josephson current.

Fig. 3.14 shows the Josephson current calculated as the phase derivative of the ground state energy  $E_{GS}$ ,  $J = dE_{GS}/d\varphi$ , for different values of  $\xi_d$ . One notices two regimes: If the phase is close to  $\varphi = 0$ , the system will be in the BCS-like state. As there is no magnetic moment in this phase, the ground state corresponds to a 0-junction. Thus the current is proportional to  $+\sin(\varphi)$ . If  $\varphi$  increases, the energy of the BCS-like state increases (as can be understood in the effective local limit, where  $E_- = U/2 - \sqrt{\xi_d^2 + \Gamma_\varphi^2}$ ). When the BCS-like state crosses with the spin doublet, the ground state changes and the dot becomes singly occupied. This magnetic moment leads to a discontinuous jump in the Josephson current and the formation of a  $\pi$ -junction. Again, we notice that the spin doublet is stabilized in the particle hole symmetric case.

### 3.7 A first glance at more complex systems

After having analyzed the effective local Hamiltonian for the single dot system, a double dot structure embedded between two superconducting leads shall be analyzed as a first glance to more complex systems. As depicted in figure 3.15, the second dot is assumed to be decoupled from the electrodes for simplicity (“T-geometry”).

The generalization of the single dot to the double dot system is fairly simple. The Hamiltonian now consists of two dot Hamiltonians  $H_{D_1}$  and  $H_{D_2}$ , the Coulomb interaction  $U_i$  ( $i=1,2$ ) on both of the dots,  $U_{12}$  between the dots, a spin-spin exchange interaction  $I\vec{S}_1 \cdot \vec{S}_2$  and an inter-dot tunneling  $H_{T_{12}}$ . Furthermore, the leads are tunnel coupled to the first dot just as in the single dot case, yielding the total Hamiltonian

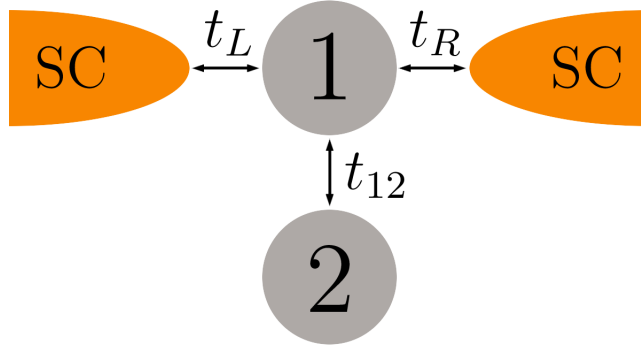


Figure 3.15: Double quantum dot coupled to superconducting leads (SC) via tunneling  $t_L$  and  $t_R$ . The inter-dot tunnel coupling is  $t_{12}$ .

$$H = H_L + H_R + H_{D_1} + H_{D_2} + H_{T_L} + H_{T_R} + H_{T_{12}} + U_{12}n_1n_2 + I\vec{S}_1 \cdot \vec{S}_2 . \quad (3.34)$$

The different Hamiltonians read

$$H_i = \sum_{\vec{k}, \sigma} \epsilon_{\vec{k}, i} c_{\vec{k}, \sigma, i}^\dagger c_{\vec{k}, \sigma, i} - \sum_{\vec{k}} \Delta_{\vec{k}, i} c_{\vec{k}, \uparrow, i}^\dagger c_{-\vec{k}, \downarrow, i}^\dagger - \sum_{\vec{k}} \Delta_{\vec{k}, i}^* c_{-\vec{k}, \downarrow, i} c_{\vec{k}, \uparrow, i} , \quad (3.35)$$

$$H_{T_i} = \sum_{\vec{k}, \sigma} (t_{\vec{k}, i} d_{\sigma, 1}^\dagger c_{\vec{k}, \sigma, i} + t_{\vec{k}, i}^* c_{\vec{k}, \sigma, i}^\dagger d_{\sigma, 1}) , \quad (3.36)$$

$$H_{T_{12}} = \sum_{\sigma} (t_{12} d_{\sigma, 1}^\dagger d_{\sigma, 2} + t_{12}^* d_{\sigma, 2}^\dagger d_{\sigma, 1}) , \quad (3.37)$$

$$\begin{aligned} H_{D_j} &= \sum_{\sigma} \epsilon_j n_{\sigma, j} + U_j n_{\uparrow, j} n_{\downarrow, j} \\ &= \sum_{\sigma} \tilde{\epsilon}_j n_{\sigma, j} + \frac{U_j}{2} (n_{\uparrow, j} + n_{\downarrow, j} - 1)^2 - \frac{U_j}{2} , \end{aligned} \quad (3.38)$$

with the spin  $\sigma$  populations  $n_{\sigma, j} = d_{\sigma, j}^\dagger d_{\sigma, j}$ . The energy  $\tilde{\epsilon}_j$  is given by  $\tilde{\epsilon}_j = \epsilon_j + \frac{U_j}{2}$ . The shift  $-\frac{U_j}{2}$  in  $H_{D_j}$  will be omitted. The conduction bands in the leads are again supposed to be flat and the tunnel matrix elements are taken to be  $t \in \mathbb{R}$ . Also,  $t$  and the gap  $\Delta$  are modeled as independent of both  $i$  and  $\vec{k}$ .

Especially interesting is the case of a local moment on the second dot, i.e. a singly occupied spin doublet. For that purpose,  $U_2$  is sent to infinity while keeping  $\tilde{\epsilon}_2$  finite. This assumption implies several simplification of the total Hamiltonian. First of all, the inter-dot Coulomb interaction  $U_{12}n_1n_2$  now becomes  $U_{12}n_1$  and can be incorporated into the first dot's energy level. Secondly, as the second dot is always singly occupied,  $H_{D_2}$  yields a constant shift of the total energy and can thus be omitted. Thirdly, tunneling processes between the two dots are suppressed by Coulomb blockade and virtual processes simply result in a positive (antiferromagnetic) shift of the spin-spin coupling  $I$ . Thus, the associated Hamiltonian  $H_{T_{12}}$  can be discarded. These remarks motivate the reduction of the Hamiltonian to

$$H_{eff} = H_L + H_R + H_{T_L} + H_{T_R} + \tilde{H}_D + I\vec{S}_1 \cdot \vec{S}_2 \quad (3.39)$$

where  $\tilde{H}_D = \sum_{\sigma} \xi_d n_{\sigma,1} + \frac{U_1}{2} (n_{\uparrow,j} + n_{\downarrow,j} - 1)^2$  and  $\xi_d = \epsilon_1 + \frac{U_1}{2} + U_{12}$ .

### 3.7.1 Effective local Hamiltonian

The effective Hamiltonian is derived just as in the single dot case. As the second dot's occupation is fixed to 1, the Hilbert space associated with this system is spanned by the basis  $\{|0_1\rangle, |\uparrow_1\rangle, |\downarrow_1\rangle, |\uparrow\downarrow_1\rangle\} \otimes \{|\uparrow_2\rangle, |\downarrow_2\rangle\}$  and has the dimension 8.

The associated eigenbasis is given by

$$\begin{array}{l}
 |1\rangle = |\uparrow_1\rangle \otimes |\uparrow_2\rangle \\
 |2\rangle = \frac{1}{\sqrt{2}} (|\uparrow_1\rangle \otimes |\downarrow_2\rangle + |\downarrow_1\rangle \otimes |\uparrow_2\rangle) \\
 |3\rangle = |\downarrow_1\rangle \otimes |\downarrow_2\rangle \\
 |4\rangle = \frac{1}{\sqrt{2}} (|\uparrow_1\rangle \otimes |\downarrow_2\rangle - |\downarrow_1\rangle \otimes |\uparrow_2\rangle) \\
 |5\rangle = (u|\uparrow\downarrow_1\rangle + v^*|0_1\rangle) \otimes |\uparrow_2\rangle \\
 |6\rangle = (-v^*|\uparrow\downarrow_1\rangle + u|0_1\rangle) \otimes |\uparrow_2\rangle \\
 |7\rangle = (u|\uparrow\downarrow_1\rangle + v^*|0_1\rangle) \otimes |\downarrow_2\rangle \\
 |8\rangle = (-v^*|\uparrow\downarrow_1\rangle + u|0_1\rangle) \otimes |\downarrow_2\rangle
 \end{array}
 \left. \begin{array}{l} \\ \\ \\ \\ \\ \\ \\ \\ \end{array} \right\} \begin{array}{l} \text{spin triplet} \\ \\ \text{spin singlet} \\ \\ \text{BCS-like states} \end{array}$$

with  $u = |u|e^{i\theta_u}$  and  $v = |v|e^{i\theta_v}$ ,  $|u|^2 = \frac{1}{2} \left( 1 + \frac{\xi_d}{\sqrt{\xi_d^2 + \Gamma_{\varphi}^2}} \right)$ ,  $|v|^2 = \frac{1}{2} \left( 1 - \frac{\xi_d}{\sqrt{\xi_d^2 + \Gamma_{\varphi}^2}} \right)$  (again,  $u$  and  $v$  are chosen to be  $\in \mathbb{R}$ ,  $\Gamma_{\varphi} = \Gamma \frac{2}{\pi} \arctan \left( \frac{D}{\Delta} \right) \cos \left( \frac{\varphi}{2} \right)$ ,  $D$  denotes half the electronic bandwidth in the leads and the matrix notation is  $|1\rangle = (1, 0, 0, 0, 0, 0, 0, 0)^T$  etc.). In this basis,  $H_{eff}$  is given by

$$H_{eff} = \begin{pmatrix} \frac{I}{4} + \xi_d & 0 & 0 & 0 & 0 & 0 & 0 & 0 \\ 0 & \frac{I}{4} + \xi_d & 0 & 0 & 0 & 0 & 0 & 0 \\ 0 & 0 & \frac{I}{4} + \xi_d & 0 & 0 & 0 & 0 & 0 \\ 0 & 0 & 0 & -\frac{3J}{4} + \xi_d & 0 & 0 & 0 & 0 \\ 0 & 0 & 0 & 0 & E_+ & 0 & 0 & 0 \\ 0 & 0 & 0 & 0 & 0 & E_- & 0 & 0 \\ 0 & 0 & 0 & 0 & 0 & 0 & E_+ & 0 \\ 0 & 0 & 0 & 0 & 0 & 0 & 0 & E_- \end{pmatrix} \quad (3.40)$$

where  $E_{\pm} = \pm \sqrt{\xi_d^2 + \Gamma_{\varphi}^2} + \xi_d + \frac{U_1}{2}$ . Like for the simple dot, the low energy BCS-like states  $|6\rangle$  and  $|8\rangle$  minimize their energy for  $\varphi = 0$ , thus corresponding to a 0-junction.

### 3.7.2 Phase diagram for the effective Hamiltonian

Having derived the effective Hamiltonian (3.40), phase diagrams can be drawn. Figure 3.16 shows several of them for the case of infinite bandwidth, i.e.  $D \rightarrow \infty$  (for the sake of simplicity). Three different phases are accessible: if the spin-spin interaction  $I$  is strong, the dot will either be in the triplet or singlet regime, according to whether the coupling is ferromagnetic or antiferromagnetic. If the spin-spin interaction is small and the Coulomb interaction is not too strong, the system will be in the degenerated BCS-like states  $|6\rangle$  and  $|8\rangle$ . Due to their higher energies, neither  $|5\rangle$  nor  $|7\rangle$  can become the ground state.

When the first dot's energy level is moved away from the particle-hole symmetry  $\xi_d = 0$ , the BCS-like phase is stabilized. This can be understood by analogies with the non-interacting and non-superconducting double dot: whereas the doubly occupied state

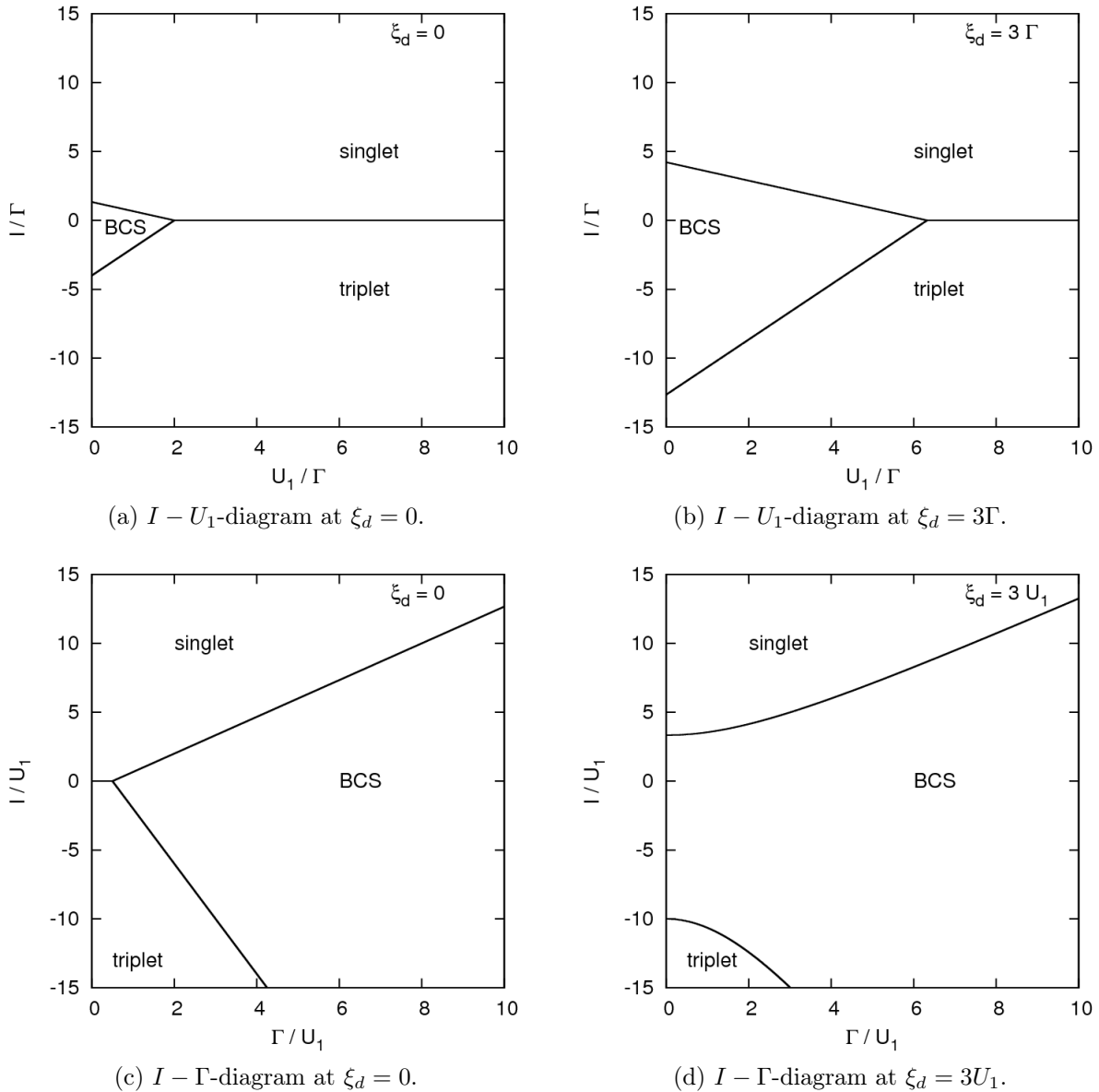


Figure 3.16: Phase diagrams of the double dot,  $n_2$  fixed at 1 and  $\varphi = 0$ .

will be the ground states if the level has a negative energy, the dot will be empty for positive energies. In any case, the singly occupied state is never the ground state. Thus, the BCS-like phase is stabilized if  $\xi_d \neq 0$ .

Increasing tunnel coupling also stabilizes the BCS-like state, which is quite natural as it is the latter that induces the superconductivity on the dot. Finally, a rising Coulomb interaction suppresses the BCS-like state, as the latter is a superposition of the empty and the doubly occupied state, thus being affected by the Coulomb interaction.

### 3.8 Summary

In this section we summarize the main results of this chapter. First, it has been shown how the Hamiltonian of a quantum dot coupled to superconducting leads can be mapped on an effective local model if the superconducting gap  $\Delta$  is much bigger than the characteristic

energy scales of the dot. This limit can quite generally be regarded as a low frequency expansion of the Green's function of the dot rather than the limit  $\Delta \rightarrow \infty$  used in the literature. This enabled us to extend the effective local Hamiltonian to leads with a finite electronic bandwidth.

We have then set up a perturbation theory around this effective local Hamiltonian and established self-consistent equations for the energy renormalizations of the Andreev bound states. We have derived those equations based on the fact that the latter correspond to transitions between different states of the effective local Hamiltonian.

In a subsequent section, we used our formalism to calculate physical quantities such as the Andreev bound state energies or superconducting correlations, and understood how these evolve as a function of gate voltage, hybridization, Coulomb interaction and superconducting gap amplitude. It has been shown that our simple approach agrees well with NRG data in a vast range of parameters, with the main limitation that the Kondo temperature is not described quantitatively near particle-hole symmetry. However, most experimentally interesting regimes should be described correctly by the simple equations we have derived.

Finally, the generalization of this approach to more complex molecular systems has shortly been envisioned analyzing the example of a double quantum dot.

The simplicity and portability constitute the main advantages of our approach, if one is interested in the Andreev bound states only, compared to extended numerical simulations. As the perturbative description is analytical and based on atomic-like levels, it should in principle be able to describe more complex systems like multiple quantum dots or molecules with several orbitals coupled to superconducting environments. Finally, extensions of our formalism to the computation of the tunneling current at realistic gap values in three-terminal geometries [43] relevant for STM experiments should certainly deserve further scrutiny.

# Chapter 4

## Perturbation theory in the Coulomb interaction

### 4.1 Introduction

In the last chapter, we have been interested in a perturbation expansion around a limit where the typical frequencies of the dot were much smaller than the gap, i.e.  $\omega_n \ll \Delta$ . By a simple self-consistency condition, the validity of this perturbation expansion could be pushed down to fairly small gaps, as was shown by comparison to NRG data.

Nevertheless, if one is interested in the physics for very small gaps  $\Delta$ , one must use a different approximation scheme. One possibility is to use a perturbation expansion around the non-interacting limit, as has already been done to some extent in the literature for superconductor-dot-superconductor systems (either with a second order perturbation expansion [68], eventually formulated self-consistently [16, 46], or using discretized models [69–71]).

In the non-interacting limit, exact solutions are easily found. This has been done in section 2.2; we shall therefore only shortly recall some essential results.

The total Hamiltonian  $H$  including the Coulomb interaction  $U$  is decomposed as  $H = H_0 + H_{pert}$  with

$$H_0 = \sum_{i=L,R} (H_i + H_{T_i}) + \sum_{\sigma} \epsilon_d n_{\sigma} \text{ and} \quad (4.1)$$

$$H_{pert} = U n_{\uparrow} n_{\downarrow}, \quad (4.2)$$

where  $H_i$  are the Hamiltonians of the leads, considered to be standard s-wave BCS Hamiltonians,  $H_{T_i}$  describes the tunnel coupling between the dot and the lead  $i$ ,  $\epsilon_d$  the energy level of the dot, and  $n_{\sigma} = d_{\sigma}^{\dagger} d_{\sigma}$  is the spin  $\sigma$  population operator of the dot (see section 2.1).

The imaginary time Green's function of the dot in Nambu matrix notation has been derived via the equation of motion and reads

$$\widehat{G}_{d,d}^0(i\omega_n) = \begin{pmatrix} i\omega_n - \epsilon_d + \frac{i\omega_n \Gamma_0(i\omega_n)}{\sqrt{\Delta^2 - (i\omega_n)^2}} & \frac{\Delta \Gamma_{\varphi}(i\omega_n)}{\sqrt{\Delta^2 - (i\omega_n)^2}} \\ \frac{\Delta \Gamma_{\varphi}(i\omega_n)}{\sqrt{\Delta^2 - (i\omega_n)^2}} & i\omega_n + \epsilon_d + \frac{i\omega_n \Gamma_0(i\omega_n)}{\sqrt{\Delta^2 - (i\omega_n)^2}} \end{pmatrix}^{-1}, \quad (4.3)$$

where  $\omega_n$  is a fermionic Matsubara frequency,  $\Delta$  the superconducting gap in the electrodes and

$$\Gamma_\varphi(i\omega_n) = \Gamma \frac{2}{\pi} \arctan \left( \frac{D}{\sqrt{\Delta^2 - (i\omega_n)^2}} \right) \cos \left( \frac{\varphi}{2} \right), \quad (4.4)$$

with half the bandwidth of the leads  $D$ , the superconducting phase difference  $\varphi$  between the leads and the hybridization  $\Gamma = 2\pi t^2 \rho_0$  ( $\rho_0 = 1/(2D)$ ) is the electronic density of states in the leads and  $t$  is the tunnel matrix element between leads and dot).

Unfortunately, the non-interacting limit is fairly unrealistic. In experiments with carbon nanotubes, the Coulomb interaction often turns out to be one of the biggest energy scales of the dot (if not the biggest [13, 50, 72]), which gives rise to the famous Coulomb blockade (see section 1.2). Similar observations have been made in small semiconductor quantum dots [2, 34]. In order to describe the physics correctly it is thus necessary to push the perturbation theory as far as possible. Especially, the first order will not be sufficient.

There should also be a regime where both the gap and the Coulomb interaction have intermediate values. In this case, both perturbation theories (in  $U$  and around the effective local limit) are supposed to yield quantitatively similar results; this would be an additional verification of the two perturbative approaches. On the other hand, there will certainly be regimes where only one of the two approaches is valid, and we will thus have two complementary calculation schemes at hand.

As an additional interest, the perturbation expansion in the Coulomb interaction is known to be a so-called conserving approximation, that has some very fundamental symmetry properties. Whereas the latter are well-known for the case of a quantum dot coupled to normal leads, their generalizations to the case of superconducting leads have so far not been analyzed to our knowledge. This will be done in the following chapter 5.

## 4.2 Perturbation expansion

### 4.2.1 First order

The perturbation theory is done for the full propagators  $G_{ij}(i\omega_n)$ , the  $(i, j)$  indicating the respective matrix element of the full Nambu Green's function  $\widehat{G}_{d,d}(i\omega_n)$  (see equation (4.3)). They are calculated by means of the Dyson equation. The latter expresses the full Green's function in terms of the bare Green's function  $\widehat{G}_{d,d}^0(i\omega_n)$ ,  $G_{ij}^0(i\omega_n)$  and the self-energy  $\widehat{\Sigma}(i\omega_n)$  as

$$\begin{aligned} \widehat{G}_{d,d}(i\omega_n) &= \widehat{G}_{d,d}^0(i\omega_n) + \widehat{G}_{d,d}^0(i\omega_n) \widehat{\Sigma}(i\omega_n) \widehat{G}_{d,d}(i\omega_n) \\ &= \widehat{G}_{d,d}^0(i\omega_n) + \widehat{G}_{d,d}^0(i\omega_n) \widehat{\Sigma}^{(1)}(i\omega_n) \widehat{G}_{d,d}^0(i\omega_n) + \mathcal{O}(U^2). \end{aligned} \quad (4.5)$$

The first order self-energy  $\widehat{\Sigma}^{(1)}(i\omega_n)$  is thus easily obtained by the first order perturbation expansion of the Green's function. A short calculation (see appendix I.1) yields

$$\Sigma_{11}^{(1)}(i\omega_n) = U \langle d_{\downarrow}^{\dagger} d_{\downarrow} \rangle_0 = -U G_{22}^0(\tau = 0^+) , \quad (4.6)$$

$$\Sigma_{12}^{(1)}(i\omega_n) = U \langle d_{\downarrow} d_{\uparrow} \rangle_0 = U G_{12}^0(\tau = 0) , \quad (4.7)$$

$$\Sigma_{21}^{(1)}(i\omega_n) = U \langle d_{\uparrow}^{\dagger} d_{\downarrow}^{\dagger} \rangle_0 = U G_{21}^0(\tau = 0) , \quad (4.8)$$

$$\Sigma_{22}^{(1)}(i\omega_n) = -U \langle d_{\uparrow}^{\dagger} d_{\uparrow} \rangle_0 = -U G_{11}^0(\tau = 0^-) \quad (4.9)$$

$(\Sigma_{ij}^{(1)}(i\omega_n))$  is the  $(i, j)$  matrix element of  $\widehat{\Sigma}^{(1)}(i\omega_n)$ .

The first order self-energies are thus nothing but the well known Hartree term and its anomalous equivalents, the superconducting correlations. We also want to point out that the  $(i, j)$  matrix element of  $\Sigma$  is the self-energy that enters the full Green's function  $G_{ji}$  (and *not*  $G_{ij}$ ). Denoting the bare Green's functions as

$$\begin{aligned} G_{11}^0 &= \text{---} \xrightarrow{\uparrow} \text{---} , & G_{12}^0 &= \text{---} \xleftarrow{\downarrow} \text{---} \xrightarrow{\uparrow} \text{---} , \\ G_{21}^0 &= \text{---} \xrightarrow{\uparrow} \text{---} \xleftarrow{\downarrow} \text{---} , & G_{22}^0 &= \text{---} \xleftarrow{\downarrow} \text{---} , \end{aligned}$$

the self-energies can diagrammatically be represented as

$$\begin{aligned} \Sigma_{11}^{(1)} &= - \text{---} \bullet \begin{array}{c} \downarrow \circlearrowleft \\ \vdots \\ \bullet \end{array} , & \Sigma_{12}^{(1)} &= \text{---} \bullet \begin{array}{c} \uparrow \circlearrowleft \\ \vdots \\ \bullet \end{array} \downarrow , \\ \Sigma_{21}^{(1)} &= \text{---} \bullet \begin{array}{c} \downarrow \circlearrowleft \\ \vdots \\ \bullet \end{array} \uparrow , & \Sigma_{22}^{(1)} &= - \text{---} \bullet \begin{array}{c} \uparrow \circlearrowleft \\ \vdots \\ \bullet \end{array} . \end{aligned}$$

### 4.2.2 Second order

The second order terms are much more tedious to calculate analytically than the first order ones. Luckily, the diagrammatic calculation technique offers a uniquely efficient way to evaluate the irreducible second order self-energies. Decomposing the Nambu Green's function and self-energy to the different orders in  $U$ ,

$$\widehat{G}_{d,d}(i\omega_n) = \widehat{G}_{d,d}^0(i\omega_n) + \widehat{G}_{d,d}^{(1)}(i\omega_n) + \widehat{G}_{d,d}^{(2)}(i\omega_n) + \dots \quad \text{and} \quad (4.10)$$

$$\widehat{\Sigma}(i\omega_n) = \widehat{\Sigma}^{(1)}(i\omega_n) + \widehat{\Sigma}^{(2)}(i\omega_n) + \dots , \quad (4.11)$$

the Dyson equation

$$\widehat{G}_{d,d}(i\omega_n) = \widehat{G}_{d,d}^0(i\omega_n) + \widehat{G}_{d,d}^0(i\omega_n) \widehat{\Sigma}(i\omega_n) \widehat{G}_{d,d}(i\omega_n) \quad (4.12)$$

implies

$$\widehat{G}_{d,d}^{(1)}(i\omega_n) = \widehat{G}_{d,d}^0(i\omega_n) \widehat{\Sigma}^{(1)}(i\omega_n) \widehat{G}_{d,d}^0(i\omega_n) \quad \text{and} \quad (4.13)$$

$$\widehat{G}_{d,d}^{(2)}(i\omega_n) = \underbrace{\widehat{G}_{d,d}^0(i\omega_n) \widehat{\Sigma}^{(1)}(i\omega_n) \widehat{G}_{d,d}^0(i\omega_n) \widehat{\Sigma}^{(1)}(i\omega_n) \widehat{G}_{d,d}^0(i\omega_n)}_{\text{reducible terms}} + \underbrace{\widehat{G}_{d,d}^0(i\omega_n) \widehat{\Sigma}^{(2)}(i\omega_n) \widehat{G}_{d,d}^0(i\omega_n)}_{\text{irreducible terms}}. \quad (4.14)$$

Because of the matrix character of the above equations, it is sufficient to calculate only one of the matrix elements of  $\widehat{G}_{d,d}^{(2)}(i\omega_n)$  in order to identify all second order irreducible self energy matrix elements  $\Sigma_{ij}^{(2)}(i\omega_n)$ . In their diagrammatic form, they read

$$\Sigma_{11}^{(2)} = \begin{array}{cccccccc} \begin{array}{c} \uparrow \\ \circlearrowleft \\ \bullet \\ \text{---} \\ \bullet \\ \circlearrowright \\ \downarrow \end{array} & \begin{array}{c} \uparrow \\ \circlearrowleft \\ \bullet \\ \text{---} \\ \bullet \\ \circlearrowright \\ \downarrow \end{array} & \begin{array}{c} \downarrow \\ \circlearrowleft \\ \bullet \\ \text{---} \\ \bullet \\ \circlearrowright \\ \uparrow \end{array} & \begin{array}{c} \downarrow \\ \circlearrowleft \\ \bullet \\ \text{---} \\ \bullet \\ \circlearrowright \\ \downarrow \end{array} & \begin{array}{c} \downarrow \\ \circlearrowleft \\ \bullet \\ \text{---} \\ \bullet \\ \circlearrowright \\ \uparrow \end{array} & \begin{array}{c} \downarrow \\ \circlearrowleft \\ \bullet \\ \text{---} \\ \bullet \\ \circlearrowright \\ \downarrow \end{array} & \begin{array}{c} \downarrow \\ \circlearrowleft \\ \bullet \\ \text{---} \\ \bullet \\ \circlearrowright \\ \uparrow \end{array} & \begin{array}{c} \downarrow \\ \circlearrowleft \\ \bullet \\ \text{---} \\ \bullet \\ \circlearrowright \\ \downarrow \end{array} \\ - & - & - & - & - & - & + & + \\ \end{array},$$

$$\Sigma_{12}^{(2)} = - \begin{array}{cccccccc} \begin{array}{c} \uparrow \\ \circlearrowleft \\ \bullet \\ \text{---} \\ \bullet \\ \circlearrowright \\ \downarrow \end{array} & \begin{array}{c} \uparrow \\ \circlearrowleft \\ \bullet \\ \text{---} \\ \bullet \\ \circlearrowright \\ \downarrow \end{array} & \begin{array}{c} \downarrow \\ \circlearrowleft \\ \bullet \\ \text{---} \\ \bullet \\ \circlearrowright \\ \uparrow \end{array} & \begin{array}{c} \downarrow \\ \circlearrowleft \\ \bullet \\ \text{---} \\ \bullet \\ \circlearrowright \\ \downarrow \end{array} & \begin{array}{c} \downarrow \\ \circlearrowleft \\ \bullet \\ \text{---} \\ \bullet \\ \circlearrowright \\ \uparrow \end{array} & \begin{array}{c} \downarrow \\ \circlearrowleft \\ \bullet \\ \text{---} \\ \bullet \\ \circlearrowright \\ \downarrow \end{array} & \begin{array}{c} \downarrow \\ \circlearrowleft \\ \bullet \\ \text{---} \\ \bullet \\ \circlearrowright \\ \uparrow \end{array} & \begin{array}{c} \downarrow \\ \circlearrowleft \\ \bullet \\ \text{---} \\ \bullet \\ \circlearrowright \\ \downarrow \end{array} \\ - & - & - & - & + & + & + & - \\ \end{array},$$

$$\Sigma_{21}^{(2)} = - \left[ \begin{array}{c} \downarrow \text{---} \text{---} \uparrow \\ \text{---} \text{---} \text{---} \text{---} \\ \uparrow \end{array} \right] - \left[ \begin{array}{c} \downarrow \text{---} \text{---} \\ \text{---} \text{---} \text{---} \text{---} \\ \uparrow \end{array} \right] - \left[ \begin{array}{c} \uparrow \text{---} \text{---} \\ \text{---} \text{---} \text{---} \text{---} \\ \downarrow \end{array} \right] + \left[ \begin{array}{c} \uparrow \text{---} \text{---} \downarrow \\ \text{---} \text{---} \text{---} \text{---} \\ \downarrow \end{array} \right] + \left[ \begin{array}{c} \downarrow \uparrow \\ \text{---} \text{---} \text{---} \text{---} \\ \uparrow \downarrow \end{array} \right] - \left[ \begin{array}{c} \downarrow \uparrow \\ \text{---} \text{---} \text{---} \text{---} \\ \uparrow \downarrow \end{array} \right],$$

$$\Sigma_{22}^{(2)} = \left[ \begin{array}{c} \downarrow \text{---} \text{---} \\ \text{---} \text{---} \text{---} \text{---} \\ \uparrow \end{array} \right] - \left[ \begin{array}{c} \downarrow \text{---} \text{---} \uparrow \\ \text{---} \text{---} \text{---} \text{---} \\ \uparrow \end{array} \right] - \left[ \begin{array}{c} \uparrow \text{---} \text{---} \downarrow \\ \text{---} \text{---} \text{---} \text{---} \\ \downarrow \end{array} \right] - \left[ \begin{array}{c} \uparrow \text{---} \text{---} \\ \text{---} \text{---} \text{---} \text{---} \\ \downarrow \end{array} \right] - \left[ \begin{array}{c} \uparrow \\ \text{---} \text{---} \text{---} \text{---} \\ \downarrow \end{array} \right] + \left[ \begin{array}{c} \uparrow \\ \text{---} \text{---} \text{---} \text{---} \\ \downarrow \end{array} \right].$$

### 4.2.3 Skeleton expansion

Quite generally, a perturbation expansion only to the second order may have difficulties to describe the physics of a given system correctly in a realistic regime of parameters. This is especially the case for the Coulomb interaction on a quantum dot considered here because the latter is often one of the biggest energy scales involved. It is therefore necessary to sum up the most important diagrams, desirably to infinite order. A fairly often used resummation technique are so-called skeleton diagrams, that resum all graphs with the same “external” structure.

The starting point is the observation that for every given diagram, the perturbation expansion also contains diagrams with all possible self-energy decorations on all internal lines. These diagrams can *uniquely* be classified by their external lines. Removing all internal self energy decorations of a given diagram, one is left with the corresponding skeleton diagram.

The skeleton of a diagram is thus obtained by cutting out all internal self energy insertions, i.e. replacing “partly dressed” propagators with bare ones wherever possible. Then, the bare propagators are replaced by full propagators. This way all diagrams with the same skeleton are summed up. Figure 4.1 illustrates the reduction of a diagram to its skeleton. As all internal self energy insertions have been removed, a skeleton diagram

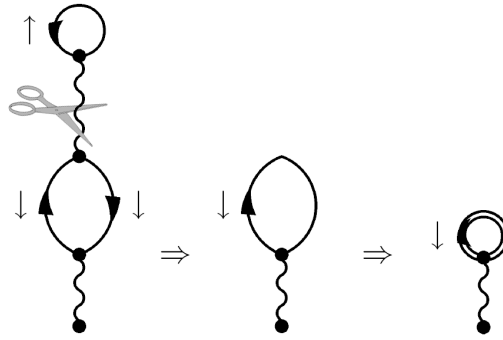


Figure 4.1: How to obtain a skeleton diagram: cut all internal self energy insertions and replace the remaining bare propagators by their fully dressed correspondents.

may also be classified as a diagram that can not be separated into two diagrams by cutting two lines.

To make a long story short, the skeleton diagram technique allows to partially resum diagrams to infinite order, thereby expressing the self energy as a function of the full propagator, that itself contains the self energy. One is thus left with a self-consistency problem.

For the perturbation series in powers of the Coulomb interaction, the skeleton expansion of the self energies up to the second order can easily be obtained starting from the diagrams in section 4.2.1 and 4.2.2. Applying the rules discussed above, one finds

$$\begin{aligned}
 \Sigma_{11} &= - \left[ \text{Diagram 1} \right] - \left[ \text{Diagram 2} \right] + \left[ \text{Diagram 3} \right], \\
 \Sigma_{12} &= \left[ \text{Diagram 4} \right] + \left[ \text{Diagram 5} \right] - \left[ \text{Diagram 6} \right], \\
 \Sigma_{21} &= \left[ \text{Diagram 7} \right] + \left[ \text{Diagram 8} \right] - \left[ \text{Diagram 9} \right],
 \end{aligned}$$

$$\Sigma_{22} = - \begin{array}{c} \uparrow \\ \text{---} \circ \text{---} \\ | \\ \bullet \end{array} - \begin{array}{c} \uparrow \\ \text{---} \circ \text{---} \\ | \\ \text{---} \uparrow \text{---} \\ | \\ \text{---} \downarrow \text{---} \\ | \\ \bullet \end{array} + \begin{array}{c} \uparrow \\ \text{---} \circ \text{---} \\ | \\ \text{---} \downarrow \text{---} \\ | \\ \text{---} \uparrow \text{---} \\ | \\ \text{---} \downarrow \text{---} \\ | \\ \bullet \end{array} .$$

Thereby, the full Green's functions are denoted by

$$\begin{aligned} G_{11} &= \begin{array}{c} \uparrow \\ \text{---} \text{---} \text{---} \\ | \\ \bullet \end{array} , & G_{12} &= \begin{array}{c} \downarrow \quad \uparrow \\ \text{---} \text{---} \text{---} \\ | \\ \bullet \end{array} , \\ G_{21} &= \begin{array}{c} \uparrow \quad \downarrow \\ \text{---} \text{---} \text{---} \\ | \\ \bullet \end{array} , & G_{22} &= \begin{array}{c} \downarrow \\ \text{---} \text{---} \text{---} \\ | \\ \bullet \end{array} . \end{aligned}$$

The above skeleton diagrams may also be transposed to analytic formulas. Doing so yields

$$\begin{aligned} \Sigma_{11}(i\omega_n) &= -U G_{22}(\tau = 0^+) - U^2 \int_0^\beta d\tau e^{i\omega_n \tau} G_{11}(\tau) G_{22}(\tau) G_{22}(-\tau) \\ &\quad + U^2 \int_0^\beta d\tau e^{i\omega_n \tau} G_{12}(\tau) G_{21}(\tau) G_{22}(-\tau) , \end{aligned} \quad (4.15)$$

$$\begin{aligned} \Sigma_{12}(i\omega_n) &= U G_{12}(\tau = 0) + U^2 \int_0^\beta d\tau e^{i\omega_n \tau} G_{11}(\tau) G_{22}(\tau) G_{12}(-\tau) \\ &\quad - U^2 \int_0^\beta d\tau e^{i\omega_n \tau} G_{21}(\tau) G_{12}(\tau) G_{12}(-\tau) , \end{aligned} \quad (4.16)$$

$$\begin{aligned} \Sigma_{21}(i\omega_n) &= U G_{21}(\tau = 0) + U^2 \int_0^\beta d\tau e^{i\omega_n \tau} G_{11}(\tau) G_{22}(\tau) G_{21}(-\tau) \\ &\quad - U^2 \int_0^\beta d\tau e^{i\omega_n \tau} G_{12}(\tau) G_{21}(\tau) G_{21}(-\tau) , \end{aligned} \quad (4.17)$$

$$\begin{aligned} \Sigma_{22}(i\omega_n) &= -U G_{11}(\tau = 0^-) - U^2 \int_0^\beta d\tau e^{i\omega_n \tau} G_{22}(\tau) G_{11}(\tau) G_{11}(-\tau) \\ &\quad + U^2 \int_0^\beta d\tau e^{i\omega_n \tau} G_{12}(\tau) G_{21}(\tau) G_{11}(-\tau) . \end{aligned} \quad (4.18)$$

The self-energies thus all have the generic form of a Hartree-type diagram and two so-called sunrise diagrams. In the limit  $\Delta \rightarrow 0$ , the first order terms reduce to the well-known spin-unpolarized Hartree-Fock terms. Due to the finite gap, additional diagrams involving anomalous propagators also contribute to the self-energies.

## 4.2.4 Particle hole symmetry

### Green's function

The particle hole symmetry corresponds to the case where the energy level of the quantum equals minus half the Coulomb interaction, i.e.  $\epsilon_d = -U/2$  or  $\xi_d = 0$ . Then, both the empty and doubly occupied state have zero energy, whereas the singly occupied states have a negative energy of  $-U/2$ . The ground state is thus the spin doublet. Transitions from this state toward either the empty state (addition of a hole) or the doubly occupied state (addition of an electron) are equally probable, thus the name of particle hole symmetry. Mathematically, the particle hole symmetry corresponds to the invariance of the Hamiltonian to an exchange of creation and annihilation operators according to

$$d_{\uparrow} \leftrightarrow d_{\downarrow}^{\dagger}, \quad (4.19)$$

$$d_{\uparrow}^{\dagger} \leftrightarrow d_{\downarrow} \quad (4.20)$$

Note that because of the BCS-terms in the Hamiltonian one has to exchange creation and annihilation operators of distinct spin species. Yet, none of the two spins is preferential. Therefore, the expectation value of the spin populations read

$$\langle d_{\uparrow}^{\dagger} d_{\uparrow} \rangle = \langle d_{\downarrow}^{\dagger} d_{\downarrow} \rangle = \frac{1}{2}. \quad (4.21)$$

In particular, this implies that the first order self-energies  $\Sigma_{11}^{(1)}$  and  $\Sigma_{22}^{(1)}$  are

$$\Sigma_{11}^{(1)} = \frac{U}{2} = -\epsilon_d \text{ and} \quad (4.22)$$

$$\Sigma_{22}^{(1)} = -\frac{U}{2} = \epsilon_d. \quad (4.23)$$

The value of the off-diagonal self-energies  $\Sigma_{12}^{(1)}$  and  $\Sigma_{21}^{(1)}$  can unfortunately not be derived from symmetry considerations. Nevertheless, equations (4.19) and (4.20) indicate that they are identical. For the remainder, we define

$$\Sigma_{12}^{(1)} = \Sigma_{21}^{(1)} = U \langle d_{\downarrow} d_{\uparrow} \rangle =: \Delta_{eff}. \quad (4.24)$$

With these considerations at hand, one can now turn to the derivation of the explicit analytic form of the skeleton expansion. As outlined in section 4.2.3, the latter is constructed only with full Green's functions.

As has been mentioned in the last section, the skeleton expansion expresses the self-energies as a function of the full propagators; one thus has to solve equations (4.15)-(4.18) self-consistently. Unfortunately, a fully self-consistent calculation scheme can lead to unphysical resummations. For instance, it is known from reference [73] that the Hubbard bands may be lost. One therefore has to work with Hartree shifted propagators, that correspond to the correct low frequency expansion of the self-energies. This technique yields in general better results.

The Hartree-Fock shifted propagators are defined by



(a) Typical neglected diagram

(b) Typical summed diagram

Figure 4.2: Examples for diagrams that are summed up (a) or not (b).

$$\widehat{\widetilde{G}}_{d,d}^{-1}(i\omega_n) := \widehat{G}_{d,d}^0{}^{-1}(i\omega_n) - \widehat{\Sigma}^{(1)}(i\omega_n) , \quad (4.25)$$

and correspond to the spin-unpolarized mean-field propagators. The absorption of these first order shift, that have been evaluated for the particle hole symmetric case, limits the validity of this perturbative approach to particle hole symmetry. Furthermore, as one is dealing with a perturbation theory around a weakly interacting limit, the perturbation expansion will only be reliable in the phase that is adiabatically connected to the noninteracting limit. In the case of superconducting leads, the latter is a BCS-like spin singlet stabilized by the proximity effect.

The “partly dressed” propagators are then used, instead of the actual full propagators, to compute the self-energy. The error due to this simplification is of the order  $\mathcal{O}(U^3)$ , which is anyway the error of the second order perturbation expansion considered here. In terms of diagrams, the use of these propagators in the skeleton expansion corresponds to the neglect of skeleton diagrams higher than third order and some diagrams contributing to the second order skeleton diagram. More precisely, this prescription neglects diagrams where a “sunrise” term (the one loop second order term) is inserted directly into another sunrise term, as indicated in figure 4.2 (a). Diagrams containing third (and higher) order skeleton diagrams are neglected as well. On the contrary, terms where two “sunrises” are separated by at least one Hartree term (i.e. first order loop) are summed up to infinite order, as shown in figure 4.2 (b).

The partly dressed Green’s function  $\widehat{\widetilde{G}}_{d,d}$  explicitly reads

$$\widehat{\widetilde{G}}_{d,d}^{-1}(i\omega_n) = \begin{pmatrix} i\omega_n + \frac{i\omega_n\Gamma_0(i\omega_n)}{\sqrt{\Delta^2-(i\omega_n)^2}} & \frac{\Delta\Gamma_\varphi(i\omega_n)}{\sqrt{\Delta^2-(i\omega_n)^2}} - \Delta_{eff} \\ \frac{\Delta\Gamma_\varphi(i\omega_n)}{\sqrt{\Delta^2-(i\omega_n)^2}} - \Delta_{eff} & i\omega_n + \frac{i\omega_n\Gamma_0(i\omega_n)}{\sqrt{\Delta^2-(i\omega_n)^2}} \end{pmatrix} := \begin{pmatrix} g_0^{-1} & f_0^{-1} \\ f_0^{-1} & g_0^{-1} \end{pmatrix} . \quad (4.26)$$

In the particle hole symmetric case, the two normal Green’s functions are thus identical, and so are the anomalous ones. Hence, we define

$$\widetilde{G}_{11} = \widetilde{G}_{22} = \frac{1}{2} \left( \frac{1}{g_0^{-1} + f_0^{-1}} + \frac{1}{g_0^{-1} - f_0^{-1}} \right) =: \mathcal{G} , \quad (4.27)$$

$$\widetilde{G}_{12} = \widetilde{G}_{21} = \frac{1}{2} \left( \frac{1}{g_0^{-1} + f_0^{-1}} - \frac{1}{g_0^{-1} - f_0^{-1}} \right) =: \mathcal{F} . \quad (4.28)$$

Due to the symmetric form of the Nambu matrix Green's function  $\widehat{G}_{d,d}$ , the self-energy derived with the skeleton expansion is also symmetrical,

$$\widehat{\Sigma} = \begin{pmatrix} \Sigma_{\mathcal{G}} & \Sigma_{\mathcal{F}} \\ \Sigma_{\mathcal{F}} & \Sigma_{\mathcal{G}} \end{pmatrix}, \quad (4.29)$$

and thus is the full Green's function  $\widehat{G}_{d,d}$  defined by

$$\widehat{G}_{d,d}^{-1}(i\omega_n) = \widehat{G}_{d,d}^{-1}(i\omega_n) - \widehat{\Sigma}(i\omega_n). \quad (4.30)$$

The matrix elements of the latter read

$$G_{11} = G_{22} = \frac{1}{2} \left( \frac{1}{g_0^{-1} - \Sigma_{\mathcal{G}} + f_0^{-1} - \Sigma_{\mathcal{F}}} + \frac{1}{g_0^{-1} - \Sigma_{\mathcal{G}} - f_0^{-1} + \Sigma_{\mathcal{F}}} \right), \quad (4.31)$$

$$G_{12} = G_{21} = \frac{1}{2} \left( \frac{1}{g_0^{-1} - \Sigma_{\mathcal{G}} + f_0^{-1} - \Sigma_{\mathcal{F}}} - \frac{1}{g_0^{-1} - \Sigma_{\mathcal{G}} - f_0^{-1} + \Sigma_{\mathcal{F}}} \right). \quad (4.32)$$

### Self-consistency

Within the (approximated) skeleton resummation scheme, the first order energy corrections have been absorbed into “partly dressed” Green's functions. Thus, only the second order self-energy corrections need to be calculated. This must be done in such a manner that the superconducting correlations are described self-consistently, i.e. such that the equation

$$\Delta_{eff} = U \langle d_{\downarrow} d_{\uparrow} \rangle \stackrel{!}{=} -\frac{U}{\pi} \text{Im} \left\{ \int_{-\infty}^{\infty} d\omega G_{12}^R(\omega) \right\} \quad (4.33)$$

is satisfied ( $G_{12}^R(\omega)$  denotes the fully dressed retarded real time anomalous Green's function). This boundary condition is most efficiently evaluated numerically.

### 4.2.5 Explicit calculation of the skeleton self energy

The next step in the calculation of the dressed Green's functions is the derivation of explicit formulas for the evaluation of  $\Sigma_{\mathcal{G}}^R(\omega)$  and  $\Sigma_{\mathcal{F}}^R(\omega)$ , the retarded real time self energies. For the particle hole symmetric case, the results of section 4.2.3 become

$$\Sigma_{\mathcal{G}}(i\omega_n) = -U^2 \int_0^{\beta} d\tau e^{i\omega_n \tau} \mathcal{G}(\tau) \mathcal{G}(\tau) \mathcal{G}(-\tau) + U^2 \int_0^{\beta} d\tau e^{i\omega_n \tau} \mathcal{F}(\tau) \mathcal{F}(\tau) \mathcal{G}(-\tau), \quad (4.34)$$

$$\Sigma_{\mathcal{F}}(i\omega_n) = U^2 \int_0^{\beta} d\tau e^{i\omega_n \tau} \mathcal{G}(\tau) \mathcal{G}(\tau) \mathcal{F}(-\tau) - U^2 \int_0^{\beta} d\tau e^{i\omega_n \tau} \mathcal{F}(\tau) \mathcal{F}(\tau) \mathcal{F}(-\tau). \quad (4.35)$$

These expressions now need to be transposed into the real time formalism. In order to simplify the following discussions as much as possible, we will consider a generalized

self-energy form

$$\Sigma_{123} = -U^2 \int_0^\beta d\tau e^{i\omega_n\tau} \mathcal{G}_1(\tau) \mathcal{G}_2(\tau) \mathcal{G}_3(-\tau) .$$

The analytic continuation is greatly simplified by the Kramers-Kronig identity that expresses the Matsubara frequency Green's function in terms of the imaginary part of the real time Green's function,

$$\mathcal{G}(i\omega_n) = -\frac{1}{\pi} \int_{-\infty}^{\infty} d\mathcal{E} \frac{\text{Im} \{ \mathcal{G}^R(\mathcal{E}) \}}{i\omega_n - \mathcal{E}} . \quad (4.36)$$

Using this formula, one is left with sums over Matsubara frequencies of some explicit, analytic functions. These sums can then be rewritten as integrals in the complex plane using the fact that the fermionic Matsubara frequencies are the poles of the analytically continued Fermi-Dirac distribution  $n_F(z)$ . Explicit calculations may be found in appendix I.2.1. At the end of the day, one ends up with a fairly simple expression that reads

$$\begin{aligned} \Sigma_{123}^{R''}(\omega) &= \frac{U^2}{\pi^2} \int_{-\infty}^{\infty} d\epsilon_1 \int_{-\infty}^{\infty} d\epsilon_2 \int_{-\infty}^{\infty} d\epsilon_3 \\ &\times \mathcal{G}_1^{R''}(\epsilon_1) \mathcal{G}_2^{R''}(\epsilon_2) \mathcal{G}_3^{R''}(-\epsilon_3) \delta(\omega - \epsilon_1 - \epsilon_2 - \epsilon_3) \\ &\times [n_F(\epsilon_1)n_F(\epsilon_2)n_F(\epsilon_3) + n_F(-\epsilon_1)n_F(-\epsilon_2)n_F(-\epsilon_3)] . \end{aligned} \quad (4.37)$$

Thereby, double apostrophes indicate imaginary parts, i.e.  $\text{Im} \{ \mathcal{G} \} =: \mathcal{G}''$ . Real part will from now on be indicated by simple apostrophes, i.e.  $\text{Re} \{ \mathcal{G} \} =: \mathcal{G}'$ . For Green's functions and self-energies, the latter can generally be obtained from the imaginary parts by the Kramers-Kronig relation

$$\Sigma_{123}^{R'}(\omega) = -\mathcal{P} \frac{1}{\pi} \int_{-\infty}^{\infty} d\mathcal{E} \frac{\Sigma_{123}^{R''}(\mathcal{E})}{\omega - \mathcal{E}} .$$

The results of this section, and especially equation (4.37), concords with other work [46, 68].

### Specifics for superconducting leads

In the present case, i.e. a quantum dot coupled to superconducting leads, the density of states of the dot is characterized by a gap between  $-\Delta$  and  $\Delta$ , where  $\Delta$  is the gap of the electrodes. Inside this gap, the discrete Andreev bound states are formed.

Due to their singular character, one needs to calculate the bound state contributions to the self-energies carefully. The evaluation of equation (4.37) is correspondingly somewhat tedious. We shall therefore here only motivate the results physically, but explicit calculations can be found in appendix I.2.2.

What are the different contributions to the self-energies? First, one should keep in mind that all contributions to the self-energies (4.34) and (4.35) have the form of a sunrise term (see equation (4.37) for the generic formula). The corresponding Feynman graph is

$$\Sigma_{\text{sunrise}} = \text{Diagram} .$$

Each contributing process thus involves three electrons (or holes). As there are only two Andreev bound states in the phase connected adiabatically to the limit  $U = 0$ , one of these electrons (or holes) necessarily needs to propagate in the electrodes and therefore has an energy higher than the gap  $\Delta$ . The two other electrons (or holes) may either be in an Andreev bound state or in the electrodes. We can therefore identify three kinds of processes:

- Processes with two electrons in ABS and one electron in the leads  
 $\Rightarrow$  energy higher than  $\Delta + 2 \times \text{ABS energy}$
- Processes with one electrons in ABS and two electrons in the leads  
 $\Rightarrow$  energy higher than  $2 \times \Delta + 1 \times \text{ABS energy}$
- Processes with all three electrons in the leads  $\Rightarrow$  energy higher than  $3 \times \Delta$

This means especially that there are no processes with energies lower than  $\Delta + 2 \times \text{ABS energy}$  (at least in the phase adiabatically connected to the non-interacting limit). Therefore, the imaginary part of the self-energies (being proportional to the density of states induced by the considered processes) also shows a gap between  $\pm (\Delta + 2 \times \text{ABS energy})$ . Furthermore, the imaginary part of the self-energies has no Andreev bound state like singularities inside the gap.

With the above considerations and the calculations in appendix I.2.2, it is straightforward to obtain the full Green's functions. The only minor obstacle is the self-consistent determination of the self consistent parameter according to equation (4.33). This can easily be achieved by a simple iterative calculation scheme, that actually converges without difficulties.

## 4.3 Results

### 4.3.1 Density of states and Green's functions

At last, we shall give some results derived with the self-consistent perturbation theory presented in the last sections. We shall first turn to the density of states. We shortly recall that the perturbation theory is set up around the spin singlet state. Therefore, it is only valid in the singlet phase. If the gap  $\Delta$  is big, this singlet is a BCS-like state (see chapter 3). If the gap is small, the proximity effect becomes less important, and a simple BCS-like state will be suppressed by the Coulomb interaction. Instead, the system can form a Kondo-like singlet.

It is well-known that the Kondo effect can not be described by a simple perturbation theory as the one we are dealing with here. Therefore, the Kondo-like state is *not* a real Kondo singlet. Also, the transition to this state, that would appear for  $\Delta \approx k_B T_K$  for a Kondo singlet (and thus be an exponentially decreasing with increasing Coulomb interaction according to  $T_K \sim \exp(-\pi U/(8\Gamma))$ ) will rather scale as  $U^{-2}$  at large  $U$  for the second order expansion considered here. Finally, we want to stress that the singlet-doublet transition (whether it is a BCS-like or a Kondo-like singlet) results in a crossing of the Andreev bound states and the Fermi level (see section 3.6.1).

One expects two fundamentally different regimes. If the gap  $\Delta$  is much smaller than the other energy scales, the dot should behave similarly to the case of coupling to normal

leads. Of course, the density of states will be cut at  $\pm\Delta$  and discrete sub-gap peaks, the Andreev bound states, will appear. Nevertheless, the latter will have a very small spectral weight. By analogies with the non-superconducting case, one would rather expect that there will be a shift of spectral weight from the central, Fermi-liquid excitations peak toward two so-called Hubbard bands at  $\pm U/2$ . These generally large resonances correspond to the transitions between single occupation and a doubly occupied or empty dot, i.e. energy differences of  $U/2$  at particle hole symmetry.

Figure 4.3 indeed shows that if the gap is small, the density of states is very similar to the non-superconducting case (shown by a blue dashed line in the plots). Especially, the formation of Hubbard bands around  $\pm U/2$  is clearly observed. Furthermore, one finds that the Andreev bound states have an almost negligible spectral weight (see zooms into the gap). Finally, we find that the stronger the Coulomb interaction, the closer the ABS move to the Fermi level, which is nothing but the precursor of the transition from the Kondo-like singlet to the spin doublet.

If the gap becomes of the same order or bigger than the Coulomb interaction, the density of states changes remarkably. In this case, the Hubbard bands, located at  $U/2$ , would be inside the gap - which obviously is not possible.

The physics behind this can be understood with what has been outlined in section 4.2.5. As the superconducting gap  $\Delta$  becomes the most important energy scale, the virtual transitions renormalizing the density of states will now predominantly depend on the energy of the Andreev bound states and the gap  $\Delta$ . Especially, these virtual processes (and thus the self-energies) will have energies higher than  $\Delta + 2 \times$  energy of ABS. This can be seen in figure 4.4, that shows the normal and anomalous self energy (note that for  $U = 3\Gamma$ ,  $\Delta = 2\Gamma$ , the bound states are located at  $\omega \approx \pm 0.035\Gamma$ , see Fig. 4.4 (b)). Furthermore, one would expect the Andreev bound states to have a big spectral weight, which is indeed what is shown in figure 4.5. As a final remark, the Coulomb interaction can be seen to reduce the spectral weight of the Andreev bound states (as it opposes a Cooper-pair like wavefunction). For strong Coulomb interactions the dot again approaches the transition toward the spin 1/2 doublet, and the bound states are located close to the Fermi level.

### 4.3.2 Andreev bound state energies and phase diagram

We have already seen in figures 4.3 and 4.4 that a phase transition between a Kondo-like singlet state and the spin 1/2 doublet occurs if the Coulomb interaction is strong. Figure 4.6 shows the transition line between these two phases (compare to figure 3.5). The perturbation theory in  $U$  matches qualitatively both the effective local Hamiltonian approach as well as the NRG data by Bauer et al. [8] The transition line derived by the perturbation theory in  $U$  decays slower than the two other curves, which is the signature of the above mentioned  $U^{-2}$ -dependence of the quasiparticle weight at large  $U$ . Nevertheless, as the plot only shows a regime of intermediate Coulomb interaction, this dependence is not fully established yet.

As a second check, we now turn to the energy corrections outside the transition line. Figure 4.7 shows the renormalized energies for variable gap and two different values of the hybridization. All three methods, namely the perturbation theory in the Coulomb interaction, the effective local Hamiltonian and the NRG data by Yoshioka and Ohashi [23] show again the same qualitative features. The bound state first renormalizes to-

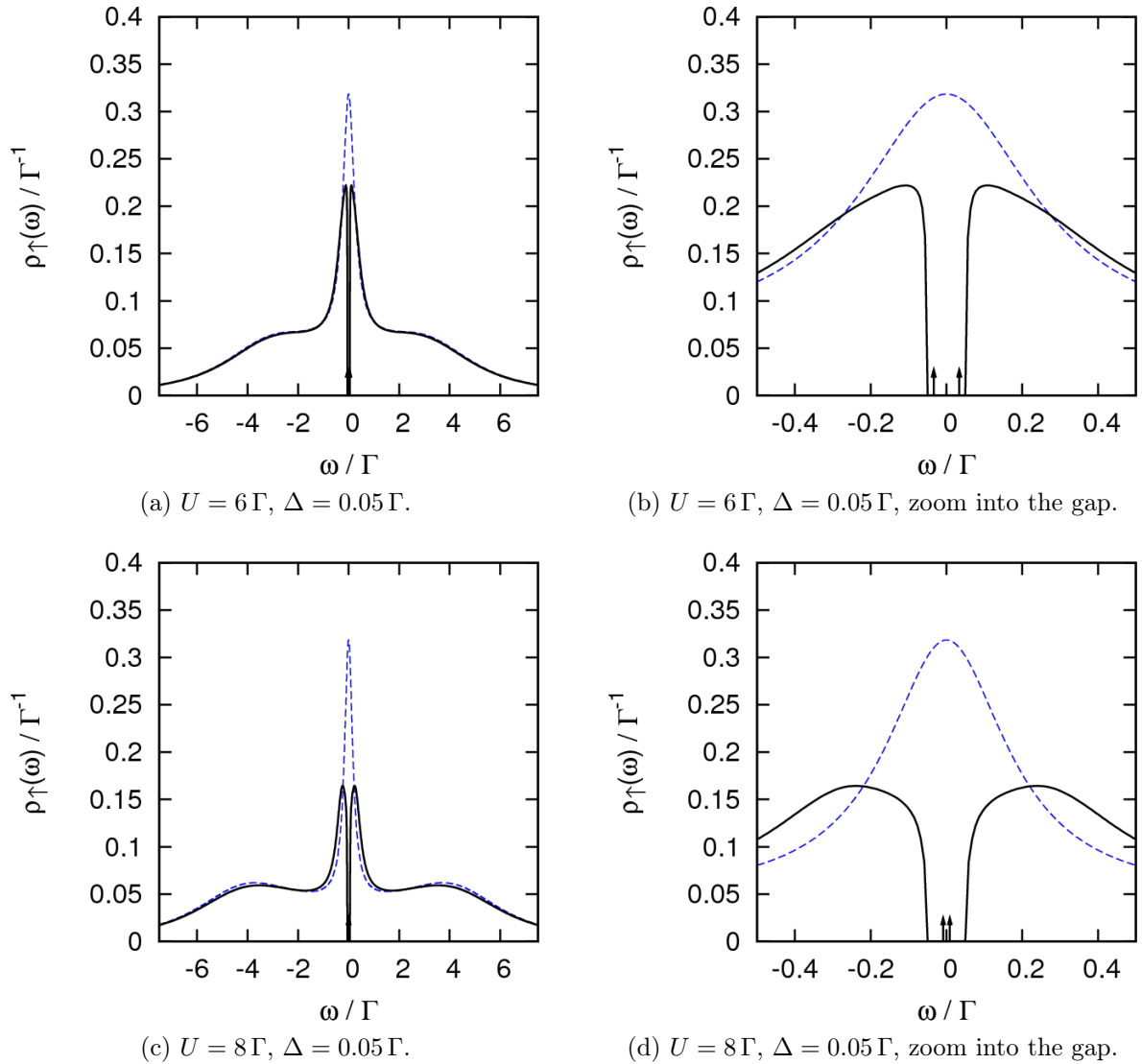


Figure 4.3: Spin up density of states  $\rho_{\uparrow}(\omega)$  for large Coulomb interactions  $U$  and small gaps  $\Delta$  (solid black curves). The bandwidth is given by  $D = 1000\Gamma$ . The corresponding density of states for a quantum dot coupled to normal electrodes (but with all other parameters identical) is indicated by the blue dashed curves. Andreev bound states are depicted by arrows (but have very small spectral weight).

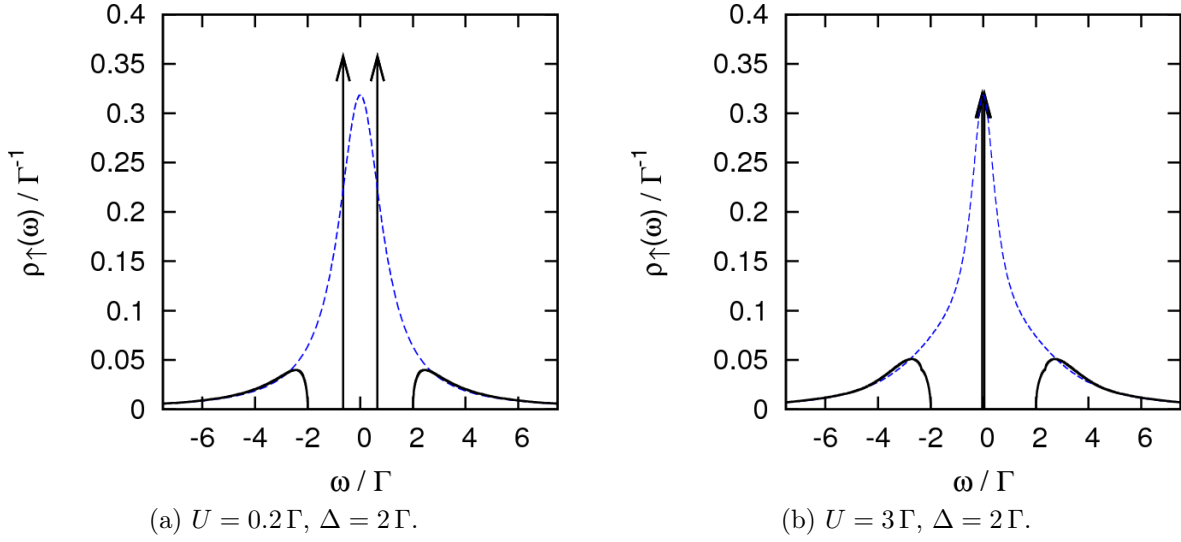


Figure 4.4: Spin up density of states  $\rho_{\uparrow}(\omega)$  for small Coulomb interactions  $U$  and large gaps  $\Delta$  (solid black curves). The bandwidth is given by  $D = 1000\Gamma$ . The corresponding density of states for a quantum dot coupled to normal electrodes (but with all other parameters identical) is indicated by the blue dashed curves. Andreev bound states are depicted by arrows.

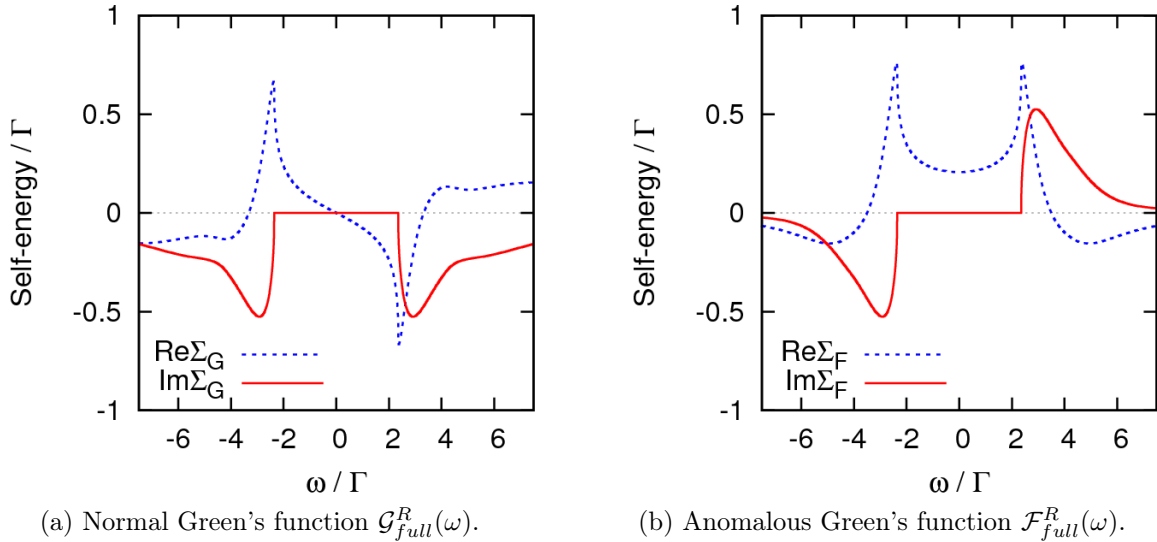


Figure 4.5: Normal self-energy  $\Sigma_G^R(\omega)$  and anomalous self-energy  $\Sigma_F^R(\omega)$  of the dot for a gap of  $\Delta = 2\Gamma$ , Coulomb interaction  $U = 3\Gamma$  and a bandwidth of  $D = 1000\Gamma$ .

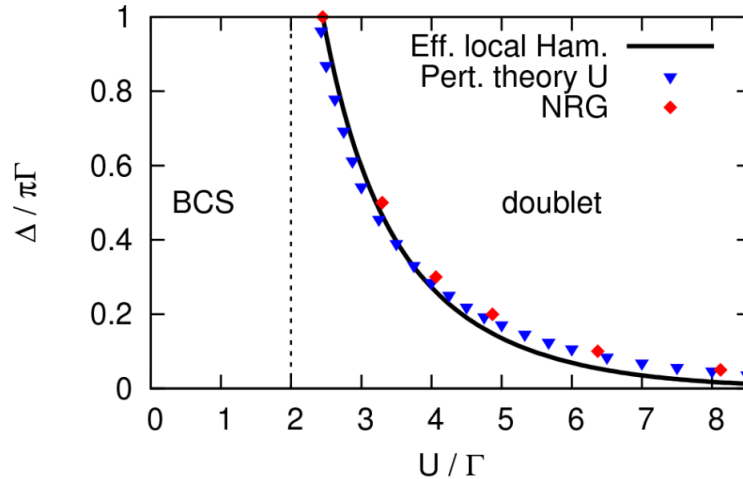


Figure 4.6: Transition line between the singlet and doublet phase for  $\pi\Gamma = 0.2D$  and  $\varphi = 0$ . The black solid line indicates the transition line calculated by the effective local Hamiltonian approach. The red diamonds show NRG data by Bauer et al. [8] The blue triangles are the result of the perturbation theory in the Coulomb interaction.

ward lower energies. If the gap becomes very small, the bound state energy remains “pinned” to  $-\Delta$  because the bound state is not allowed to leave the gap. Furthermore, an increasing hybridization results in a stronger proximity effect, i.e. more pronounced renormalizations.

The plot reveals that the two perturbative methods actually complete each other. In the large gap regime, i.e. in the spin doublet phase, the effective local Hamiltonian approach yields excellent results (as has been discussed in chapter 3). The perturbation theory in  $U$  on the other hand is only controlled and valid in the singlet phase, i.e. for negative bound state energies. If the gap is not too small, we find a regime where both analytic approaches basically yield the same results. For very small gaps, the effective local Hamiltonian approach loses its validity, whereas the perturbation theory in the Coulomb interaction matches perfectly the NRG data (unless the Coulomb interaction becomes very big).

### 4.3.3 Superconducting correlations

At last, we want to investigate the superconducting correlations. Again, we compare the perturbation theory in  $U$  to the effective local Hamiltonian approach to the NRG data by Bauer et al. [8]. Figure 4.8 affirms that the perturbation theory in  $U$  works very well in the singlet phase. It is thus truly complementary to the effective local Hamiltonian approach: The latter fits the NRG data especially in the spin doublet phase (see also section 3.6.5), that is not at all described by the perturbation theory in  $U$ .

## 4.4 Summary

Before turning to the Luttinger-Ward functional for a quantum dot coupled to superconducting leads, we want to summarize shortly the main findings of this chapter. First, we want to point out that the perturbation expansion around the non-interacting limit

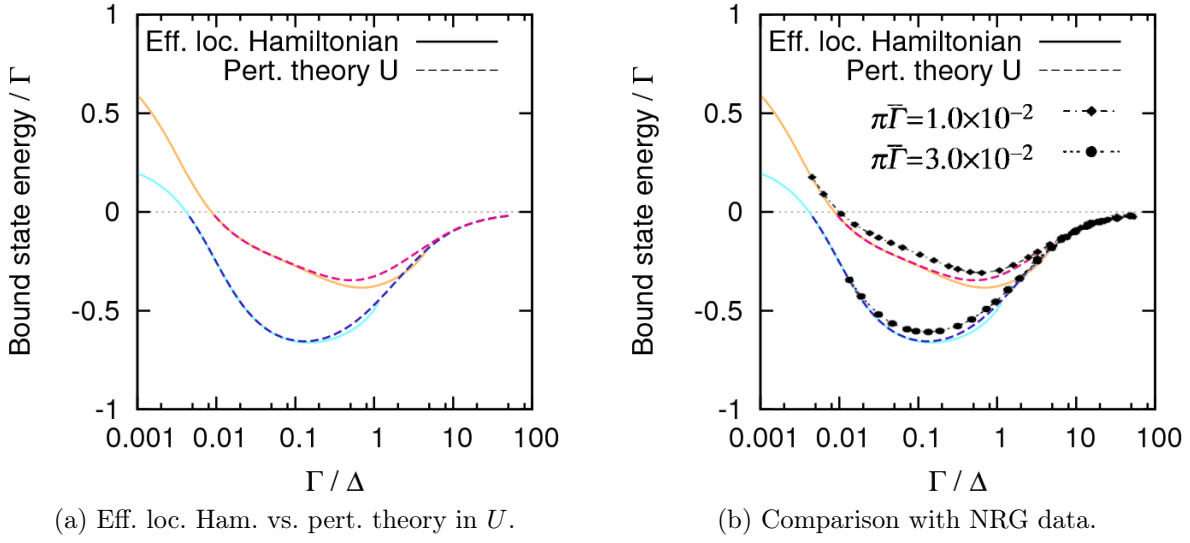


Figure 4.7: Renormalization of the low energy Andreev bound state. The orange solid and the violet dashed line correspond to  $\pi\Gamma = 2U$ , the light and dark blue curves to  $\pi\Gamma = 6U$ . In all cases, the bandwidth  $D$  is  $D = 200U$ . Subfigure (b) shows a comparison to NRG data from reference [23],  $\bar{\Gamma} = \Gamma/D$ .

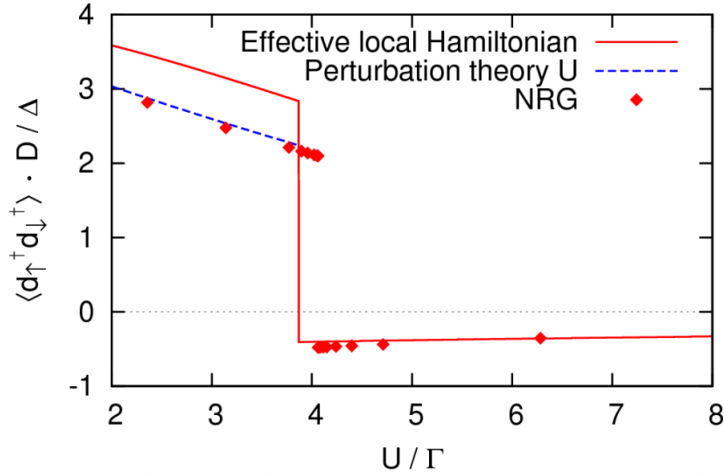


Figure 4.8: Superconducting correlations as a function of the Coulomb interaction  $U$  (for  $\pi\Gamma = 0.2D$ ,  $\Delta = 0.06D$  and  $\xi_d = 0$ ). The symbols correspond to NRG data from Ref. [8]. The red solid line is the result of the self-consistent approach discussed in section 3, the blue dashed line is the result of the perturbation theory in the Coulomb interaction.

considered here has already been established by Vecino, Martín-Rodero and Levy Yeyati [46]. Nevertheless, their paper mainly focuses on limiting situations, as for instance a zero bandwidth limit, the limit  $\Delta \gg \Gamma$  or  $\Delta \ll \Gamma$ . On the other hand, a paper by Dell'Anna and collaborators [16] deals with the Josephson current through a Josephson quantum dot. Although they also used a perturbation expansion in the Coulomb interaction to the second order, only the first order terms have been treated self-consistently.

We compared the results of the perturbation theory in  $U$  for intermediate regimes to both NRG calculations and the renormalized effective local Hamiltonian approach developed in chapter 3. We have shown that as long as the gap is not too small, and as long as the dot is in the phase adiabatically connected to the limit  $U = 0$ , all three approaches yield similar results. Furthermore, we have pointed out that the perturbation expansion in powers of the Coulomb interaction and the effective local Hamiltonian approach are actually complementary. The effective local Hamiltonian describes the physics in the spin doublet phase accurately, but fails for very small gaps. On the other hand, the perturbation expansion in  $U$  can not describe the spin doublet phase, because the latter is not adiabatically connected to the non-interacting limit. It does work well, on the contrary, in the small gap regime.

# Chapter 5

## Luttinger-Ward functional and Friedel sum rule

### 5.1 Luttinger-Ward functional

#### 5.1.1 Introduction

As stated in section 4.2.3, the skeleton expansion allows to sum up an infinity of diagrams. While one would naively expect such a resummation to improve the convergence and exactness of the perturbation theory, this is only true if the summed diagrams are chosen carefully.

As a simple example, consider a case where some diagrams increase the energy of a given state and a second set lowers its energy. If one would sum up e.g. only the first set of diagrams, the energy level might be overestimated dramatically. To make a long story short it is thus important to carefully select the diagrams one sums up.

The choice of physically important diagrams is generally guided by intuition. Yet, one would always like to end up with an approximation that respects the conservation laws of the system like energy or momentum conservation. A simple criterion to check whether an approximation is “conserving” or not has been provided by Baym and Kadanoff [74, 75]. They showed that conservation laws are respected if the resulting self energy  $\Sigma$ , considered as a functional of the full Green’s functions  $G$ , can itself be written as a derivative of a functional  $\Phi$ ,

$$\Sigma[G] = \frac{\delta\Phi}{\delta G} . \quad (5.1)$$

As will become clear later on, the functional  $\Phi$  is nothing but the self-energy diagrams, closed by a full propagator  $G$ .

In an earlier paper, Luttinger and Ward had already analyzed how symmetries of this functional  $\Phi$  relate to equations the self energy must fulfill [76]. Therefore,  $\Phi$  is also called the Luttinger-Ward functional. Ever since, symmetries of Luttinger-Ward functionals have been exploited in order to derive rather fundamental properties of (conserving) perturbation series, as for instance the Friedel sum rule [77, 78]. The latter quite generally relates the total charge displaced by an impurity to the scattering of electrons at the Fermi level by that impurity, stating that the number of displaced electrons  $n_d$  relates to the sum of all scattering phase shifts  $\delta_l$  of the partial waves  $l$  as

$$n_d = \frac{2}{\pi} \sum_l (2l + 1) \delta_l . \quad (5.2)$$

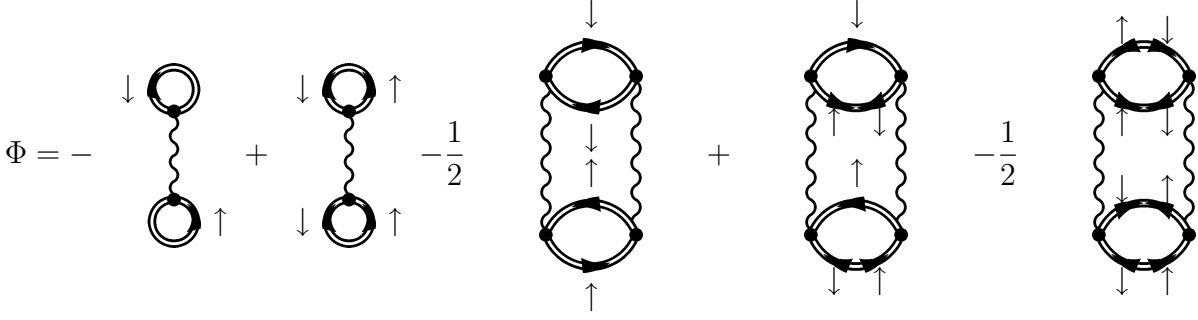
Because the phase shifts  $\delta_l$  also relate to the extra states induced by the impurity, the Friedel sum rule indicates that the number of extra states below the Fermi level must be such that the accommodated charge exactly screens the charge of the impurity (see for example textbooks like [79]).

Whereas the Luttinger-Ward functional and the resulting Friedel sum rule have been studied extensively for several systems (as for instance the Fermi liquid models [79, 80], more specifically the Anderson impurity model [78] and interacting electrons [77], Mott insulators (see [81, 82] and references therein) or semiconductors [83]), the case of a quantum dot coupled to superconducting leads has so far not been treated (in a previous work by Alastalo et al., the expression of the Luttinger-Ward functional  $\Phi$  has been obtained up to the second order in  $U$ , but no further calculations like the derivation of the Friedel sum rule have been performed [68]). In the remainder of this chapter, the Luttinger-Ward functional for the case of a single quantum dot connected to superconducting electrodes will thus be analyzed for the first time. Symmetries of the Luttinger-Ward functional shall be used to derive the superconducting generalization of the Friedel sum rule for this system. This equation is a useful condition for the self-consistent determination of parameters like local superconducting correlations and may constitute an important ingredient to non-conserving schemes like the local moment approach (LMA) (see [84, 85] and references therein).

### 5.1.2 Explicit form up to second order

Equation (5.1) serves as a starting point for the derivation of the explicit form of the Luttinger-Ward functional. It states that we need to set up a functional of *full* propagators such that its functional derivative equals the self-energies. A natural starting point is thus to look at the self-energies in their skeleton expansion; the latter indeed only involves full propagators.

The effect of a derivative is, roughly spoken, to remove one of the entities that is derived for (as in  $\frac{d}{dx} x \cdot x \sim x$ ). Here, this corresponds to removing one of the full Green's functions. The functional  $\Phi$  we are looking for is thus nothing but the skeleton self-energies with an additional full Green's function. As  $\Phi$  has no frequency dependence, but the self energy  $\Sigma^R(\omega)$  does, this additional Green's function closes the two open vertices of the self-energy diagrams. More precisely, for a given diagram of the self-energy  $\Sigma_{ij}$ , the corresponding term in  $\Phi$  is obtained by simply closing the diagram with a full propagator  $G_{ij}$ . Diagrammatically and up to the second order in  $U$ ,  $\Phi$  is given by:



These diagrams can of course be transposed into analytic formulas, which yields

$$\begin{aligned}
\Phi &= \sum_{m=1,2} \sum_n \frac{\beta}{2m} \text{tr} \left\{ \widehat{G}_{d,d}(i\omega_n) \widehat{\Sigma}^{(m)}(i\omega_n) \right\} \\
&= -U\beta \int_0^\beta d\tau \delta(\tau) [G_{11}(\tau)G_{22}(\tau) - G_{12}(\tau)G_{21}(\tau)] \\
&\quad - \frac{U^2}{2}\beta \int_0^\beta d\tau [G_{11}(\tau)G_{22}(\tau) - G_{12}(\tau)G_{21}(\tau)] \cdot [G_{11}(-\tau)G_{22}(-\tau) - G_{12}(-\tau)G_{21}(-\tau)] .
\end{aligned} \tag{5.3}$$

The self-energies (4.15)-(4.18) can now indeed be written as

$$\Sigma_{ij}(i\omega_n) = \frac{\delta\Phi}{\delta G_{ij}} . \tag{5.4}$$

At this point, we want to stress that the Luttinger-Ward functional, up to the second order, factorizes into determinants of the Nambu Green's function  $\widehat{G}_{d,d}(i\omega_n)$ . This property will be important for the derivation of the symmetries of  $\Phi$ . As we are only analyzing the explicit form of  $\Phi$  up to the second order, this factorization and the resulting symmetries a priori only hold for the second order expansion. Nevertheless, we suspect this factorization to be linked to the invariance of  $\Phi$  to an orthogonal transformation of the Nambu spinor basis (i.e.  $SU(2)$  spin symmetry). Therefore, the invariances we will derive below might hold to infinite order and not only to the second one. Work in this direction is in progress.

### 5.1.3 Symmetries of the Luttinger-Ward functional

The Luttinger-Ward functional  $\Phi$  has a number of symmetries, i.e. invariances under transformations of the Green's functions  $G_{ij}$ . The most simple one is a global frequency shift,

$$G_{ij}(i\omega_n) \rightarrow G_{ij}(i\omega_n + i\delta\omega) \quad \forall i, j, n . \tag{5.5}$$

It is straightforward to see that this invariance holds for all orders of the perturbation expansion:

$$\begin{aligned}
\Phi &= \sum_{m=1}^{\infty} \sum_n \frac{\beta}{2m} \text{tr} \left\{ \widehat{G}_{d,d}(i\omega_n) \widehat{\Sigma}^{(m)}(i\omega_n) \right\} \\
&\rightarrow \sum_{m=1}^{\infty} \sum_n \frac{\beta}{2m} \text{tr} \left\{ \widehat{G}_{d,d}(i\omega_n + i\delta\omega) \widehat{\Sigma}^{(m)}(i\omega_n + i\delta\omega) \right\} \\
&\stackrel{\text{index shift}}{=} \sum_{m=1}^{\infty} \sum_n \frac{\beta}{2m} \text{tr} \left\{ \widehat{G}_{d,d}(i\omega_n) \widehat{\Sigma}^{(m)}(i\omega_n) \right\} .
\end{aligned} \tag{5.6}$$

As shall be shown now, the invariance under a global frequency shift results from a number of more specific symmetries. The latter will be derived by evaluating the effect of a small frequency shift

$$G_{ij}(i\omega_n) \rightarrow G_{ij}(i\omega_n) + i\delta\omega \frac{\partial G_{kl}(i\omega_n)}{\partial(i\omega_n)} , \tag{5.7}$$

that can also be written as

$$G_{ij}(\tau) \rightarrow G_{ij}(\tau) + i\tau\delta\omega G_{kl}(\tau) . \tag{5.8}$$

Two types of invariances are to be distinguished, namely those that mix different Green's functions and those that do not. The four "non-mixing invariances" are

$$\left. \begin{aligned} G_{11}(i\omega_n) &\rightarrow G_{11}(i\omega_n) + i\delta\omega \frac{\partial G_{11}(i\omega_n)}{\partial(i\omega_n)} \\ G_{12}(i\omega_n) &\rightarrow G_{12}(i\omega_n) + i\delta\omega \frac{\partial G_{12}(i\omega_n)}{\partial(i\omega_n)} \end{aligned} \right\} \forall n , \tag{5.9}$$

$$\left. \begin{aligned} G_{11}(i\omega_n) &\rightarrow G_{11}(i\omega_n) + i\delta\omega \frac{\partial G_{11}(i\omega_n)}{\partial(i\omega_n)} \\ G_{21}(i\omega_n) &\rightarrow G_{21}(i\omega_n) + i\delta\omega \frac{\partial G_{21}(i\omega_n)}{\partial(i\omega_n)} \end{aligned} \right\} \forall n , \tag{5.10}$$

$$\left. \begin{aligned} G_{22}(i\omega_n) &\rightarrow G_{22}(i\omega_n) + i\delta\omega \frac{\partial G_{22}(i\omega_n)}{\partial(i\omega_n)} \\ G_{12}(i\omega_n) &\rightarrow G_{12}(i\omega_n) + i\delta\omega \frac{\partial G_{12}(i\omega_n)}{\partial(i\omega_n)} \end{aligned} \right\} \forall n , \tag{5.11}$$

$$\left. \begin{aligned} G_{22}(i\omega_n) &\rightarrow G_{22}(i\omega_n) + i\delta\omega \frac{\partial G_{22}(i\omega_n)}{\partial(i\omega_n)} \\ G_{21}(i\omega_n) &\rightarrow G_{21}(i\omega_n) + i\delta\omega \frac{\partial G_{21}(i\omega_n)}{\partial(i\omega_n)} \end{aligned} \right\} \forall n . \tag{5.12}$$

Here shall only be stated the proof of the first invariance, the others can be understood similarly. In terms of imaginary time, equation (5.9) becomes

$$\begin{aligned} G_{11}(\tau) &\rightarrow G_{11}(\tau) + i\tau\delta\omega G_{11}(\tau) \\ G_{12}(\tau) &\rightarrow G_{12}(\tau) + i\tau\delta\omega G_{12}(\tau) \end{aligned} . \tag{5.13}$$

The first order term of the Luttinger-Ward functional only contains Green's functions at imaginary time  $\tau = 0$ . Therefore, this term is trivially invariant under the above transformation. The second order term, when expanded to the order  $\mathcal{O}(\delta\omega^1)$ , becomes

$$\begin{aligned}
\Phi^{(2)} &= -\frac{U^2}{2}\beta \int_0^\beta d\tau [G_{11}(\tau)G_{22}(\tau) - G_{12}(\tau)G_{21}(\tau)] \cdot [G_{11}(-\tau)G_{22}(-\tau) - G_{12}(-\tau)G_{21}(-\tau)] \\
&\rightarrow \Phi^{(2)} \cdot (1 + i\tau\delta\omega) \cdot (1 - i\tau\delta\omega) = \Phi^{(2)} \cdot (1 + i\tau\delta\omega - i\tau\delta\omega) = \Phi^{(2)} .
\end{aligned} \tag{5.14}$$

The transformations (5.9)-(5.12) thus leave the functional  $\Phi$  invariant. The global frequency shift invariance of  $\Phi$  is nothing but the combination of (5.9) and (5.12).

The Luttinger-Ward functional is also invariant under four transformations that mix the normal and anomalous propagators. The invariances in question are

$$\left. \begin{aligned} G_{11}(i\omega_n) &\rightarrow G_{11}(i\omega_n) + i\delta\omega \frac{\partial G_{21}(i\omega_n)}{\partial(i\omega_n)} \\ G_{12}(i\omega_n) &\rightarrow G_{12}(i\omega_n) + i\delta\omega \frac{\partial G_{22}(i\omega_n)}{\partial(i\omega_n)} \end{aligned} \right\} \forall n, \quad (5.15)$$

$$\left. \begin{aligned} G_{11}(i\omega_n) &\rightarrow G_{11}(i\omega_n) + i\delta\omega \frac{\partial G_{12}(i\omega_n)}{\partial(i\omega_n)} \\ G_{21}(i\omega_n) &\rightarrow G_{21}(i\omega_n) + i\delta\omega \frac{\partial G_{22}(i\omega_n)}{\partial(i\omega_n)} \end{aligned} \right\} \forall n, \quad (5.16)$$

$$\left. \begin{aligned} G_{22}(i\omega_n) &\rightarrow G_{22}(i\omega_n) + i\delta\omega \frac{\partial G_{21}(i\omega_n)}{\partial(i\omega_n)} \\ G_{12}(i\omega_n) &\rightarrow G_{12}(i\omega_n) + i\delta\omega \frac{\partial G_{11}(i\omega_n)}{\partial(i\omega_n)} \end{aligned} \right\} \forall n, \quad (5.17)$$

$$\left. \begin{aligned} G_{22}(i\omega_n) &\rightarrow G_{22}(i\omega_n) + i\delta\omega \frac{\partial G_{12}(i\omega_n)}{\partial(i\omega_n)} \\ G_{21}(i\omega_n) &\rightarrow G_{21}(i\omega_n) + i\delta\omega \frac{\partial G_{22}(i\omega_n)}{\partial(i\omega_n)} \end{aligned} \right\} \forall n. \quad (5.18)$$

The proof of invariance (5.15) is exemplary for the others. The latter can be written as

$$\begin{aligned} G_{11}(\tau) &\rightarrow G_{11}(\tau) + i\tau\delta\omega G_{21}(\tau) \\ G_{12}(\tau) &\rightarrow G_{12}(\tau) + i\tau\delta\omega G_{22}(\tau) \end{aligned} \quad (5.19)$$

The first order term is thus again trivially invariant, as it involves only Green's functions at  $\tau = 0$ . The second order term is invariant because

$$\begin{aligned} &G_{11}(\tau)G_{22}(\tau) - G_{12}(\tau)G_{21}(\tau) \\ \rightarrow &G_{11}(\tau)G_{22}(\tau) - G_{12}(\tau)G_{21}(\tau) + G_{21}(\tau)G_{22}(\tau) - G_{22}(\tau)G_{21}(\tau) \\ = &G_{11}(\tau)G_{22}(\tau) - G_{12}(\tau)G_{21}(\tau). \end{aligned} \quad (5.20)$$

### Symmetries of the Luttinger-Ward functional at particle hole symmetry

As there are only two different propagators at particle-hole symmetry (see section 4.2.4),  $\mathcal{G}$  and  $\mathcal{F}$ , the eight Luttinger-Ward functional invariances derived above condense into two simple equations, that read

$$\left. \begin{aligned} \mathcal{G}(i\omega_n) &\rightarrow \mathcal{G}(i\omega_n) + i\delta\omega \frac{\partial \mathcal{G}(i\omega_n)}{\partial(i\omega_n)} \\ \mathcal{F}(i\omega_n) &\rightarrow \mathcal{F}(i\omega_n) + i\delta\omega \frac{\partial \mathcal{F}(i\omega_n)}{\partial(i\omega_n)} \end{aligned} \right\} \forall n \text{ and} \quad (5.21)$$

$$\left. \begin{aligned} \mathcal{G}(i\omega_n) &\rightarrow \mathcal{G}(i\omega_n) + i\delta\omega \frac{\partial \mathcal{F}(i\omega_n)}{\partial(i\omega_n)} \\ \mathcal{F}(i\omega_n) &\rightarrow \mathcal{F}(i\omega_n) + i\delta\omega \frac{\partial \mathcal{G}(i\omega_n)}{\partial(i\omega_n)} \end{aligned} \right\} \forall n. \quad (5.22)$$

## 5.2 Superconducting Friedel sum rule at particle hole symmetry

### 5.2.1 Luttinger-Ward equations

In this section, equations (5.21) and (5.22) shall be transposed from imaginary time to real time in order to check them in some simple limiting cases analytically in the following

section. In the following, the discussion will be simplified by using a generic self-energy  $\Sigma_\alpha(i\omega_n)$  and a generic Green's function  $G_\beta(i\omega_n)$ .

The self-energy  $\Sigma_\alpha(i\omega_n)$  can be written as the functional derivative of the Luttinger-Ward functional,

$$\Sigma_\alpha(i\omega_n) = \frac{\delta\Phi}{\delta G_\alpha(i\omega_n)}. \quad (5.23)$$

Let us consider the case where the functional  $\Phi = \Phi[G_\alpha, G_\beta, \dots]$  is invariant under the transformation  $G_\alpha(\omega_n) \rightarrow G_\alpha(\omega_n) + i\delta\omega \frac{\partial G_\beta}{\partial(i\omega_n)}$ , i.e.

$$\begin{aligned} \Phi[G_\alpha, G_\beta, \dots] &= \Phi\left[G_\alpha + i\delta\omega \frac{\partial G_\beta}{\partial(i\omega_n)}, G_\beta, \dots\right] \\ &= \Phi[G_\alpha, G_\beta, \dots] + \sum_{\omega_n} i\delta\omega \frac{\delta\Phi}{\delta G_\alpha} \frac{\partial G_\beta}{\partial(i\omega_n)}. \end{aligned} \quad (5.24)$$

Now integrating by parts, one ends up with

$$\sum_{\omega_n} \frac{\partial \Sigma_\alpha(i\omega_n)}{\partial(i\omega_n)} G_\beta = 0. \quad (5.25)$$

The next step is to perform the analytic continuation of this equation, i.e. to find its retarded real time formulation. This can be achieved by writing sums over Matsubara frequencies as an integral in the complex plane via the residues of the Fermi-Dirac distribution function. This yields

$$\int_{-\infty}^{\infty} d\omega n_F(\omega) \operatorname{Im} \left\{ \frac{\partial \Sigma_\alpha^R(\omega)}{\partial\omega} G_\beta^R(\omega) \right\} = 0. \quad (5.26)$$

For the symmetries derived above, the equations corresponding to (5.26) read

$$\operatorname{Im} \left\{ \int_{-\infty}^{\infty} d\omega n_F(\omega) \left( G_{11}^R(\omega) \frac{\partial \Sigma_{\mathcal{G}}^R}{\partial\omega} + G_{12}^R(\omega) \frac{\partial \Sigma_{\mathcal{F}}^R}{\partial\omega} \right) \right\} = 0, \quad (5.27)$$

$$\operatorname{Im} \left\{ \int_{-\infty}^{\infty} d\omega n_F(\omega) \left( G_{11}^R(\omega) \frac{\partial \Sigma_{\mathcal{F}}^R}{\partial\omega} + G_{12}^R(\omega) \frac{\partial \Sigma_{\mathcal{G}}^R}{\partial\omega} \right) \right\} = 0. \quad (5.28)$$

In the limit  $\Delta \rightarrow 0$ , equations (5.27) and (5.28) both reduce to the well known Luttinger equation for a quantum dot coupled to normal leads [77, 78]. Following the lines of reference [78], we shall exploit these two equations to simplify

$$\begin{aligned} (G_{11}^R + G_{12}^R) \frac{\partial}{\partial\omega} \frac{1}{G_{11}^R + G_{12}^R} &= -\frac{\partial}{\partial\omega} \ln(G_{11}^R + G_{12}^R) \\ &= (G_{11}^R + G_{12}^R) \frac{\partial}{\partial\omega} \left( g_0^{-1R} + f_0^{-1R} - \Sigma_{\mathcal{G}}^R - \Sigma_{\mathcal{F}}^R \right). \end{aligned} \quad (5.29)$$

Plugging (5.27) and (5.28) into this equation and taking the zero temperature limit yields the rather simple formula

$$\text{Im} \left\{ \int_{-\infty}^0 d\omega \left( \frac{\partial}{\partial \omega} \ln (G_{11}^R + G_{12}^R) + (G_{11}^R + G_{12}^R) \left( \frac{\partial g_0^{-1R}}{\partial \omega} + \frac{\partial f_0^{-1R}}{\partial \omega} \right) \right) \right\} = 0. \quad (5.30)$$

In a perfectly symmetric way, one may also derive

$$\text{Im} \left\{ \int_{-\infty}^0 d\omega \left( \frac{\partial}{\partial \omega} \ln (G_{11}^R - G_{12}^R) + (G_{11}^R - G_{12}^R) \left( \frac{\partial g_0^{-1R}}{\partial \omega} - \frac{\partial f_0^{-1R}}{\partial \omega} \right) \right) \right\} = 0. \quad (5.31)$$

These expressions can be simplified further on. Indeed,

$$\int_{-\infty}^0 d\omega \frac{\partial}{\partial \omega} \ln (G_{11}^R \pm G_{12}^R) = [\ln (G_{11}^R \pm G_{12}^R)]_{-\infty}^0. \quad (5.32)$$

For complex numbers  $z$ , the logarithm is defined by  $\ln(z) = \ln(\|z\| e^{i \arg(z)}) = \ln(\|z\|) + i \arg(z)$ . Taking the imaginary part of the above equation will therefore simply yield the argument of expression inside the logarithm. Yet, the latter expression is the sum or difference of two retarded Green's functions. Therefore, this argument must be  $\arg(z) \in \{-\pi, 0\}$ . We thus obtain

$$\text{Im} \left\{ \int_{-\infty}^0 d\omega \frac{\partial}{\partial \omega} \ln (G_{11}^R \pm G_{12}^R) \right\} = \left[ -\arctan \left( \frac{\text{Re} \{G_{11}^R \pm G_{12}^R\}}{\text{Im} \{G_{11}^R \pm G_{12}^R\}} \right) - \frac{\pi}{2} \right]_{-\infty}^0. \quad (5.33)$$

Because the self energies  $\Sigma_{\mathcal{G}}^R(\omega)$  and  $\Sigma_{\mathcal{F}}^R(\omega)$  tend to zero for  $\omega \rightarrow -\infty$ , the phase of the Green's functions at  $\omega \rightarrow -\infty$  can easily be evaluated based on the known expressions for  $U = 0$ . Considering for example

$$G_{11}^R(\omega) + G_{12}^R(\omega) = \frac{1}{g_0^{-1R}(\omega) + f_0^{-1R}(\omega) - \Sigma_{\mathcal{G}}^R(\omega) - \Sigma_{\mathcal{F}}^R(\omega)} \xrightarrow{\omega \rightarrow -\infty} \frac{1}{g_0^{-1R}(\omega) + f_0^{-1R}(\omega)}, \quad (5.34)$$

one can easily understand that both  $\text{Re} \{G_{11}^R + G_{12}^R\}$  and  $\text{Im} \{G_{11}^R + G_{12}^R\}$  will tend to  $0^-$ . Nevertheless, as the imaginary part tends much slower to zero than the real part, their ratio will tend to infinity. A similar consideration holds for  $G_{11}^R - G_{12}^R$ . Thus, one ends up with

$$\text{Im} \left\{ \int_{-\infty}^0 d\omega \frac{\partial}{\partial \omega} \ln (G_{11}^R \pm G_{12}^R) \right\} = \frac{\pi}{2} - \arctan \left( \frac{\text{Re} \{G_{11}^R(0) \pm G_{12}^R(0)\}}{\text{Im} \{G_{11}^R(0) \pm G_{12}^R(0)\}} \right). \quad (5.35)$$

The Green's functions and self energies at  $\omega = 0$  have several very useful properties. First of all, the imaginary parts of the self energies vanish inside that gap and thus in particular at  $\omega = 0$ . Furthermore, the imaginary part of the self energy  $\Sigma_{\mathcal{G}}^R(\omega)$  has to be symmetric, just as the Green's functions  $\mathcal{G}^R$  and  $G_{11}^R$ . From the Kramers-Kronig

relation, one finds thus that the real part of  $\Sigma_{\mathcal{G}}^R(\omega)$  is antisymmetric in  $\omega$ , and in particular  $\Sigma_{\mathcal{G}}^R(\omega = 0) = 0$ . This implies, together with equations (I.17) and (I.18), that

$$G_{11}^R(\omega = 0) = i\eta \quad (5.36)$$

and

$$G_{12}^{R''}(\omega = 0) = 0 . \quad (5.37)$$

On the other hand,

$$G_{12}^{R'}(\omega = 0) \neq 0 \quad (5.38)$$

due to superconducting correlations. These properties obviously simplify equation (5.35) considerably. Putting everything together allows to write down the final version of the Luttinger-Ward equations, that read

$$-\frac{1}{\pi} \int_{-\infty}^0 d\omega \operatorname{Im} \left\{ (G_{11}^R + G_{12}^R) \frac{\partial (g_0^{-1R} + f_0^{-1R})}{\partial \omega} \right\} = \frac{1}{2} - \frac{1}{2} \operatorname{sgn} \left( \Sigma_{\mathcal{F}}^{R'}(0) - f_0^{-1R'}(0) \right) , \quad (5.39)$$

$$-\frac{1}{\pi} \int_{-\infty}^0 d\omega \operatorname{Im} \left\{ (G_{11}^R - G_{12}^R) \frac{\partial (g_0^{-1R} - f_0^{-1R})}{\partial \omega} \right\} = \frac{1}{2} + \frac{1}{2} \operatorname{sgn} \left( \Sigma_{\mathcal{F}}^{R'}(0) - f_0^{-1R'}(0) \right) . \quad (5.40)$$

Equations (5.39) and (5.40) are worth looking at in more detail. They state that at zero temperature and in the singlet phase of the quantum dot, there are two quantized entities. These quantities are either 1 or 0 depending on the value of the anomalous Green's function at  $\omega = 0$ .

This is a result known from the non-superconducting case. There, the left hand side of equations (5.39) and (5.40) is the charge added to the system by the presence of the interacting quantum dot, the so-called excess charge. In the superconducting case, such a simple physical interpretation is not possible. If the excess charge is calculated, one ends up with an expression similar but not equal to equation (5.39). We attribute this to the non-conservation of the charge in a superconducting system.

Anyhow, equations (5.39) and (5.40) above are powerful boundary conditions that need to be satisfied as long as one stays adiabatically connected to the  $U = 0$  phase. If the ground state changes to a spin doublet, the basic perturbation theory around the singlet phase considered here will show singularities and equations (5.39) and (5.40) will be violated.

## 5.2.2 Some simple limiting cases

### Non-interacting quantum dot ( $U = 0$ )

In this section, we shall check equations (5.39) and (5.40) in some simple limiting cases. At first, the non-interacting case  $U = 0$  will be considered.

The self-energies vanish identically, and so does the self-consistent parameter  $\Delta_{eff} = U \langle d_{\downarrow} d_{\uparrow} \rangle$ . Therefore, already equations (5.27) and (5.28) are trivially satisfied, and thus

are all the subsequent ones. As the imaginary part of the anomalous Green's function is antisymmetric with respect to  $\omega = 0$  (see equation (I.16) for  $\Delta_{eff} = 0$ ),  $\Delta_{eff} = 0$  is indeed self-consistent (see equation (4.33)).

### First order approximation

In the formalism we have derived above, the first order corrections to the Green's functions have been absorbed into the "partly dressed" propagators. The latter have subsequently been used for the skeleton expansion of the self energies. Therefore, the self-energies only start at the second order (that is disregarded in a first order approximation). As a consequence, equations (5.27) and (5.28) are trivially satisfied for a first order approximation.

### Effective local Hamiltonian

In the effective local limit, corresponding to the large gap limit of the total Hamiltonian, an exact solution for the interacting problem exists. In order to simplify the discussions at much as possible, we shall further consider the limit of infinite electronic bandwidth in the leads, i.e.  $D \rightarrow \infty$ . The generalization of the below considerations to finite bandwidth is straightforward. The system has four eigenstates, that read for particle hole symmetry

$$\begin{aligned}
|\uparrow\rangle & & , \text{ energy } E_{\uparrow} & = 0 \\
|\downarrow\rangle & & , \text{ energy } E_{\downarrow} & = 0 \\
|+\rangle & = \frac{1}{\sqrt{2}} (|\uparrow\downarrow\rangle + |0\rangle) & , \text{ energy } E_{+} & = \frac{U}{2} + |\Gamma_{\varphi}| \\
|-\rangle & = \frac{1}{\sqrt{2}} (-|\uparrow\downarrow\rangle + |0\rangle) & , \text{ energy } E_{-} & = \frac{U}{2} - |\Gamma_{\varphi}| ,
\end{aligned} \tag{5.41}$$

with  $\Gamma_{\varphi} = \Gamma + \cos\left(\frac{\varphi}{2}\right)$ .

Because Coulomb interaction is taken into account, the exact Green's functions can only be calculated in Lehmann representation (i.e. not using Wick's theorem). They depend on whether the ground state is the BCS-like spin singlet  $|-\rangle$  or the spin 1/2 doublet and read

$$G_{11}^R(\omega) = \begin{cases} \frac{1}{2} \left( \frac{1}{\omega+i\eta+|\Gamma_{\varphi}|-\frac{U}{2}} + \frac{1}{\omega+i\eta-|\Gamma_{\varphi}|+\frac{U}{2}} \right) & , \frac{U}{2} < |\Gamma_{\varphi}| \text{ (singlet phase)} \\ \frac{1}{2} \left( \frac{1}{\omega+i\eta+|\Gamma_{\varphi}|-\frac{U^2}{4}} \frac{1}{\omega+i\eta+|\Gamma_{\varphi}|} + \frac{1}{\omega+i\eta-|\Gamma_{\varphi}|-\frac{U^2}{4}} \frac{1}{\omega+i\eta-|\Gamma_{\varphi}|} \right) & , \frac{U}{2} > |\Gamma_{\varphi}| \text{ (doublet phase)} , \end{cases} \tag{5.42}$$

$$G_{12}^R(\omega) = \begin{cases} \frac{1}{2} \left( \frac{1}{\omega+i\eta+|\Gamma_{\varphi}|-\frac{U}{2}} - \frac{1}{\omega+i\eta-|\Gamma_{\varphi}|+\frac{U}{2}} \right) & , \frac{U}{2} < |\Gamma_{\varphi}| \text{ (singlet phase)} \\ \frac{1}{2} \left( \frac{1}{\omega+i\eta+|\Gamma_{\varphi}|-\frac{U^2}{4}} \frac{1}{\omega+i\eta+|\Gamma_{\varphi}|} - \frac{1}{\omega+i\eta-|\Gamma_{\varphi}|-\frac{U^2}{4}} \frac{1}{\omega+i\eta-|\Gamma_{\varphi}|} \right) & , \frac{U}{2} > |\Gamma_{\varphi}| \text{ (doublet phase)} . \end{cases} \tag{5.43}$$

Sticking to the notation defined in (4.31) and (4.32), i.e.

$$G_{11}^R = \frac{1}{2} \left( \frac{1}{g_0^{-1R} - \Sigma_{\mathcal{G}}^R + f_0^{-1R} - \Sigma_{\mathcal{F}}^R} + \frac{1}{g_0^{-1R} - \Sigma_{\mathcal{G}}^R - f_0^{-1R} + \Sigma_{\mathcal{F}}^R} \right), \quad (5.44)$$

$$G_{12}^R = \frac{1}{2} \left( \frac{1}{g_0^{-1R} - \Sigma_{\mathcal{G}}^R + f_0^{-1R} - \Sigma_{\mathcal{F}}^R} - \frac{1}{g_0^{-1R} - \Sigma_{\mathcal{G}}^R - f_0^{-1R} + \Sigma_{\mathcal{F}}^R} \right), \quad (5.45)$$

one can identify

$$g_0^{-1R} = \omega + i\eta, \quad (5.46)$$

$$f_0^{-1R} = |\Gamma_\varphi|, \quad (5.47)$$

$$\Sigma_{\mathcal{G}}^R = \begin{cases} 0 & , \frac{U}{2} < |\Gamma_\varphi| \text{ (singlet phase)} \\ \frac{U^2}{4} \frac{\omega + i\eta}{(\omega + i\eta)^2 - \Gamma_\varphi^2} & , \frac{U}{2} > |\Gamma_\varphi| \text{ (doublet phase)}, \end{cases} \quad (5.48)$$

$$\Sigma_{\mathcal{F}}^R = \begin{cases} \frac{U}{2} & , \frac{U}{2} < |\Gamma_\varphi| \text{ (singlet phase)} \\ -\frac{U^2}{4} \frac{|\Gamma_\varphi|}{(\omega + i\eta)^2 - \Gamma_\varphi^2} & , \frac{U}{2} > |\Gamma_\varphi| \text{ (doublet phase)}. \end{cases} \quad (5.49)$$

Quite interestingly, the exact self energies are purely first order in  $U$  in the singlet phase and purely second order in the doublet phase [24]. The abrupt transition between these two self-energy dependences shows how a simple perturbation theory around the singlet phase breaks down as soon as the doublet becomes the ground state. As mentioned before, and as we shall see in a moment, this implies especially that the Luttinger-Ward equations (5.39) and (5.40) (based explicitly on the perturbation expansion) are only valid in the singlet phase.

The evaluation of the Luttinger-Ward equations in the singlet phase is rather simple. The self-energies are purely real, and so are  $g_0^{-1R}$  and  $f_0^{-1R}$  and the Green's functions apart the Andreev bound states. To be completely consistent with section 4.2.4, the first order self-energies are again incorporated into the now “partly dressed” propagators. Then,

$$g_0^{-1R} = \omega + i\eta, \quad (5.50)$$

$$f_0^{-1R} = |\Gamma_\varphi| - \Delta_{eff} \text{ and } \Delta_{eff} = \frac{U}{2}, \quad (5.51)$$

$$\Sigma_{\mathcal{G}}^R = 0, \quad (5.52)$$

$$\Sigma_{\mathcal{F}}^R = 0. \quad (5.53)$$

Thus, the imaginary part of the Green's functions reads

$$\text{Im} \{ G_{11}^R + G_{12}^R \} = -\pi\delta(\omega + |\Gamma_\varphi| - \frac{U}{2}) \quad (5.54)$$

$$\text{Im} \{ G_{11}^R - G_{12}^R \} = -\pi\delta(\omega - |\Gamma_\varphi| + \frac{U}{2}) \quad (5.55)$$

As the self-energies vanish within this definition, one might simply apply the proof given above for the first order. Yet, it is instructive to evaluate equations (5.39) and (5.40) at least once. We start off by computing

$$\begin{aligned}
& -\frac{1}{\pi} \int_{-\infty}^0 d\omega \operatorname{Im} \left\{ (G_{11}^R + G_{12}^R) \frac{\partial (g_0^{-1R} + f_0^{-1R})}{\partial \omega} \right\} \\
&= -\frac{1}{\pi} \int_{-\infty}^0 d\omega \operatorname{Im} \{ G_{11}^R + m G_{12}^R \} \frac{\partial (g_0^{-1R} + f_0^{-1R})}{\partial \omega} \\
&= -\frac{1}{\pi} \int_{-\infty}^0 d\omega \left( -\pi \delta(\omega + |\Gamma_\varphi| - \frac{U}{2}) \right) \cdot (1 + 0) .
\end{aligned} \tag{5.56}$$

In the singlet phase,  $|\Gamma_\varphi| - U/2 > 0$ , which yields

$$-\frac{1}{\pi} \int_{-\infty}^0 d\omega \operatorname{Im} \left\{ (G_{11}^R + G_{12}^R) \frac{\partial (g_0^{-1R} + f_0^{-1R})}{\partial \omega} \right\} = 1 . \tag{5.57}$$

An analogous calculation yields

$$-\frac{1}{\pi} \int_{-\infty}^0 d\omega \operatorname{Im} \left\{ (G_{11}^R - G_{12}^R) \frac{\partial (g_0^{-1R} - f_0^{-1R})}{\partial \omega} \right\} = 0 . \tag{5.58}$$

For the Luttinger-Ward equations (5.39) and (5.40) to be satisfied, this imposes

$$1 \stackrel{!}{=} \frac{1}{2} - \frac{1}{2} \operatorname{sgn} \left( \frac{U}{2} - |\Gamma_\varphi| \right) , \tag{5.59}$$

$$0 \stackrel{!}{=} \frac{1}{2} + \frac{1}{2} \operatorname{sgn} \left( \frac{U}{2} - |\Gamma_\varphi| \right) , \tag{5.60}$$

which is obviously true in the singlet phase. The last part of the consistency check is the evaluation of  $\Delta_{eff}$ . According to

$$\begin{aligned}
\Delta_{eff} = U \langle d_\downarrow d_\uparrow \rangle &= -\frac{U}{\pi} \operatorname{Im} \left\{ \int_{-\infty}^{\infty} d\omega G_{12}^R(\omega) \right\} \\
&= -\frac{U}{\pi} \int_{-\infty}^{\infty} d\omega \left( -\frac{\pi}{2} \right) \cdot \left( \delta(\omega + |\Gamma_\varphi| - \frac{U}{2}) - \delta(\omega - |\Gamma_\varphi| + \frac{U}{2}) \right) \\
&= \frac{U}{2} .
\end{aligned} \tag{5.61}$$

The exact solution in the wide gap  $\Delta$  limit thus indeed satisfies the Luttinger-Ward equations and the self-consistency of the local pairing amplitude. Before ending by some remarks on the evaluation of the Luttinger-Ward equations in a general regime, we shall show that in the spin doublet phase (i.e. the one not adiabatically connected to non-interacting limit), the Luttinger-Ward equations are violated. First of all, we notice that

$$\Delta_{eff} = U \langle d_\downarrow d_\uparrow \rangle = 0 ,$$

because there are no superconducting correlations on a purely singly occupied dot. Therefore,

$$g_0^{-1R} = \omega + i\eta, \quad (5.62)$$

$$f_0^{-1R} = |\Gamma_\varphi|, \quad (5.63)$$

$$\Sigma_{\mathcal{G}}^R = \frac{U^2}{4} \frac{\omega + i\eta}{(\omega + i\eta)^2 - \Gamma_\varphi^2}, \quad (5.64)$$

$$\Sigma_{\mathcal{F}}^R = -\frac{U^2}{4} \frac{|\Gamma_\varphi|}{(\omega + i\eta)^2 - \Gamma_\varphi^2}. \quad (5.65)$$

Again, self energies as well as  $g_0^{-1R}$  and  $f_0^{-1R}$  are real, so that only the bound states contribute. For equation (5.39), the contribution of the latter is given by

$$\text{Im} \{G_{11}^R + G_{12}^R\} = \frac{1}{2} \left( -\pi\delta\left(\omega + |\Gamma_\varphi| - \frac{U}{2}\right) - \pi\delta\left(\omega + |\Gamma_\varphi| + \frac{U}{2}\right) \right) \quad (5.66)$$

Using the fact that the doublet phase is characterized by  $\frac{U}{2} > |\Gamma_\varphi|$ , we obtain analogously to equation (5.56)

$$\begin{aligned} & -\frac{1}{\pi} \int_{-\infty}^0 d\omega \text{Im} \left\{ (G_{11}^R + G_{12}^R) \frac{\partial (g_0^{-1R} + f_0^{-1R})}{\partial \omega} \right\} \\ &= -\frac{1}{\pi} \int_{-\infty}^0 d\omega \frac{1}{2} \left( -\pi\delta\left(\omega + |\Gamma_\varphi| - \frac{U}{2}\right) - \pi\delta\left(\omega + |\Gamma_\varphi| + \frac{U}{2}\right) \right) \cdot (1 + 0) = \frac{1}{2}. \end{aligned} \quad (5.67)$$

In order to respect the Luttinger-Ward equation (5.39), we would thus need to have

$$\frac{1}{2} \stackrel{!}{=} \frac{1}{2} - \frac{1}{\pi} \arctan \left( \frac{\frac{U^2}{4|\Gamma_\varphi|} - |\Gamma_\varphi|}{\eta} \right) = 0. \quad (5.68)$$

This is of course wrong, which shows that the Luttinger-Ward equations based on the perturbation theory set up in chapter 4 are in general only valid in the singlet phase.

### Numerical evaluation for arbitrary parameters

We shall finish with some remarks on the numerical evaluation of the Luttinger-Ward equations in general parameter regime. As they are singular contributions to equations (5.39) and (5.40), one needs to deal with the Andreev bound states separately. Nevertheless, also the evaluation of the integrals corresponding to the continuum of states above the gap is numerically somewhat tricky, because the gap edge has a singular contribution as well. These singularities can be avoided by subtracting the first order Luttinger-Ward equations (that have been shown to be always satisfied in the singlet phase). Indeed, the integral

$$-\frac{1}{\pi} \int_{-\infty}^0 d\omega \text{Im} \left\{ (G_{11}^R \pm G_{12}^R) \frac{\partial (g_0^{-1R} \pm f_0^{-1R})}{\partial \omega} - (\mathcal{G}^R \pm \mathcal{F}^R) \frac{\partial (g_0^{-1R} \pm f_0^{-1R})}{\partial \omega} \right\} \quad (5.69)$$

turn out to converge much better than the simple equations (5.39) and (5.40). The Luttinger-Ward equations have been checked for the perturbative approach for various parameters (e.g. for all the results presented in section 4.3); they are satisfied within numerical precision.



# Chapter 6

## Conclusion

### 6.1 Summary and Conclusions

The beginning of this diploma thesis was devoted to the rederivation of some well-known results. After having gained some information on the electronic structure of a non-interacting single quantum dot, the Josephson current through this system has been reanalyzed. It has been checked that the latter has two contributions, namely one of the bound states inside the gap and one of a continuum of states outside the gap. These contributions were found to have opposite signs. Using a perturbation theory around the weak hybridization limit, it has further been explained that the total Josephson current changes its sign if the quantum dot becomes magnetic (i.e. observation of a  $0 - \pi$  transition).

The next chapter presented a new perturbative calculation scheme around an effective local Hamiltonian. In order to obtain the latter, the total Hamiltonian was transposed into an action-based description. The effective local Hamiltonian corresponds to the low frequency limit of this action, i.e. the limit where the superconducting gap is much bigger than the characteristic frequencies of the dot. In this limit, the dot is described by superconducting atomic states. Within the effective local Hamiltonian approach, the energies of the Andreev bound states are described as the energy differences of the superconducting atomic states.

We have then set up a self-consistent perturbation theory around the effective local Hamiltonian that describes how the superconducting atomic states mix if the gap decreases. This leads to a non-trivial renormalization of the Andreev bound states. By comparison to recent NRG data, we could show that our approach accurately describes the Andreev bound states as well as the superconducting correlations on the dot as a function of gate voltage, hybridization, Coulomb interaction and superconducting gap amplitude. As a major limitation, the Kondo regime could only be captured qualitatively, because of vertex corrections that have not been included in our energy corrections.

Due to its simple and reliable description of the Andreev bound states, the effective local Hamiltonian approach should be readily applicable to describe future spectroscopic measurements. The main advantage of our formalism, compared to numerical calculations, is that it is based on simple, analytic equations. It should thus not be very difficult to transpose it to more complex systems, like double dots. Indeed, a short glance at a generalization of our approach to double dots completed this part of the thesis.

The fourth chapter described a perturbation theory in the Coulomb interaction. As

the latter can be a large energy scale in experimental systems, the perturbation expansion had to be pushed to the second order. Using a skeleton expansion, we were able to resum certain diagrams to infinite order. Nevertheless, this perturbation theory, set up around the non-interacting limit, is only valid in the singlet phase of the quantum dot. In this phase, the physics is indeed very well described, as has been shown by comparison to both numerical data and results obtained with the effective local Hamiltonian approach.

We found that the intermediate coupling regime was satisfactorily described by all three approaches. Still, the two analytic approaches are complementary. For large gaps, when the proximity effect becomes less important and the dot is in a spin doublet phase, only the effective local Hamiltonian is able to give correct results. On the other hand, the latter cannot describe the low gap regime. This regime, on the contrary, is well captured by the perturbation expansion in the Coulomb interaction. The two analytic approaches thus constitute a set of tools that describes almost any experimentally relevant regime quantitatively (except for the Kondo regime at very large Coulomb interaction and near particle hole symmetry).

The fifth and last chapter dealt with the derivation of the Luttinger-Ward functional of a quantum dot connected to superconducting electrodes. The explicit expression of the latter has been found up to the second order based on the perturbation expansion in the Coulomb interaction. The symmetries of the Luttinger-Ward functional allowed us to derive two Luttinger-Ward equations. We found two quantized entities (instead of just one for the case of normal electrodes), linked to the normal and anomalous propagators. These equations, that may serve as powerful boundary conditions in numerical studies, have been checked analytically in some simple limiting cases, but also numerically in a general regime of parameters for the second order perturbation calculation of chapter 4.

## 6.2 Outlook

A first objective is to increase the validity and exactness of the low frequency expansion. It would be especially desirable to capture the Kondo temperature correctly by eventually including the vertex corrections.

A second aim would be to further analyze the double dot structure, for example using the perturbative approach developed in this thesis (i.e. around the low frequency limit). Yet, different approaches may be necessary for different regimes.

Furthermore, it would certainly be of great interest to try and generalize the invariances of the Luttinger-Ward functional to infinite order. Also, one might use them as self-consistency conditions in, for instance, a generalized local moment approach (LMA) calculation.

Finally, a generalization of the effective local Hamiltonian approach to non-equilibrium situations, i.e. applied bias voltage across the junction, would be desirable. In this context, recent work by Governale, Pala and König [43, 60, 64] might be a promising starting point. Based on a diagrammatic technique, they analyzed the out-of-equilibrium physics of a quantum dot coupled to superconducting and normal electrodes. The spectroscopy of Andreev bound states by such a device, which could for instance be an STM (scanning tunneling microscope, see below), is also envisioned. Yet, their work only deals with the large gap limit  $\Delta \rightarrow \infty$ . The combination of our perturbation theory around the effective local Hamiltonian and their diagrammatic approach is a promising candidate for the description of the out-of-equilibrium physics of a superconducting quantum dot

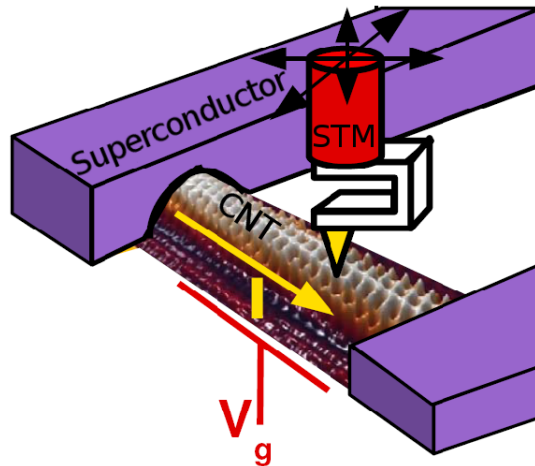


Figure 6.1: Sketch of a STM Andreev spectroscopy experiment [11] (see text).

in a general regime of parameters.

### 6.2.1 Andreev bound state spectroscopy

As discussed in the introduction, we expect the effective local Hamiltonian approach developed in this thesis to describe Andreev bound state spectroscopy experiments. ABS spectroscopy has been discussed recently for microwave experiments [10] and noise measurements [12] on quantum dots. Additionally, the spectrum of a superconducting quantum dot could be measured by a transport setup through a STM, as has been suggested in reference [43]. Indeed, STM spectroscopy experiments on carbon nanotubes are scheduled in the near future at the CNRS Grenoble [11]. Figure 6.1 shows a sketch of the intended experimental setup. A carbon nanotube (CNT) connected to superconducting electrodes corresponds to the quantum dot considered in this thesis. In order to measure the density of states of the latter, a STM tip will be placed on top of the nanotube. The energy levels of the carbon nanotube can be controlled by means of a gate voltage  $V_g$ . Eventually, a bias voltage can be applied, so that a current  $I$  would flow across the junction.

In contrast to more standard transport experiments, where the current through electrodes and dot as a function of an applied bias voltage across the junction is measured, this device has the striking advantage that the hybridization of the nanotube to the superconducting electrodes can be controlled separately from the tunnel coupling to the STM tip. This way, the carbon nanotube can be coupled sufficiently strongly to the superconducting electrodes for the proximity effect to be well-established, while the density of states is probed by a weak tunneling link. This is indeed an advantage compared to more standard transport experiments, where it is difficult to perform a true tunnel spectroscopy in regimes where the proximity effect is important.



# Appendix A

## Some conventions on Matsubara Green's functions

Quite often, the Matsubara imaginary-time formalism is used to calculate Green's functions. It allows to treat the perturbation expansions of the time evolution operator  $U(t, t')$  and the Boltzmann factor  $e^{-\beta H}$  ( $\beta = \frac{1}{kT}$ ) in one single go. Nevertheless, one should always bear in mind that the Matsubara formalism is only valid for time independent Hamiltonians (including possible perturbations). If a perturbation is time dependent, a non-equilibrium formalism (e.g. Keldysh formalism) has to be used.

The real time Green's functions like the retarded Green's function  $G^R(\vec{r}, \sigma, t; \vec{r}', \sigma', t') = -i\theta(t' - t)\langle[\Psi_\sigma(\vec{r}, t), \Psi_{\sigma'}^\dagger(\vec{r}', t')]_{\pm}\rangle$  have the form of a correlation function (with commutators for bosons and anticommutators for fermions). The Matsubara formalism is based on correlation functions that generalize these Green's functions. The innovation is the use of an imaginary time, basically "replacing"  $it$  by  $\tau$ . Deeper insight in this formalism can be found in textbooks [53]. Here shall only be given some definitions and properties concerning Matsubara Green's functions.

A Matsubara Green's function is defined by

$$\mathcal{C}_{AB}(\tau, \tau') := -\langle T_\tau A(\tau) B(\tau') \rangle, \quad (\text{A.1})$$

where  $A$  and  $B$  are two observables and  $T_\tau$  is the imaginary-time ordering operator. Two central properties of  $\mathcal{C}_{AB}(\tau, \tau')$  are

$$\mathcal{C}_{AB}(\tau, \tau') = \mathcal{C}_{AB}(\tau - \tau', 0) := \mathcal{C}_{AB}(\tau) \quad (\text{A.2})$$

$$\mathcal{C}_{AB}(\tau) = \pm \mathcal{C}_{AB}(\tau + \beta) \quad (\text{A.3})$$

(+ for bosons and  $-$  for fermions).

Very often, Fourier transforms of Matsubara Green's functions have to be dealt with. These are defined by

$$\mathcal{C}_{AB}(i\omega_n) = \int_0^\beta d\tau e^{i\omega_n \tau} \mathcal{C}_{AB}(\tau) \quad (\text{A.4})$$

with the Matsubara frequencies

$$\omega_n = \begin{cases} \frac{2n\pi}{\beta} & , \text{ for bosons} \\ \frac{(2n+1)\pi}{\beta} & , \text{ for fermions.} \end{cases} \quad (\text{A.5})$$

The inverse transformation is given by

$$\mathcal{C}_{AB}(\tau) = \frac{1}{\beta} \sum_{n=-\infty}^{\infty} e^{-i\omega_n\tau} \mathcal{C}_{AB}(i\omega_n). \quad (\text{A.6})$$

The real frequency Green's functions (retarded and advanced) can be recovered once the Matsubara Green's functions are evaluated by an analytic continuation:

$$C_{AB}^R(\omega) = \mathcal{C}_{AB}(i\omega_n \rightarrow \omega + i\eta) \quad (\text{A.7})$$

$$C_{AB}^A(\omega) = \mathcal{C}_{AB}(i\omega_n \rightarrow \omega - i\eta) \quad (\text{A.8})$$

with  $\eta \rightarrow 0^+$ .

While working with Matsubara Green's functions, sums over Matsubara frequencies of the form

$$\frac{1}{\beta} \sum_{i\omega_n} \mathcal{C}_{AB}(i\omega_n) e^{i\omega_n\tau}, \tau > 0$$

might be encountered. In order to evaluate these, the residue theorem can be used. To do so, functions with poles at the Matsubara frequencies are needed. These functions are (for bosons and fermions respectively) the well-known bosonic and fermionic distribution functions (if they are considered as functions of  $z \in \mathbb{C}$ ):

$$n_B(z) = \frac{1}{e^{\beta z} - 1}, \quad \text{poles for } z = \frac{i2n\pi}{\beta} \quad (\text{A.9})$$

$$n_F(z) = \frac{1}{e^{\beta z} + 1}, \quad \text{poles for } z = \frac{i(2n+1)\pi}{\beta} \quad (\text{A.10})$$

The residues of these functions are  $\text{res}(n_B; i\omega_n) = \frac{1}{\beta}$  and  $\text{res}(n_F; i\omega_n) = -\frac{1}{\beta}$ . Thus, fermionic Matsubara sums can be rewritten as

$$\frac{1}{\beta} \sum_{i\omega_n} \mathcal{C}_{AB}(i\omega_n) e^{i\omega_n\tau} = - \oint_c \frac{dz}{2\pi i} n_F(z) \mathcal{C}_{AB}(i\omega_n) \quad (\text{A.11})$$

(similar formulas exist for bosonic Green's function). Thereby,  $c$  labels a contour enclosing all poles of the distribution function.

Finally, the Matsubara Green's function can be calculated, just as real-time Green's functions, via the equation of motion technique. This technique is nothing but the transcript of the Schrödinger equation to Green's functions. The basic ingredient is the use of the Heisenberg equation of motion for an operator  $A(t)$ , given by  $i\frac{d}{dt}A(t) = [A(t), H] + i(\frac{\partial}{\partial t}A_S(t))_H$  (noting  $A(t)$  an operator in the Heisenberg picture,  $A_S(t)$  the same operator in the Schrödinger picture and  $(\cdot)_H$  the entity  $(\cdot)$  in the Heisenberg picture). In terms of imaginary-time, this equation yields

$$\frac{d}{d\tau}A(\tau) = \frac{\partial}{\partial\tau}A(\tau) = [H, A(\tau)]. \quad (\text{A.12})$$

The imaginary unit  $i$  has disappeared as a consequence of the imaginary-time formalism. Applying these relations to the Matsubara Green's function, the equation of motion reads (with  $+$  for bosons and  $-$  for fermions):

$$\begin{aligned}
\frac{d}{d\tau}\mathcal{C}_{AB}(\tau) &= \frac{\partial}{\partial\tau}\{-\theta(\tau)\langle A(\tau)B(0)\rangle - (\pm)\theta(-\tau)\langle B(0)A(\tau)\rangle\} \\
&= -\delta(\tau)\langle A(\tau)B(0) - (\pm)B(0)A(\tau)\rangle - \langle T_\tau[H, A](\tau)B(0)\rangle \\
&= -\delta(\tau)\langle [A(0), B(0)]_\pm\rangle - \langle T_\tau[H, A](\tau)B(0)\rangle
\end{aligned} \tag{A.13}$$



# Appendix B

## Analytic continuation

Whilst dealing with Green's functions, it is often convenient to work in the Matsubara imaginary-time formalism. Nevertheless, physical quantities are related to the real-time Green's functions. To establish the link between these two, Lehmann representation for generic imaginary-time Green's functions  $\mathcal{C}_{AB}(\tau, \tau')$  and retarded real-time Green's functions  $C_{AB}^R(t, t')$  can be used. The latter are defined by

$$\mathcal{C}_{AB}(\tau, \tau') = -\langle T_\tau A(\tau)B(\tau') \rangle \quad (\text{B.1})$$

and

$$C_{AB}^R(t, t') = -i\theta(t - t')\langle [A(t), B(t')]_\pm \rangle. \quad (\text{B.2})$$

These expressions can readily be Fourier transformed and rewritten in Lehmann representation, which yields

$$C_{AB}(i\omega_n) = \frac{1}{Z} \sum_{n, n'} \frac{\langle n|A|n'\rangle\langle n'|B|n\rangle}{i\omega_n + E_n - E_{n'}} (e^{-\beta E_n} - (\pm)e^{-\beta E_{n'}}) \quad (\text{B.3})$$

and

$$C_{AB}^R(\omega) = \frac{1}{Z} \sum_{n, n'} \frac{\langle n|A|n'\rangle\langle n'|B|n\rangle}{\omega + E_n - E_{n'} + i\eta} (e^{-\beta E_n} - (\pm)e^{-\beta E_{n'}}), \quad (\text{B.4})$$

where  $Z$  is the system's partition function,  $|n\rangle$  and  $|n'\rangle$  the eigenstates of its Hamiltonian. The sign  $+$  ( $-$ ) is for bosonic (fermionic) operators and  $\eta \rightarrow 0^+$ .

Now, the remarks in appendix A on the recovery of the retarded Green's function from the Matsubara Green's function by an analytic continuation  $i\omega_n \rightarrow \omega + i\eta$  are obvious. Nevertheless, this analytic continuation needs to be done carefully. Especially, the above derivation only holds if the Matsubara Green's function has the form of a rational function.

The analytic continuation is not always trivial. Fortunately, working the above Lehmann representation, a helpful relation can be derived:

$$\begin{aligned} C_{AB}^R(\omega) &= \frac{1}{Z} \sum_{n, n'} \frac{\langle n|A|n'\rangle\langle n'|B|n\rangle}{\omega + E_n - E_{n'} + i\eta} (e^{-\beta E_n} - (\pm)e^{-\beta E_{n'}}) \\ &= \frac{1}{Z} \sum_{n, n'} \langle n|A|n'\rangle\langle n'|B|n\rangle (e^{-\beta E_n} - (\pm)e^{-\beta E_{n'}}) \cdot \left( \mathcal{P} \frac{1}{\omega + E_n - E_{n'}} - i\pi\delta(\omega + E_n - E_{n'}) \right), \end{aligned} \quad (\text{B.5})$$

and thus

$$\text{Im}\{C_{AB}^R(\omega)\} = \frac{-i\pi}{Z} \sum_{n,n'} \langle n|A|n'\rangle \langle n'|B|n\rangle (e^{-\beta E_n} - (\pm)e^{-\beta E_{n'}}) \delta(\omega + E_n - E_{n'}) . \quad (\text{B.6})$$

Using this equation, the Matsubara Green's function can be written as

$$\mathcal{C}_{AB}(i\omega_n) = - \int \frac{d\mathcal{E}}{\pi} \frac{\text{Im}\{C_{AB}^R(\mathcal{E})\}}{i\omega_n - \mathcal{E}} = \int \frac{d\mathcal{E}}{\pi} \frac{\text{Im}\{C_{AB}^R(\mathcal{E})\}}{\omega_n^2 - \mathcal{E}^2} (i\omega_n + \mathcal{E}) . \quad (\text{B.7})$$

Finally, an instructive example shall be inspected, i.e. the analytic continuation of the function

$$\mathcal{C}(i\omega_n) = \frac{1}{\sqrt{\Delta^2 + \omega_n^2}} = \frac{1}{\sqrt{\Delta^2 - (i\omega_n)^2}} . \quad (\text{B.8})$$

The latter is particularly interesting because an analytic continuation of this type is needed in section 2.2.2.

If  $|\Delta| > |\omega_n|$ , the continuation is straightforward and yields

$$C^R(\omega) = \frac{1}{\sqrt{\Delta^2 - (\omega + i\eta)^2}} \stackrel{|\Delta| \geq |\omega_n|}{=} \frac{1}{\sqrt{\Delta^2 - \omega^2}} . \quad (\text{B.9})$$

If  $|\Delta| < |\omega_n|$ , the continuation is a priori not obvious:

$$C^R(\omega) = \frac{1}{\sqrt{\Delta^2 - (\omega + i\eta)^2}} \stackrel{|\Delta| \leq |\omega_n|}{=} \frac{1}{\sqrt{-(\omega^2 - \Delta^2)}} \stackrel{?}{=} \begin{cases} \frac{+i}{\sqrt{\omega^2 - \Delta^2}} \\ \frac{-i}{\sqrt{\omega^2 - \Delta^2}} \end{cases} \quad (\text{B.10})$$

Which of the two signs is the right one? Or may there be different signs for different values of  $\omega$ ? These questions can be answered using equation (B.7). Firstly,  $\mathcal{C}(i\omega_n) = \frac{1}{\sqrt{\Delta^2 + \omega_n^2}}$  is an even function of  $\omega_n$  and entirely real. This means that  $\text{Im}\{C^R(\mathcal{E})\}$  needs to be an odd function of  $\mathcal{E}$ . Furthermore,  $\mathcal{C}(i\omega_n)$  is  $> 0$ , which yields the ansatz

$$C^R(\omega) = \begin{cases} \frac{1}{\sqrt{\Delta^2 - \omega^2}} , & |\Delta| > |\omega_n| \\ \frac{+i \text{sgn}(\omega)}{\sqrt{\omega^2 - \Delta^2}} , & |\Delta| < |\omega_n| . \end{cases} \quad (\text{B.11})$$

Using equation (B.7) it can easily be checked that this is indeed the correct analytic continuation.

# Appendix C

## Derivation of the superconducting single dot's Green's functions

The Green's functions of the non-interacting superconducting single dot system are most conveniently derived in Nambu notation using the spinors defined in section 2.2.1. The Green's functions then become  $2 \times 2$  matrices. The dot's Green's function is given by

$$\begin{aligned} \widehat{G}_{d,d}^0(\tau) &= -\langle T_\tau \Psi_D(\tau) \Psi_D^\dagger(0) \rangle \\ &= \begin{pmatrix} -\langle T_\tau d_\uparrow(\tau) d_\uparrow^\dagger(0) \rangle & -\langle T_\tau d_\uparrow(\tau) d_\downarrow(0) \rangle \\ -\langle T_\tau d_\downarrow^\dagger(\tau) d_\uparrow^\dagger(0) \rangle & -\langle T_\tau d_\downarrow^\dagger(\tau) d_\downarrow(0) \rangle \end{pmatrix}. \end{aligned} \quad (\text{C.1})$$

The system's other Green's function are defined by

$$\widehat{G}_{\vec{k},d}^{U=0}(\tau) = -\langle T_\tau \Psi_{\vec{k},i}(\tau) \Psi_D^\dagger(0) \rangle, \quad (\text{C.2})$$

$$\widehat{G}_{\vec{k},\vec{k}'}^{U=0}(\tau) = -\langle T_\tau \Psi_{\vec{k},i}(\tau) \Psi_{\vec{k}',i}^\dagger(0) \rangle. \quad (\text{C.3})$$

They are evaluated using the equation of motion (see appendix A),

$$\frac{d}{d\tau} \widehat{G}_{AB}(\tau) = -\delta(\tau) \langle \{A(0), B(0)\} \rangle - \langle T_\tau \left( \frac{d}{d\tau} A \right) (\tau) B(0) \rangle. \quad (\text{C.4})$$

Thus, the imaginary-time derivatives of the different spinors need to be calculated:

$$\begin{aligned} \frac{\partial}{\partial \tau} d_\uparrow(\tau) &= [H_0, d_\uparrow(\tau)] = -\epsilon_d d_\uparrow(\tau) - \sum_{\vec{k},i} t e^{i\frac{1}{2}\varphi_i} c_{\vec{k},\uparrow,i}(\tau), \\ \frac{\partial}{\partial \tau} d_\downarrow^\dagger(\tau) &= [H_0, d_\downarrow^\dagger(\tau)] = \epsilon_d d_\downarrow^\dagger(\tau) + \sum_{\vec{k},i} t e^{-i\frac{1}{2}\varphi_i} c_{\vec{k},\downarrow,i}^\dagger(\tau) \\ \Rightarrow \frac{\partial}{\partial \tau} \Psi_D(\tau) &= -\widehat{H}_D \Psi_D(\tau) - \sum_{\vec{k},i} \widehat{H}_{T_i} \Psi_{\vec{k},i}(\tau). \end{aligned} \quad (\text{C.5})$$

$$\begin{aligned}
\frac{\partial}{\partial \tau} c_{\vec{k}, \uparrow, i}(\tau) &= [H_0, c_{\vec{k}, \uparrow, i}(\tau)] = -\epsilon_{\vec{k}, i} c_{\vec{k}, \uparrow, i}(\tau) + \Delta c_{-\vec{k}, \downarrow, i}^\dagger(\tau) - t e^{-i\frac{1}{2}\varphi_i} d_\uparrow(\tau), \\
\frac{\partial}{\partial \tau} c_{-\vec{k}, \downarrow, i}^\dagger(\tau) &= [H_0, c_{-\vec{k}, \downarrow, i}^\dagger(\tau)] = \epsilon_{-\vec{k}, i} c_{-\vec{k}, \downarrow, i}^\dagger(\tau) + \Delta_* c_{\vec{k}, \uparrow, i}(\tau) + t e^{i\frac{1}{2}\varphi_i} d_\downarrow^\dagger(\tau) \\
\Rightarrow \frac{\partial}{\partial \tau} \Psi_{\vec{k}}(\tau) &= -\hat{H}_{\vec{k}, i} \Psi_{\vec{k}, i}(\tau) - \hat{H}_{T_i}^\dagger \Psi_D(\tau). \tag{C.6}
\end{aligned}$$

Using (C.4) - (C.6), the time derivatives of the Green's functions (C.1) - (C.3) take the form

$$\frac{\partial}{\partial \tau} \hat{G}_{d,d}^0(\tau) = -\delta(\tau) \mathbf{1} - \hat{H}_D \hat{G}_{d,d}^0(\tau) - \sum_{\vec{k}, i} \hat{H}_{T_i} \hat{G}_{\vec{k}, d}^{U=0}(\tau), \tag{C.7}$$

$$\frac{\partial}{\partial \tau} \hat{G}_{\vec{k}, d}^{U=0}(\tau) = -\hat{H}_{\vec{k}, i} \hat{G}_{\vec{k}, d}^{U=0}(\tau) - \hat{H}_{T_i}^\dagger \hat{G}_{d,d}^0(\tau). \tag{C.8}$$

Fourier transforming and combining these expressions yields

$$\hat{G}_{d,d}^0(i\omega_n) = \left( i\omega_n \mathbf{1} - \hat{H}_D - \sum_{\vec{k}, i} \hat{H}_{T_i} \left( i\omega_n \mathbf{1} - \hat{H}_{\vec{k}, i} \right)^{-1} \hat{H}_{T_i}^\dagger \right)^{-1}, \tag{C.9}$$

$$\hat{G}_{\vec{k}, d}^{U=0}(i\omega_n) = \left( i\omega_n \mathbf{1} - \hat{H}_{\vec{k}, i} \right)^{-1} \hat{H}_{T_i}^\dagger \hat{G}_{d,d}^0(i\omega_n). \tag{C.10}$$

With these considerations, the actual expression of the Green's function  $\hat{G}_{d,d}^0(\tau)$  can be computed. The most difficult step is the inversion of a  $2 \times 2$  matrix, i.e.

$$\begin{aligned}
\left( i\omega_n \mathbf{1} - \hat{H}_{\vec{k}, i} \right)^{-1} &= \begin{pmatrix} i\omega_n - \epsilon_{\vec{k}, i} & \Delta \\ \Delta & i\omega_n + \epsilon_{\vec{k}, i} \end{pmatrix}^{-1} \\
&= \frac{1}{(i\omega_n)^2 - \epsilon_{\vec{k}, i}^2 - \Delta^2} \begin{pmatrix} i\omega_n + \epsilon_{\vec{k}, i} & -\Delta \\ -\Delta & i\omega_n - \epsilon_{\vec{k}, i} \end{pmatrix}. \tag{C.11}
\end{aligned}$$

The next step is the calculation of

$$\sum_{\vec{k}, i} \hat{H}_{T_i} \left( i\omega_n \mathbf{1} - \hat{H}_{\vec{k}, i} \right)^{-1} \hat{H}_{T_i}^\dagger = \sum_i \hat{H}_{T_i} \hat{G}_i^0 \hat{H}_{T_i}^\dagger \tag{C.12}$$

with

$$\hat{G}_i^0 = \sum_{\vec{k}} \frac{1}{(i\omega_n)^2 - \epsilon_{\vec{k}, i}^2 - \Delta^2} \begin{pmatrix} i\omega_n + \epsilon_{\vec{k}, i} & -\Delta \\ -\Delta & i\omega_n - \epsilon_{\vec{k}, i} \end{pmatrix}. \tag{C.13}$$

In the above equation,  $\hat{G}_i^0$  is the bare Green's function, i.e. decoupled from the dot, for the lead  $i$  ( $i = L, R$ ). In order to evaluate  $\hat{G}_i^0$ , the electrons in the leads are supposed to be in a flat and infinite band with a constant density of states  $\rho_0$ , which leads to

$$\begin{aligned}
\widehat{G}_i^0 &= \sum_{\vec{k}} \frac{1}{(i\omega_n)^2 - \epsilon_{\vec{k},i}^2 - \Delta^2} \begin{pmatrix} i\omega_n + \epsilon_{\vec{k},i} & -\Delta \\ -\Delta & i\omega_n - \epsilon_{\vec{k},i} \end{pmatrix} \\
&\rightarrow \int_{-\infty}^{\infty} d\epsilon \rho_0 \frac{1}{(i\omega_n)^2 - \epsilon^2 - \Delta^2} \begin{pmatrix} i\omega_n + \epsilon & -\Delta \\ -\Delta & i\omega_n - \epsilon \end{pmatrix} \\
&= \frac{\pi\rho_0}{\sqrt{\Delta^2 - (i\omega_n)^2}} \begin{pmatrix} -i\omega_n & \Delta \\ \Delta & -i\omega_n \end{pmatrix}.
\end{aligned} \tag{C.14}$$

Putting everything together yields the final expression of the dot's Green's function,

$$\widehat{G}_{d,d}^0(i\omega_n) = \frac{1}{\text{Det}(i\omega_n)} \begin{pmatrix} i\omega_n + \epsilon_d - \sum_i t^2 G_{i,22}^0 & -\sum_i t^2 e^{-i\varphi_i} G_{i,12}^0 \\ -\sum_i t^2 e^{i\varphi_i} G_{i,21}^0 & i\omega_n - \epsilon_d - \sum_i t^2 G_{i,11}^0 \end{pmatrix}, \tag{C.15}$$

where  $G_{i,\alpha\beta}^0$  denotes the matrix element  $\widehat{G}_i^0|_{\alpha,\beta}$  and

$$\begin{aligned}
\text{Det}(i\omega_n) &= \left| \widehat{G}_{d,d}^0(i\omega_n)^{-1} \right| \\
&= (i\omega_n(1 + \alpha(i\omega_n)) - \epsilon_d) \cdot (i\omega_n(1 + \alpha(i\omega_n)) + \epsilon_d) \\
&\quad - \left( \alpha(i\omega_n)\Delta \cos\left(\frac{\varphi}{2}\right) \right)^2.
\end{aligned} \tag{C.16}$$

In the above equation,  $\varphi = \varphi_L - \varphi_R$  is the phase difference of the two superconducting electrodes and

$$\alpha(i\omega_n) = \frac{2\pi\rho_0 t^2}{\sqrt{\Delta^2 - (i\omega_n)^2}} = \frac{\Gamma}{\sqrt{\Delta^2 - (i\omega_n)^2}}. \tag{C.17}$$



# Appendix D

## The Bogoliubov transformation for the effective local Hamiltonian

The diagonalization of the quantum dot system's effective BCS Hamiltonian can be achieved using a transformation proposed by Bogoliubov. In the present case of an effective local Hamiltonian, the first step is to rewrite  $H_{eff} = \sum_{\sigma} \xi_d d_{\sigma,1}^{\dagger} d_{\sigma,1} - \left( \Gamma_{\varphi} d_{\uparrow,1}^{\dagger} d_{\downarrow,1}^{\dagger} + h.c. \right) + \frac{U_1}{2} \left( \sum_{\sigma} d_{\sigma,1}^{\dagger} d_{\sigma,1} - 1 \right)^2$  with  $\Gamma_{\varphi} = \Gamma 2/\pi \arctan(D/\Delta) \cos(\varphi/2)$  in Nambu notation. For the non-magnetic subspace, this yields

$$H_{eff} = \begin{pmatrix} d_{\uparrow,1}^{\dagger} \\ d_{\downarrow,1}^{\dagger} \end{pmatrix}^{\dagger} \begin{pmatrix} \xi_d & -\Gamma_{\varphi} \\ -\Gamma_{\varphi}^* & -\xi_d \end{pmatrix} \begin{pmatrix} d_{\uparrow,1} \\ d_{\downarrow,1} \end{pmatrix} + \xi_d + \frac{U_1}{2}. \quad (\text{D.1})$$

The Bogoliubov transformation consists of the ansatz

$$\begin{pmatrix} \gamma_{\uparrow} \\ \gamma_{\downarrow} \end{pmatrix} = \begin{pmatrix} u^* & v \\ -v^* & u \end{pmatrix} \begin{pmatrix} d_{\uparrow,1} \\ d_{\downarrow,1} \end{pmatrix}. \quad (\text{D.2})$$

The constraint for  $\gamma_{\sigma}$  to be a fermionic operator yields  $|u|^2 + |v|^2 = 1$ , derivable by a straightforward calculation using the commutation relations. This is why  $|u|$  and  $|v|$  can be written as  $|u| = \cos(\theta)$  and  $|v| = \sin(\theta)$ . These new operators are now inserted into  $H_{eff}$ . The above transformation diagonalizes the Hamiltonian if the equations

$$\tan(2\theta) = -\frac{|\Gamma_{\varphi}|}{\xi_d} \text{ and} \quad (\text{D.3})$$

$$\theta_u + \theta_v = \frac{\varphi_L + \varphi_R}{2} \quad (\text{D.4})$$

are fulfilled (where the notations  $u = |u|e^{i\theta_u}$  and  $v = |v|e^{i\theta_v}$  have been used). Using these results yields

$$H_{eff} = \begin{pmatrix} \gamma_{\uparrow} \\ \gamma_{\downarrow} \end{pmatrix}^{\dagger} \begin{pmatrix} E_+ & 0 \\ 0 & E_- \end{pmatrix} \begin{pmatrix} \gamma_{\uparrow} \\ \gamma_{\downarrow} \end{pmatrix}, \quad (\text{D.5})$$

with  $E_{\pm} = \pm \sqrt{\xi_d^2 + \Gamma_{\varphi}^2} + \xi_d + \frac{U_1}{2}$ . In addition, it can be shown that  $|u|^2 = \frac{1}{2} \left( 1 + \frac{\xi_d}{\sqrt{\xi_d^2 + \Gamma_{\varphi}^2}} \right)$  and  $|v|^2 = \frac{1}{2} \left( 1 - \frac{\xi_d}{\sqrt{\xi_d^2 + \Gamma_{\varphi}^2}} \right)$ . Finally, as the absolute value of the superconductors'

phases is without physical meaning, equation (D.4) implies that  $u, v \in \mathbb{R}$  is always a possible choice.

# Appendix E

## Some basics of quantum field theory

### E.1 Introduction

Quantum field theory (often referred to with the abbreviation QFT) has been developed in the mid-20<sup>th</sup>-century and can be regarded as the quantum mechanics analogue of the classical Hamilton-Lagrange formalism. In the latter, the (classical) trajectory  $q(t)$  of a particle corresponds to an extremum of the action  $S[q(t)] = \int_{t_1}^{t_2} L[q(t), \dot{q}(t), t] dt$ .

The idea behind quantum field theory is to generalize this formalism to quantum mechanics, which has initially been formulated in a Hamiltonian approach. Pioneer work was done by Richard P. Feynman [86], who developed the so-called Feynman path integral for single particles. Different to classical particles, a quantum particle does not need to obey strict energy and momentum conservation, but has a Heisenberg uncertainty. Thus, also trajectories which are not the “optimal”, classical one are possible. Now, in terms of an action-based description, this means that not only the classical trajectory, but also other trajectories “close” to the classical one contribute to the action  $\mathcal{S}[q(t)] = \int_{t_1}^{t_2} L[q(t), \dot{q}(t), t] dt$ . Still, these trajectories have a smaller contribution than the classical one.

As an example for such processes, a tunneling event out of a potential well (e.g. of an electron in a free atom) may be considered. Classically, the particle has no chance of leaving the well. Nevertheless, a quantum mechanics particle may tunnel through the potential barrier and leave the well. This explains for example the spontaneous disintegration of radioactive atoms.

The generalization of the Feynman path integral to many-particle physics is called “quantum field theory”. For more explicit explanations, the reader is referred to references [87] or [88], for example.

### E.2 Grassmann numbers

As suggested by its name, the quantum field theory uses second quantization particle fields. Two types of fields need to be distinguished, namely bosonic and fermionic fields. Different to bosonic fields, which commute, fermionic fields anticommute. Whereas bosonic fields can be described by complex numbers (that commute), fermionic fields can not be dealt with in a “standard” way. Indeed, a new kind of numbers needs to be introduced: the so-called Grassmann numbers. Not very much needs to be known about them

(for instance, no norm is defined for Grassmann numbers, they can thus not be regarded as “small” or “big”), but they have some important properties.

First of all, Grassmann numbers anticommute with Grassmann numbers and fermionic operators,

$$[\eta, \eta']_+ = [\eta, c]_+ = [\eta, c^\dagger]_+ = 0 . \quad (\text{E.1})$$

In particular, this implies that  $\eta\eta = 0$ . Secondly, functions of Grassmann numbers are defined by their Taylor expansion:

$$f(\eta_1, \dots, \eta_k) = \sum_{n=0}^{\infty} \sum_{i_1, \dots, i_n=1}^k \frac{1}{n!} \frac{\partial^n f}{\partial \eta_{i_1} \cdots \partial \eta_{i_n}} \Big|_{\eta_j=0 \forall j} \eta_{i_1} \cdots \eta_{i_n} . \quad (\text{E.2})$$

Thirdly, integrals over Grassmann numbers are defined as

$$\int d\eta_i = 0 \text{ and} \quad (\text{E.3})$$

$$\int d\eta_i \eta_j = \delta_{i,j} . \quad (\text{E.4})$$

This implies that integration and differentiation of Grassmann numbers is the same:

$$\int d\eta f(\eta) = \int d\eta \left( f(0) + \frac{\partial f}{\partial \eta} \Big|_{\eta=0} \eta \right) = \frac{\partial f}{\partial \eta} \Big|_{\eta=0} = \frac{\partial f}{\partial \eta} . \quad (\text{E.5})$$

### E.3 The partition function

The basis for all calculations in quantum field theory is the partition function  $Z = \text{tr}\{e^{-\beta(H-\mu N)}\}$ . How can this trace be evaluated for a general, fermionic Hamiltonian  $H$ , containing any kind of combinations of creation and annihilation operators  $c^\dagger$  and  $c$ ? The answer of quantum field theory is the use of so-called coherent states  $|\eta\rangle$  which are eigenstates of the annihilation operator,  $c|\eta\rangle = \eta|\eta\rangle$ . The fermionic coherent states are given by

$$|\eta\rangle = \exp\{-\eta c^\dagger\} |0\rangle \quad (\text{E.6})$$

(where  $|0\rangle$  denotes the vacuum).

The analog of a hermitian conjugate of a coherent state is

$$\langle \eta| = \langle 0| \exp\{-c\bar{\eta}\} = \langle 0| \exp\{\bar{\eta}c\} . \quad (\text{E.7})$$

Note that Grassmann numbers are not complex numbers. This is why  $\bar{\eta}$  is not the complex conjugate of  $\eta$ , but has to be seen as a different and completely independent Grassmann number. Therefore, the generalization of a Gaussian integral of complex numbers,  $\int dr d\varphi e^{-z^*z} = \int d\text{Re}\{z\} d\text{Im}\{z\} e^{-z^*z} = \pi$  reads

$$\int d\eta d\bar{\eta} e^{-\bar{\eta}a\eta} = a . \quad (\text{E.8})$$

It shall again be insisted on the fact that the integration over  $\eta$  and  $\bar{\eta}$  are independent. The overlap of two coherent states is found to be

$$\langle \eta' | \eta \rangle = \exp \{ \bar{\eta}' \eta \} \quad (\text{E.9})$$

and because of equations (E.3) and (E.4), the Grassmann number's completeness relation is

$$\mathbb{1} = \int d(\bar{\eta}, \eta) e^{-\bar{\eta}' \eta} | \eta \rangle \langle \eta | . \quad (\text{E.10})$$

With these basic relations, the partition function for fermions can finally be derived. Starting point is the general definition

$$Z = \text{tr} \{ e^{-\beta(H - \mu N)} \} = \sum_n \langle n | e^{-\beta(H - \mu N)} | n \rangle . \quad (\text{E.11})$$

The above Hamiltonian is written in terms of fermionic creation and annihilation operators,  $H = H(c, c^\dagger)$ . These operators now need to be in “normal order”, i.e. all creation operators at the left side of the different terms and the annihilation operators at the right side. The Hamiltonian is then given by a sum of terms of the form  $c_i^\dagger c_j^\dagger \cdots c_k^\dagger c_l c_m \cdots c_n$ . Then, a  $\mathbb{1}$  of coherent states is injected, yielding

$$Z = \int d(\bar{\eta}, \eta) e^{-\bar{\eta}' \eta} \sum_n \langle n | \eta \rangle \langle \eta | e^{-\beta(H(c^\dagger, c) - \mu N(c^\dagger, c))} | n \rangle . \quad (\text{E.12})$$

Finally,  $\langle n | \eta \rangle \langle \eta | n \rangle = \langle -\eta | n \rangle \langle n | \eta \rangle$  is used. Note that there is a sign change due to the commutation of two fermionic fields [87]. Furthermore,  $\mathbb{1} = \sum_n | n \rangle \langle n |$  is always true. This yields

$$Z = \int d(\bar{\eta}, \eta) e^{-\bar{\eta}' \eta} \langle -\eta | e^{-\beta(H(c^\dagger, c) - \mu N(c^\dagger, c))} | \eta \rangle . \quad (\text{E.13})$$

Although it would be tempting to simply replace the fermionic operators in  $H(c^\dagger, c)$  and  $N(c^\dagger, c)$  by the corresponding Grassmann fields, different operators and Grassmann fields do in general not commute. This is why  $\beta(H(c^\dagger, c) - \mu N(c^\dagger, c))$  has to be subdivided into small intervals  $\delta = \frac{\beta}{N}$ . The exponential function can now be Taylor expanded. Terms that include two operators (which might not commute) are small as  $\delta^2$  and can be neglected,

$$\begin{aligned} \langle -\eta | e^{-\beta(H(c^\dagger, c) - \mu N(c^\dagger, c))} | \eta \rangle &= \langle -\eta | e^{-\delta \sum_{n=0}^{N-1} (H(c^\dagger, c) - \mu N(c^\dagger, c))} | \eta \rangle \\ &\approx \langle -\eta | \prod_{n=0}^{N-1} (1 - \delta (H(c^\dagger, c) - \mu N(c^\dagger, c))) | \eta \rangle . \end{aligned} \quad (\text{E.14})$$

Now, a “Grassmann- $\mathbb{1}$ ” is inserted between the different time steps and the product can be re-exponentiated. This yields

$$Z = \int \prod_{n=0}^N d(\bar{\eta}^n, \eta^n) e^{-\delta \sum_{n=0}^{N-1} [\delta^{-1} (\bar{\eta}^n - \bar{\eta}^{n+1}) \eta^n + H(\bar{\eta}^{n+1}, \eta^n) - \mu N(\bar{\eta}^{n+1}, \eta^n)]} . \quad (\text{E.15})$$

If the limit  $N \rightarrow \infty$  is taken, the partition function becomes

$$Z = \int D(\bar{\eta}, \eta) e^{-S[\bar{\eta}, \eta]} \quad \text{with} \quad (\text{E.16})$$

$$S[\bar{\eta}, \eta] = \int_0^\beta d\tau \left[ \bar{\eta} \frac{\partial}{\partial \tau} \eta + H(\bar{\eta}, \eta) - \mu N(\eta, \eta) \right]$$

with the conditions  $\bar{\eta}(0) = -\bar{\eta}(\beta)$  and  $\eta(0) = -\eta(\beta)$ . Note that in the above derivation, the definition

$$\sum_n \delta^{-1}(\bar{\eta}^n - \bar{\eta}^{n+1}) \eta^n = \sum_n \frac{\bar{\eta}^n - \bar{\eta}^{n+1}}{\delta} \eta^n \xrightarrow{N \rightarrow \infty} \int d\tau \left( -\frac{\partial}{\partial \tau} \bar{\eta} \right) \eta = \int d\tau \bar{\eta} \frac{\partial}{\partial \tau} \eta \quad (\text{E.17})$$

has been used. Nonetheless, as Grassmann numbers do not have a defined norm,  $\bar{\eta}_n - \bar{\eta}_{n+1}$  can not be regarded as small, even if  $N \rightarrow \infty$  [88]. What are the consequences of the simplification  $\frac{\bar{\eta}^n - \bar{\eta}^{n+1}}{\delta} \eta^n \xrightarrow{N \rightarrow \infty} \left( -\frac{\partial}{\partial \tau} \bar{\eta} \right) \eta$ ? If for example the Matsubara Fourier transform is taken, the term  $-\frac{\partial}{\partial \tau}$  yields an  $i\omega$ . In fact, if the above approximation is not used, this term would be replaced by  $e^{i\omega} - 1$ . This means that only quantities insensitive to high frequencies are fully captured by the above approximation. Especially the free energy may come out wrong. Nevertheless, all correlation functions will be reproduced correctly: they are given by derivatives of the free energy, which makes the integrals sufficiently insensitive to high frequencies.

Fairly often, calculations will be done in the above mentioned Matsubara frequency space. Using the standard Matsubara frequencies  $\omega_n$ , the Fourier transforms of the fields are given by

$$\eta(\tau) = \frac{1}{\beta} \sum_{\omega_n} \eta_n e^{-i\omega_n \tau} \quad \text{and} \quad \eta_n = \frac{1}{\beta} \int_0^\beta d\tau \eta(\tau) e^{i\omega_n \tau}, \quad (\text{E.18})$$

$$\bar{\eta}(\tau) = \frac{1}{\beta} \sum_{\omega_n} \bar{\eta}_n e^{i\omega_n \tau} \quad \text{and} \quad \bar{\eta}_n = \frac{1}{\beta} \int_0^\beta d\tau \bar{\eta}(\tau) e^{-i\omega_n \tau}. \quad (\text{E.19})$$

The Fourier transformation of an action

$$S[\bar{\eta}, \eta] = \int_0^\beta d\tau \left[ \sum_{i,j} \bar{\eta}_i(\tau) \left[ \left( \frac{\partial}{\partial \tau} - \mu \right) \delta_{i,j} + h_{i,j} \right] \eta_j(\tau) + \sum_{i,j,k,l} V_{i,j,k,l} \bar{\eta}_i(\tau) \bar{\eta}_j(\tau) \eta_k(\tau) \eta_l(\tau) \right] \quad (\text{E.20})$$

yields

$$S[\bar{\eta}, \eta] = \sum_{i,j,\omega_n} \bar{\eta}_{i,n} [(-i\omega_n - \mu) \delta_{i,j} + h_{i,j}] \eta_{j,n} + \frac{1}{\beta} \sum_{i,j,k,l,\{\omega_{n_i}\}} V_{i,j,k,l} \bar{\eta}_{i,n_1} \bar{\eta}_{j,n_2} \eta_{k,n_3} \eta_{l,n_4} \delta_{n_1+n_2,n_3+n_4} \quad (\text{E.21})$$

(using the identity  $\int_0^\beta d\tau e^{-i\omega_n \tau} = \beta \delta_{\omega_n,0}$ ). Note that  $(-i\omega_n - \mu) \delta_{i,j} + h_{i,j}$  is an inverse interaction-less Green's function  $G_0^{-1}(i\omega_n)$  (c.f. the Green's functions in appendix C).

# Appendix F

## Derivation of the effective action

A fairly compact and efficient way to derive the energy corrections of a perturbed system is the use of quantum field theory, a formalism that directly yields the system's partition function. Some remarks on this formalism can be found in appendix E. Just as for the creation and annihilation operators, Nambu notation is used for the Grassmann fields:

$$\Psi_{\vec{k},i}(\tau) = \begin{pmatrix} c_{\vec{k},\uparrow,i}(\tau) \\ \bar{c}_{-\vec{k},\downarrow,i}(\tau) \end{pmatrix}, \quad \bar{\Psi}_{\vec{k},i}(\tau) = (\bar{c}_{\vec{k},\uparrow,i}(\tau), c_{-\vec{k},\downarrow,i}(\tau)) ,$$

$$\Psi_d(\tau) = \begin{pmatrix} d_{\uparrow}(\tau) \\ \bar{d}_{\downarrow}(\tau) \end{pmatrix}, \quad \bar{\Psi}_d(\tau) = (\bar{d}_{\uparrow}(\tau), d_{\downarrow}(\tau)) .$$

Their Fourier transforms are given by

$$\Psi_n = \frac{1}{\sqrt{\beta}} \int_0^\beta d\tau \Psi(\tau) e^{i\omega_n \tau}, \quad \Psi(\tau) = \frac{1}{\sqrt{\beta}} \sum_{\omega_n} \Psi_n e^{-i\omega_n \tau} ,$$

$$\bar{\Psi}_n = \frac{1}{\sqrt{\beta}} \int_0^\beta d\tau \bar{\Psi}(\tau) e^{-i\omega_n \tau}, \quad \bar{\Psi}(\tau) = \frac{1}{\sqrt{\beta}} \sum_{\omega_n} \bar{\Psi}_n e^{i\omega_n \tau} ,$$

where  $\omega_n$  is a Matsubara frequency.

The partition function is

$$Z = \int \mathcal{D}(\bar{\Psi}, \Psi) e^{-S} \tag{F.1}$$

with

$$S = \sum_{\vec{k},i,\omega_n} \bar{\Psi}_{\vec{k},i,n} \underbrace{\begin{pmatrix} -i\omega_n + \epsilon_{\vec{k}} & -\Delta \\ -\Delta & -i\omega_n - \epsilon_{\vec{k}} \end{pmatrix}}_{=-\hat{G}_{\vec{k}i,\vec{k}i}^0^{-1}(i\omega_n)} \Psi_{\vec{k},i,n} \tag{F.2}$$

$$+ \sum_{\vec{k},i,\omega_n} \left( \bar{\Psi}_{d,n} \underbrace{\begin{pmatrix} te^{i\frac{1}{2}\varphi_i} & 0 \\ 0 & -te^{-i\frac{1}{2}\varphi_i} \end{pmatrix}}_{=\hat{H}_{T_i}} \Psi_{\vec{k},i,n} + \bar{\Psi}_{\vec{k},i,n} \begin{pmatrix} te^{-i\frac{1}{2}\varphi_i} & 0 \\ 0 & -te^{i\frac{1}{2}\varphi_i} \end{pmatrix} \Psi_{d,n} \right)$$

$$+ \underbrace{\sum_{\omega_n} \bar{\Psi}_{d,n} \begin{pmatrix} -i\omega_n + \epsilon_d & 0 \\ 0 & -i\omega_n - \epsilon_d \end{pmatrix} \Psi_{d,n}}_{=:S_{\text{dot,local}}} + \int d\tau U \bar{d}_{\uparrow}(\tau) \bar{d}_{\downarrow}(\tau) d_{\downarrow}(\tau) d_{\uparrow}(\tau) ,$$

where  $\mathcal{D}(\bar{\Psi}, \Psi)$  stands for the integration over all present Grassmann fields. As only the dot's state is interesting, it would be advantageous to integrate over the electrodes' fields, and we do that following reference [14]. Nonetheless, due to the mixed term involving a  $\Psi_{d,n}$  and a  $\Psi_{\vec{k},i,n}$ , the electrodes first need to be decoupled from the dot. This is done by shifting the electrodes fields' integration variables according to

$$\Psi_{\vec{k},i,n} \rightarrow \Psi'_{\vec{k},i,n} = \Psi_{\vec{k},i,n} - \Psi_{\vec{k},i,n}^0 \quad \text{and} \quad \bar{\Psi}_{\vec{k},i,n} \rightarrow \bar{\Psi}'_{\vec{k},i,n} = \bar{\Psi}_{\vec{k},i,n} - \bar{\Psi}_{\vec{k},i,n}^0. \quad (\text{F.3})$$

To get rid of the mixed terms,  $\bar{\Psi}_{\vec{k},i,n}^0$  and  $\Psi_{\vec{k},i,n}^0$  are chosen such that  $\left. \frac{\partial S}{\partial \bar{\Psi}'} \right|_{\bar{\Psi}', \Psi'=0} = \left. \frac{\partial S}{\partial \bar{\Psi}'} \right|_{\bar{\Psi}', \Psi'=0} = 0$ . This condition leads to

$$\Psi_{\vec{k},i,n}^0 = \hat{G}_{\vec{k}i, \vec{k}i}^0 \hat{H}_{T_i}^\dagger \Psi_{d,n} \quad \text{and} \quad \bar{\Psi}_{\vec{k},i,n}^0 = \bar{\Psi}_{d,n} \hat{H}_{T_i} \hat{G}_{\vec{k}i, \vec{k}i}^0. \quad (\text{F.4})$$

Incorporating these transformations into the action yields

$$S = \sum_{\vec{k},i,\omega_n} \underbrace{\left( \bar{\Psi}'_{\vec{k},i,n} \left( -\hat{G}_{\vec{k}i, \vec{k}i}^0 \right) \Psi'_{\vec{k},i,n} \right)}_{=:S_{\text{el}}} + \underbrace{\left( \bar{\Psi}_{d,n} \hat{H}_{T_i} \hat{G}_{\vec{k}i, \vec{k}i}^0 \hat{H}_{T_i}^\dagger \Psi_{d,n} \right)}_{=:S_{\text{dot}}} + S_{\text{dot,local}}. \quad (\text{F.5})$$

Now, as the electrodes have been decoupled, the integration over the fields  $\bar{\Psi}'$  and  $\Psi'$  can be performed:

$$Z = \int \mathcal{D}(\bar{\Psi}, \Psi) e^{-S} = \int \mathcal{D}(\bar{\Psi}', \Psi') e^{-S_{\text{el}}} \int \mathcal{D}(\bar{\Psi}_d, \Psi_d) e^{-S_{\text{dot}}} = Z_{\text{el}} \int \mathcal{D}(\bar{\Psi}_d, \Psi_d) e^{-S_{\text{dot}}}, \quad (\text{F.6})$$

where  $Z_{\text{el}}$  is just an irrelevant constant (which will be omitted from now on). The final results are:

$$Z = \int \mathcal{D}(\bar{\Psi}_d, \Psi_d) e^{-S_{\text{dot}}} \quad \text{with} \quad (\text{F.7})$$

$$S_{\text{dot}} = \sum_{\vec{k},i,\omega_n} \bar{\Psi}_{d,n} \hat{H}_{T_i} \hat{G}_{\vec{k}i, \vec{k}i}^0 \hat{H}_{T_i}^\dagger \Psi_{d,n} + \sum_{\omega_n} \bar{\Psi}_{d,n} \begin{pmatrix} -i\omega_n + \epsilon_d & 0 \\ 0 & -i\omega_n - \epsilon_d \end{pmatrix} \Psi_{d,n} \\ + \int d\tau U \bar{d}_\uparrow(\tau) \bar{d}_\downarrow(\tau) d_\downarrow(\tau) d_\uparrow(\tau). \quad (\text{F.8})$$

# Appendix G

## Derivation of the partition function for a single dot

The partition function is derived starting from the action's perturbation expansion in section 3.5.2. The calculations are performed in the operator formalism. The passage into this formalism

- replaces the Grassmann fields by the corresponding operators,
- replaces the  $\int e^{-S_{\text{eff}}}(\cdot)$  by  $Z_{\text{eff}}\langle(\cdot)\rangle_0$ ,
- introduces time-ordering.

This yields two types of terms. While terms like

$$\int_0^\beta d\tau \langle T_\tau d_\uparrow^\dagger(\tau) d_\downarrow^\dagger(\tau) \rangle_0 = \int_0^\beta d\tau \langle T_\tau d_\uparrow^\dagger(0) d_\downarrow^\dagger(0) \rangle_0 = \beta \langle T_\tau d_\uparrow^\dagger(\tau) d_\downarrow^\dagger(\tau) \rangle_0$$

are fairly obvious to deal with, terms like

$$\int_0^\beta d\tau \int_0^\beta d\tau' G_{\vec{k}i\vec{k}i;12}^0(\tau - \tau') \langle T_\tau d_\uparrow^\dagger(\tau) d_\downarrow^\dagger(\tau') \rangle_0$$

seem rather laborious to calculate. Fortunately, the product of two fermionic (or bosonic) Greens functions  $G_a(\tau)$  and  $G_b(\tau)$  obeys  $\int_0^\beta d\tau \int_0^\beta d\tau' G_a(\tau - \tau') G_b(\tau - \tau') = \beta \int_0^\beta d\tau G_a(\tau) G_b(\tau)$  (as can be shown using Fourier transformation). Therefore, the partition function's perturbation expansion is

$$\begin{aligned} Z &= Z_0 - Z_0 t^2 \beta \sum_{\vec{k}, i} \int_0^\beta d\tau \left( G_{\vec{k}i\vec{k}i;11}^0(\tau) \langle T_\tau d_\uparrow^\dagger(\tau) d_\uparrow(0) \rangle_0 \right. \\ &\quad - G_{\vec{k}i\vec{k}i;12}^0(\tau) e^{i\varphi_i} \langle T_\tau d_\uparrow^\dagger(\tau) d_\downarrow^\dagger(0) \rangle_0 - G_{\vec{k}i\vec{k}i;21}^0(\tau) e^{-i\varphi_i} \langle T_\tau d_\downarrow(\tau) d_\uparrow(0) \rangle_0 \\ &\quad \left. + G_{\vec{k}i\vec{k}i;22}^0(\tau) \langle T_\tau d_\downarrow(\tau) d_\downarrow^\dagger(0) \rangle_0 \right) - 2\beta |\Gamma_\varphi| \left( \langle T_\tau d_\uparrow^\dagger(0) d_\uparrow^\dagger(0) \rangle_0 + \langle T_\tau d_\downarrow(\tau) d_\uparrow(0) \rangle_0 \right). \end{aligned} \quad (\text{G.1})$$

In the above equation,  $G_{\vec{k}i\vec{k}i;lm}^0$  is the Fourier transformed Nambu matrix element  $\widehat{G}_{\vec{k}i, \vec{k}i}^0(i\omega_n) \Big|_{l,m}$  and the subscript 0 indicates that the expectation values are statistical averages calculated in the effective local limit. The leads' Green's functions are:

$$\sum_{\vec{k}} G_{\vec{k}\vec{i}\vec{k}\vec{i};11}^0(\tau) = \sum_{\vec{k}} -\frac{\text{sgn}(\tau)}{2} \left( e^{-|\tau|E_{\vec{k}}} + e^{-(\beta-|\tau|)E_{\vec{k}}} \right), \quad (\text{G.2})$$

$$G_{\vec{k}\vec{i}\vec{k}\vec{i};12}^0(\tau) = \frac{\Delta}{2E_{\vec{k}}} \left( e^{-|\tau|E_{\vec{k}}} - 2 \cosh(|\tau|E) n_F(E_{\vec{k}}) \right) \quad (\text{G.3})$$

$$\xrightarrow{T \rightarrow 0\text{K}} \frac{\Delta}{2E_{\vec{k}}} \left( e^{-|\tau|E_{\vec{k}}} - e^{-(\beta-|\tau|)E_{\vec{k}}} \right),$$

with  $E_{\vec{k}} = \sqrt{\epsilon_{\vec{k}}^2 + \Delta^2}$ . Furthermore,  $G_{\vec{k}\vec{i}\vec{k}\vec{i};21}^0(\tau) = G_{\vec{k}\vec{i}\vec{k}\vec{i};12}^0(\tau)^*$  and  $\sum_{\vec{k}} G_{\vec{k}\vec{i}\vec{k}\vec{i};22}^0(\tau) = \sum_{\vec{k}} G_{\vec{k}\vec{i}\vec{k}\vec{i};11}^0(\tau)$ .

As one cannot apply Wick's theorem because of the Coulomb interaction, the dot's Green's functions are calculated using Lehmann representation, which yields (for  $\tau > 0$ )

$$\langle T_{\tau} d_{\uparrow}^{\dagger}(\tau) d_{\uparrow}(0) \rangle_0 = \frac{1}{Z_0} \left( u^2 \left( e^{-E_{\uparrow}^0 \tau} e^{-E_{\uparrow}^0(\beta-\tau)} + e^{-E_{\downarrow}^0 \tau} e^{-E_{\downarrow}^0(\beta-\tau)} \right) + v^2 \left( e^{-E_{\uparrow}^0 \tau} e^{-E_{\uparrow}^0(\beta-\tau)} + e^{-E_{\downarrow}^0 \tau} e^{-E_{\downarrow}^0(\beta-\tau)} \right) \right), \quad (\text{G.4})$$

$$\langle T_{\tau} d_{\uparrow}^{\dagger}(\tau) d_{\downarrow}^{\dagger}(0) \rangle_0 = \frac{1}{Z_0} uv \left( e^{-E_{\downarrow}^0 \tau} e^{-E_{\downarrow}^0(\beta-\tau)} - e^{-E_{\uparrow}^0 \tau} e^{-E_{\uparrow}^0(\beta-\tau)} - e^{-E_{\downarrow}^0 \tau} e^{-E_{\uparrow}^0(\beta-\tau)} + e^{-E_{\uparrow}^0 \tau} e^{-E_{\downarrow}^0(\beta-\tau)} \right), \quad (\text{G.5})$$

$$\langle T_{\tau} d_{\downarrow}(\tau) d_{\uparrow}(0) \rangle_0 = \frac{1}{Z_0} uv \left( e^{-E_{\uparrow}^0 \tau} e^{-E_{\downarrow}^0(\beta-\tau)} - e^{-E_{\downarrow}^0 \tau} e^{-E_{\uparrow}^0(\beta-\tau)} - e^{-E_{\downarrow}^0 \tau} e^{-E_{\uparrow}^0(\beta-\tau)} + e^{-E_{\uparrow}^0 \tau} e^{-E_{\downarrow}^0(\beta-\tau)} \right), \quad (\text{G.6})$$

$$\langle T_{\tau} d_{\downarrow}(\tau) d_{\downarrow}^{\dagger}(0) \rangle_0 = \frac{1}{Z_0} \left( u^2 \left( e^{-E_{\uparrow}^0 \tau} e^{-E_{\uparrow}^0(\beta-\tau)} + e^{-E_{\downarrow}^0 \tau} e^{-E_{\downarrow}^0(\beta-\tau)} \right) + v^2 \left( e^{-E_{\downarrow}^0 \tau} e^{-E_{\uparrow}^0(\beta-\tau)} + e^{-E_{\uparrow}^0 \tau} e^{-E_{\downarrow}^0(\beta-\tau)} \right) \right). \quad (\text{G.7})$$

Using  $u^2 + v^2 = 1$ , the partition function becomes:

$$Z = Z_0 + \beta t^2 \sum_{\vec{k}, \sigma} \times \left( \frac{1}{E_{\vec{k}} - (E_{\uparrow}^0 - E_{\sigma}^0)} \left( e^{-\beta E_{\uparrow}^0} - e^{-\beta(E_{\vec{k}} + E_{\sigma}^0)} \right) + \frac{1}{E_{\vec{k}} - (E_{\downarrow}^0 - E_{\sigma}^0)} \left( e^{-\beta E_{\downarrow}^0} - e^{-\beta(E_{\vec{k}} + E_{\sigma}^0)} \right) + \frac{1}{E_{\vec{k}} + (E_{\uparrow}^0 - E_{\sigma}^0)} \left( e^{-\beta E_{\sigma}^0} - e^{-\beta(E_{\vec{k}} + E_{\uparrow}^0)} \right) + \frac{1}{E_{\vec{k}} + (E_{\downarrow}^0 - E_{\sigma}^0)} \left( e^{-\beta E_{\sigma}^0} - e^{-\beta(E_{\vec{k}} + E_{\downarrow}^0)} \right) + \frac{2\Delta}{E_{\vec{k}}} uv \left| \cos\left(\frac{\varphi}{2}\right) \right| \times \left( \frac{1}{E_{\vec{k}} + (E_{\uparrow}^0 - E_{\sigma}^0)} \left( e^{-\beta E_{\sigma}^0} - e^{-\beta(E_{\vec{k}} + E_{\uparrow}^0)} \right) - \frac{1}{E_{\vec{k}} + (E_{\downarrow}^0 - E_{\sigma}^0)} \left( e^{-\beta E_{\sigma}^0} - e^{-\beta(E_{\vec{k}} + E_{\downarrow}^0)} \right) - \frac{1}{E_{\vec{k}} - (E_{\uparrow}^0 - E_{\sigma}^0)} \left( e^{-\beta E_{\uparrow}^0} - e^{-\beta(E_{\vec{k}} + E_{\sigma}^0)} \right) + \frac{1}{E_{\vec{k}} - (E_{\downarrow}^0 - E_{\sigma}^0)} \left( e^{-\beta E_{\downarrow}^0} - e^{-\beta(E_{\vec{k}} + E_{\sigma}^0)} \right) \right) + 2\beta |\Gamma_{\varphi}| uv \left( e^{-\beta E_{\uparrow}^0} - e^{-\beta E_{\downarrow}^0} \right). \quad (\text{G.8})$$

As  $E_{\vec{k}} = \sqrt{\epsilon_{\vec{k}}^2 + \Delta^2} > 0$ , terms with an  $e^{-\beta E_{\vec{k}}}$  are exponentially suppressed for  $T \rightarrow 0$  K and can be omitted.



# Appendix H

## Explicit self consistent expression of $\delta a$

The energy shift  $\delta a = \delta E_- - \delta E_\sigma$  is calculated starting from the self consistent equation (3.29). The shift  $\delta b$  follows from equation (3.30). As these two equations are completely symmetric, only  $\delta a$  shall be discussed here. The calculation of  $\delta b$  is quasi-identical.

In equation (3.29),  $a_0 = \frac{U}{2} - \sqrt{\xi_d^2 + \Gamma_\varphi^2}$  and  $b_0 = \frac{U}{2} - \sqrt{\xi_d^2 + \Gamma_\varphi^2}$  are the initial, not renormalized parameters. For  $a_0 > 0$ ,  $\delta a$  is given by

$$\begin{aligned} \delta a &= -\frac{\Gamma}{\pi} \int_0^D d\epsilon \left( \frac{2}{E - a(\Delta)} - \frac{1}{E + b_0} - \frac{1}{E + a_0} \right. \\ &\quad \left. + \frac{\Delta}{E} uv \left| \cos\left(\frac{\varphi}{2}\right) \right| \left( \frac{2}{E - a(\Delta)} - \frac{1}{E + b_0} + \frac{1}{E + a_0} \right) \right) \\ &\quad + 2|\Gamma_\varphi| uv \end{aligned} \quad (\text{H.1})$$

(with  $E = \sqrt{\epsilon^2 + \Delta^2}$ ). The integrals can be performed analytically. Thereby, the density of states  $\rho_0 = 1/(2D)$  is assumed to be constant,  $D$  being half the electronic bandwidth of the leads. Using

$$\begin{aligned} &\int_{-D}^D d\epsilon \rho_0 \frac{1}{\sqrt{\epsilon^2 + \Delta^2} + X} \quad (\text{H.2}) \\ &= 2\rho_0 \left[ \frac{X}{\sqrt{\Delta^2 - X^2}} \left( \arctan\left(\frac{X\epsilon}{\sqrt{\Delta^2 - X^2}\sqrt{\Delta^2 + \epsilon^2}}\right) - \arctan\left(\frac{\epsilon}{\sqrt{\Delta^2 - X^2}}\right) \right) \right. \\ &\quad \left. + \ln\left(\epsilon + \sqrt{\epsilon^2 + \Delta^2}\right) \right]_0^D \end{aligned}$$

and

$$\begin{aligned} &\int_{-D}^D d\epsilon \rho_0 \frac{1}{\sqrt{\epsilon^2 + \Delta^2} + X} \quad (\text{H.3}) \\ &= 2\rho_0 \left[ -\frac{\Delta}{\sqrt{\Delta^2 - X^2}} \left( \arctan\left(\frac{X\epsilon}{\sqrt{\Delta^2 - X^2}\sqrt{\Delta^2 + \epsilon^2}}\right) - \arctan\left(\frac{\epsilon}{\sqrt{\Delta^2 - X^2}}\right) \right) \right]_0^D \end{aligned}$$

yields the explicit self-consistent equation for  $\delta a$  as a function of the gap  $\Delta$ . As only energy differences are considered, the logarithms simplify. The final expression for  $\delta a$  reads

$$\begin{aligned}
\delta a = & -\frac{\Gamma}{\pi} \left[ \frac{2a(\Delta)}{\sqrt{\Delta^2 - a(\Delta)^2}} \left( \arctan \left( \frac{a(\Delta)\epsilon}{\sqrt{\Delta^2 - a(\Delta)^2} \sqrt{\Delta^2 + \epsilon^2}} \right) + \arctan \left( \frac{\epsilon}{\sqrt{\Delta^2 - a(\Delta)^2}} \right) \right) \right. \\
& - \frac{a_0}{\sqrt{\Delta^2 - a_0^2}} \left( \arctan \left( \frac{a_0\epsilon}{\sqrt{\Delta^2 - a_0^2} \sqrt{\Delta^2 + \epsilon^2}} \right) - \arctan \left( \frac{\epsilon}{\sqrt{\Delta^2 - a_0^2}} \right) \right) \\
& - \frac{b_0}{\sqrt{\Delta^2 - b_0^2}} \left( \arctan \left( \frac{b_0\epsilon}{\sqrt{\Delta^2 - b_0^2} \sqrt{\Delta^2 + \epsilon^2}} \right) - \arctan \left( \frac{\epsilon}{\sqrt{\Delta^2 - b_0^2}} \right) \right) \\
& + uv \left| \cos \left( \frac{\varphi}{2} \right) \right| \\
& \left( \frac{2\Delta}{\sqrt{\Delta^2 - a(\Delta)^2}} \left( \arctan \left( \frac{a(\Delta)\epsilon}{\sqrt{\Delta^2 - a(\Delta)^2} \sqrt{\Delta^2 + \epsilon^2}} \right) + \arctan \left( \frac{\epsilon}{\sqrt{\Delta^2 - a(\Delta)^2}} \right) \right) \right. \\
& - \frac{\Delta}{\sqrt{\Delta^2 - a_0^2}} \left( \arctan \left( \frac{a_0\epsilon}{\sqrt{\Delta^2 - a_0^2} \sqrt{\Delta^2 + \epsilon^2}} \right) - \arctan \left( \frac{\epsilon}{\sqrt{\Delta^2 - a_0^2}} \right) \right) \\
& \left. \left. + \frac{\Delta}{\sqrt{\Delta^2 - b_0^2}} \left( \arctan \left( \frac{b_0\epsilon}{\sqrt{\Delta^2 - b_0^2} \sqrt{\Delta^2 + \epsilon^2}} \right) - \arctan \left( \frac{\epsilon}{\sqrt{\Delta^2 - b_0^2}} \right) \right) \right) \right]_0^D. \tag{H.4}
\end{aligned}$$

Whenever necessary, the analytic continuation

$$\frac{1}{\sqrt{x^2 - y^2}} \arctan \left( \frac{Z}{\sqrt{x^2 - y^2}} \right) \xrightarrow{|y| > |x|} \frac{1}{2} \frac{1}{\sqrt{y^2 - x^2}} \ln \left( \frac{1 - \frac{Z}{\sqrt{y^2 - x^2}}}{1 + \frac{Z}{\sqrt{y^2 - x^2}}} \right) \tag{H.5}$$

is understood.

# Appendix I

## Perturbation expansion in the Coulomb interaction

### I.1 First order

The first order self energies in the perturbation expansion around the non-interacting limit are calculated by expanding the dot's full Green's function

$$\widehat{G}(\tau) = \begin{pmatrix} -\langle T_\tau d_\uparrow(\tau) d_\uparrow^\dagger(0) \rangle & -\langle T_\tau d_\uparrow(\tau) d_\downarrow(0) \rangle \\ -\langle T_\tau d_\downarrow^\dagger(\tau) d_\uparrow^\dagger(0) \rangle & -\langle T_\tau d_\downarrow^\dagger(\tau) d_\downarrow(0) \rangle \end{pmatrix} \quad (\text{I.1})$$

to the first order in the Coulomb interaction  $U$ . Due to the matrix character of the Nambu notation, it is only necessary to calculate one of the four matrix elements in order to derive the complete first order self energy  $\widehat{\Sigma}$ . The latter is defined by the Matsubara frequency Dyson equation,

$$\begin{aligned} \widehat{G}_{d,d}(i\omega_n) &= \widehat{G}_{d,d}^0(i\omega_n) + \widehat{G}_{d,d}^0(i\omega_n) \widehat{\Sigma}(i\omega_n) \widehat{G}_{d,d}(i\omega_n) \\ &= \widehat{G}_{d,d}^0(i\omega_n) + \widehat{G}_{d,d}^0(i\omega_n) \widehat{\Sigma}^{(1)}(i\omega_n) \widehat{G}_{d,d}^0(i\omega_n) + \mathcal{O}(U^2) . \end{aligned} \quad (\text{I.2})$$

Expanding now for instance  $G_{11}$  to the first order, one finds

$$\begin{aligned} G_{11}(\tau) = G_{11}^0(\tau) &- U \int_0^\beta d\tau_1 G_{12}^0(\tau - \tau_1) G_{21}^0(\tau_1) G_{11}^0(0) \\ &+ U \int_0^\beta d\tau_1 G_{12}^0(\tau - \tau_1) G_{11}^0(\tau_1) G_{21}^0(0) \\ &+ U \int_0^\beta d\tau_1 G_{11}^0(\tau - \tau_1) G_{11}^0(\tau_1) G_{22}^0(0) \\ &- U \int_0^\beta d\tau_1 G_{11}^0(\tau - \tau_1) G_{21}^0(\tau_1) G_{12}^0(0) . \end{aligned} \quad (\text{I.3})$$

Fourier transformation and simple identification determines the self energies  $\Sigma_{ij}^1(i\omega_n)$  (i.e. the  $(i, j)$  matrix element of  $\Sigma^{(1)}(i\omega_n)$ ) as

$$\Sigma_{11}^{(1)}(i\omega_n) = U \langle d_{\downarrow}^{\dagger} d_{\downarrow} \rangle_0 = -U G_{22}^0(\tau = 0^+) , \quad (\text{I.4})$$

$$\Sigma_{12}^{(1)}(i\omega_n) = U \langle d_{\downarrow} d_{\uparrow} \rangle_0 = U G_{12}^0(\tau = 0) , \quad (\text{I.5})$$

$$\Sigma_{21}^{(1)}(i\omega_n) = U \langle d_{\uparrow}^{\dagger} d_{\downarrow}^{\dagger} \rangle_0 = U G_{21}^0(\tau = 0) , \quad (\text{I.6})$$

$$\Sigma_{22}^{(1)}(i\omega_n) = -U \langle d_{\uparrow}^{\dagger} d_{\uparrow} \rangle_0 = -U G_{11}^0(\tau = 0^-) . \quad (\text{I.7})$$

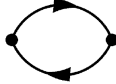
## I.2 Explicit calculation of the self-energy

### I.2.1 Deriving the explicit formula

In order to derive explicit formulas for the self-energies, the retarded real time equivalent of self-energies of the generic form

$$\Sigma_{123} = -U^2 \int_0^{\beta} d\tau e^{i\omega_n \tau} \mathcal{G}_1(\tau) \mathcal{G}_2(\tau) \mathcal{G}_3(-\tau) \quad (\text{I.8})$$

needs to be found. At first, we define  $\Pi(\tau) = -\mathcal{G}_2(\tau) \mathcal{G}_3(-\tau)$ . Diagrammatically,  $\Pi(\tau)$  is

nothing but the bubble  in the sunrise graph  constituting  $\Sigma_{123}$ . Using these definitions,  $\Sigma_{123}$  has the form

$$\begin{aligned} \Sigma_{123}(i\omega_n) &= U^2 \int_0^{\beta} d\tau e^{i\omega_n \tau} \mathcal{G}_1(\tau) \Pi(\tau) \\ &= U^2 \sum_{\omega_1, \omega_p} \frac{1}{\beta^2} \int_0^{\beta} d\tau e^{i(\omega_n - \omega_1 - \omega_p)\tau} \mathcal{G}_1(i\omega_1) \Pi(i\omega_p) \\ &= \frac{U^2}{\beta} \sum_{\omega_1} \mathcal{G}_1(i\omega_1) \Pi(i\omega_n - i\omega_1) , \end{aligned} \quad (\text{I.9})$$

where  $\omega_1$  and  $\omega_n$  are fermionic Matsubara frequencies and  $\omega_p$  is a bosonic one.

At this stage, it is very useful to note that the imaginary time version  $\mathcal{G}(i\omega_n)$  of a Green's function and the imaginary part of its retarded version  $\mathcal{G}^R(\omega)$  are related by

$$\mathcal{G}(i\omega_n) = -\frac{1}{\pi} \int_{-\infty}^{\infty} d\omega \frac{\text{Im} \{ \mathcal{G}^R(\omega) \}}{i\omega_n - \omega} , \quad (\text{I.10})$$

as can be seen in Lehmann representation. As we will encounter quite a lot of imaginary parts in the remainder of this section, they shall be indicated by a double apostrophe, i.e.  $\text{Im} \{ \mathcal{G} \} =: \mathcal{G}''$ , whereas real part will be indicated by simple apostrophes, i.e.  $\text{Re} \{ \mathcal{G} \} =: \mathcal{G}'$ . Furthermore, we will exploit the fact that the fermionic Matsubara frequencies are the poles of the analytically continued Fermi-Dirac distribution  $n_F(z)$ . Therefore, sums over Matsubara frequencies can be written as integrals in the complex plane. Evaluating the latter yields

$$\begin{aligned}\Sigma_{123}(i\omega_n) &= \frac{U^2}{\pi^2\beta} \int_{-\infty}^{\infty} d\omega \int_{-\infty}^{\infty} d\omega' \mathcal{G}_1^{R''}(\omega) \Pi^{R''}(\omega') \sum_{\omega_1} \frac{1}{i\omega_1 - \omega} \frac{1}{i\omega_n - i\omega_1 - \omega'} \quad (\text{I.11}) \\ &= \frac{U^2}{\pi^2} \int_{-\infty}^{\infty} d\omega \int_{-\infty}^{\infty} d\omega' \mathcal{G}_1^{R''}(\omega) \Pi^{R''}(\omega') \frac{-n_F(-\omega) - n_B(\omega')}{i\omega_n - \omega - \omega'} ,\end{aligned}$$

where  $n_F(\omega)$  is the Fermi-Dirac distribution and  $n_B(\omega)$  denotes the Bose-Einstein distribution. Using equation I.10 once more and performing the analytic continuation, one obtains

$$\Sigma_{123}^{R''}(\omega) = \frac{U^2}{\pi} \int_{-\infty}^{\infty} d\epsilon \mathcal{G}_1^{R''}(\epsilon) \Pi^{R''}(\omega - \epsilon) [n_F(-\epsilon) + n_B(\omega - \epsilon)] . \quad (\text{I.12})$$

$\Pi^{R''}(\omega)$  can be obtained by a perfectly analog calculation, yielding

$$\Pi^{R''}(\omega) = \frac{1}{\pi} \int_{-\infty}^{\infty} d\epsilon \mathcal{G}_2^{R''}(\omega - \epsilon) \mathcal{G}_3^{R''}(\epsilon) [n_F(\epsilon) - n_F(\omega + \epsilon)] . \quad (\text{I.13})$$

Plugging everything together one ends up with

$$\begin{aligned}\Sigma_{123}^{R''}(\omega) &= \frac{U^2}{\pi^2} \int_{-\infty}^{\infty} d\epsilon_1 \int_{-\infty}^{\infty} d\epsilon_2 \int_{-\infty}^{\infty} d\epsilon_3 \\ &\quad \times \mathcal{G}_1^{R''}(\epsilon_1) \mathcal{G}_2^{R''}(\epsilon_2) \mathcal{G}_3^{R''}(-\epsilon_3) \delta(\omega - \epsilon_1 - \epsilon_2 - \epsilon_3) \\ &\quad \times [n_F(-\epsilon_3) - n_F(\epsilon_2)] [n_F(-\epsilon_1) + n_B(\epsilon_2 + \epsilon_3)] .\end{aligned}$$

In a last step, the Fermi-Dirac and Bose-Einstein factors are simplified. Doing so yields the final result for the imaginary part of the retarded self-energy,

$$\begin{aligned}\Sigma_{123}^{R''}(\omega) &= \frac{U^2}{\pi^2} \int_{-\infty}^{\infty} d\epsilon_1 \int_{-\infty}^{\infty} d\epsilon_2 \int_{-\infty}^{\infty} d\epsilon_3 \quad (\text{I.14}) \\ &\quad \times \mathcal{G}_1^{R''}(\epsilon_1) \mathcal{G}_2^{R''}(\epsilon_2) \mathcal{G}_3^{R''}(-\epsilon_3) \delta(\omega - \epsilon_1 - \epsilon_2 - \epsilon_3) \\ &\quad \times [n_F(\epsilon_1)n_F(\epsilon_2)n_F(\epsilon_3) + n_F(-\epsilon_1)n_F(-\epsilon_2)n_F(-\epsilon_3)] .\end{aligned}$$

## I.2.2 Evaluation of the self-energies for superconducting leads

In order to calculate the self-energies via equation (4.37),  $\mathcal{G}^R(\omega)$  and  $\mathcal{F}^R(\omega)$  need to be computed by analytic continuation of (4.27) and (4.28). One obtains

$$\mathcal{G}^R(\omega) = \frac{1}{2} \left( \frac{1}{g_0^{-1R}(\omega) + f_0^{-1R}(\omega)} + \frac{1}{g_0^{-1R}(\omega) - f_0^{-1R}(\omega)} \right) , \quad (\text{I.15})$$

$$\mathcal{F}^R(\omega) = \frac{1}{2} \left( \frac{1}{g_0^{-1R}(\omega) + f_0^{-1R}(\omega)} - \frac{1}{g_0^{-1R}(\omega) - f_0^{-1R}(\omega)} \right) , \quad (\text{I.16})$$

where

$$g_0^{-1R}(\omega) = \begin{cases} (\omega + i\eta) \left( 1 + \frac{|\Gamma_0|(\omega)}{\sqrt{\Delta^2 - \omega^2}} \right) & , |\omega| < \Delta \text{ (inside gap)} \\ (\omega + i\eta) \left( 1 + \frac{|\tilde{\Gamma}_0|(\omega)}{\sqrt{\omega^2 - \Delta^2}} \right) + i\Gamma \frac{|\omega|}{\sqrt{\omega^2 - \Delta^2}} & , |\omega| > \Delta \text{ (outside gap)} \end{cases} \quad (\text{I.17})$$

and

$$f_0^{-1R}(\omega) = \begin{cases} \Delta \frac{|\Gamma_\varphi(\omega)|}{\sqrt{\Delta^2 - \omega^2}} - \Delta_{eff} & , |\omega| < \Delta \text{ (inside gap)} \\ \Delta \frac{|\tilde{\Gamma}_\varphi(\omega)|}{\sqrt{\omega^2 - \Delta^2}} + i\Gamma \left| \cos\left(\frac{\varphi}{2}\right) \right| \frac{\Delta \operatorname{sgn}(\omega)}{\sqrt{\omega^2 - \Delta^2}} - \Delta_{eff} & , |\omega| > \Delta \text{ (outside gap)}. \end{cases} \quad (\text{I.18})$$

Thereby, the definitions

$$\Gamma_\varphi(\omega) = \Gamma \frac{2}{\pi} \cos\left(\frac{\varphi}{2}\right) \arctan\left(\frac{D}{\sqrt{\Delta^2 - \omega^2}}\right) \quad (\text{I.19})$$

and

$$\tilde{\Gamma}_\varphi(\omega) = \Gamma \frac{1}{\pi} \cos\left(\frac{\varphi}{2}\right) \ln\left(\frac{D - \sqrt{\omega^2 - \Delta^2}}{D + \sqrt{\omega^2 - \Delta^2}}\right) \quad (\text{I.20})$$

have been introduced and  $\eta \rightarrow 0^+$ .

It is worth to notice that  $\mathcal{G}^R$  and  $\mathcal{F}^R$  both have discrete subgap Dirac-peak contributions if either  $g_0^{-1R}(\omega) + f_0^{-1R}(\omega)$  or  $g_0^{-1R}(\omega) - f_0^{-1R}(\omega)$  vanishes. These peaks are nothing but the Andreev bound states. Working their explicit forms, one finds that  $g_0^{-1R}(\omega) + f_0^{-1R}(\omega)$  and  $g_0^{-1R}(\omega) - f_0^{-1R}(\omega)$  are in fact symmetric with respect to  $\omega = 0$ . Thus, the peaks are located at symmetric frequencies we shall denote  $\pm\omega^0$  (we take  $\omega^0 > 0$  without loss of generality); they have equal weight for  $\mathcal{G}^{R''}$  and opposite weight for  $\mathcal{F}^{R''}$ . In order to simplify the discussions as much as possible, we thus work with a generalized Green's function, defined by

$$\mathcal{G}^{R''}(\omega) = \begin{cases} \mathcal{G}^{cont}(\omega) & , |\omega| > \Delta \\ W^+ \delta(\omega - \omega^0) + W^- \delta(\omega + \omega^0) & , |\omega| < \Delta . \end{cases} \quad (\text{I.21})$$

For a numerical evaluation of the self-energies it is obviously necessary to deal with the Andreev bound states separately because they constitute singular contributions. Furthermore, only the zero temperature limit will be considered, in which the Fermi-Dirac distributions become Heaviside step functions. Writing down all terms in equation (4.37), one finds that a self-energy term

$$\Sigma_{123}(\tau) = -U^2 \mathcal{G}_1(\tau) \mathcal{G}_2(\tau) \mathcal{G}_3(-\tau)$$

corresponds to an imaginary part of the retarded real time self-energy

$$\frac{\pi^2}{U^2} \Sigma_{123}^R''(\omega) = W_1^+ W_2^+ W_3^- \delta(\omega - \omega_1^0 - \omega_2^0 - \omega_3^0) + W_1^- W_2^- W_3^+ \delta(\omega + \omega_1^0 + \omega_2^0 + \omega_3^0) \quad (\text{I})$$

$$+ \theta(\omega - (\omega_2^0 + \omega_3^0 + \Delta)) W_2^+ W_3^- \mathcal{G}_1^{\text{cont}}(\omega - \omega_2^0 - \omega_3^0) \quad (\text{II})$$

$$+ \theta(-\omega - (\omega_2^0 + \omega_3^0 + \Delta)) W_2^- W_3^+ \mathcal{G}_1^{\text{cont}}(\omega + \omega_2^0 + \omega_3^0)$$

$$+ \theta(\omega - (\omega_1^0 + \omega_3^0 + \Delta)) W_1^+ W_3^- \mathcal{G}_2^{\text{cont}}(\omega - \omega_2^0 - \omega_3^0) \quad (\text{III})$$

$$+ \theta(-\omega - (\omega_1^0 + \omega_3^0 + \Delta)) W_1^- W_3^+ \mathcal{G}_2^{\text{cont}}(\omega + \omega_2^0 + \omega_3^0)$$

$$+ \theta(\omega - (\omega_1^0 + \omega_2^0 + \Delta)) W_1^+ W_2^+ \mathcal{G}_3^{\text{cont}}(-\omega + \omega_2^0 + \omega_3^0) \quad (\text{IV})$$

$$+ \theta(-\omega - (\omega_1^0 + \omega_2^0 + \Delta)) W_1^- W_2^- \mathcal{G}_3^{\text{cont}}(-\omega - \omega_2^0 - \omega_3^0)$$

$$+ \theta(\omega - (\omega_1^0 + 2\Delta)) \int_{\Delta}^{\omega - \Delta - \omega_1^0} d\epsilon W_1^+ \mathcal{G}_2^{\text{cont}}(\epsilon) \mathcal{G}_3^{\text{cont}}(\epsilon - \omega + \omega_1^0) \quad (\text{V})$$

$$+ \theta(-\omega - (\omega_1^0 + 2\Delta)) \int_{\omega + \Delta + \omega_1^0}^{-\Delta} d\epsilon W_1^- \mathcal{G}_2^{\text{cont}}(\epsilon) \mathcal{G}_3^{\text{cont}}(\epsilon - \omega - \omega_1^0)$$

$$+ \theta(\omega - (\omega_2^0 + 2\Delta)) \int_{\Delta}^{\omega - \Delta - \omega_2^0} d\epsilon W_2^+ \mathcal{G}_1^{\text{cont}}(\epsilon) \mathcal{G}_3^{\text{cont}}(\epsilon - \omega + \omega_2^0) \quad (\text{VI})$$

$$+ \theta(-\omega - (\omega_2^0 + 2\Delta)) \int_{\omega + \Delta + \omega_2^0}^{-\Delta} d\epsilon W_2^- \mathcal{G}_1^{\text{cont}}(\epsilon) \mathcal{G}_3^{\text{cont}}(\epsilon - \omega - \omega_2^0)$$

$$+ \theta(\omega - (\omega_3^0 + 2\Delta)) \int_{\Delta}^{\omega - \Delta - \omega_3^0} d\epsilon W_3^- \mathcal{G}_1^{\text{cont}}(\epsilon) \mathcal{G}_2^{\text{cont}}(\omega - \omega_1^0 - \epsilon) \quad (\text{VII})$$

$$+ \theta(-\omega - (\omega_3^0 + 2\Delta)) \int_{\omega + \Delta + \omega_3^0}^{-\Delta} d\epsilon W_3^+ \mathcal{G}_1^{\text{cont}}(\epsilon) \mathcal{G}_2^{\text{cont}}(\omega + \omega_1^0 + \epsilon)$$

$$+ \theta(\omega - 3\Delta) \int_{\Delta}^{\omega - 2\Delta} d\epsilon_1 \mathcal{G}_1^{\text{cont}}(\epsilon_1) \times \int_{\Delta}^{\omega - \epsilon_1 - \Delta} d\epsilon_2 \mathcal{G}_2^{\text{cont}}(\epsilon_2) \mathcal{G}_3^{\text{cont}}(\epsilon_1 + \epsilon_2 - \omega) \quad (\text{VIII})$$

$$+ \theta(-\omega - 3\Delta) \int_{2\Delta + \omega}^{-\Delta} d\epsilon_1 \mathcal{G}_1^{\text{cont}}(\epsilon_1) \times \int_{\Delta - \epsilon_1 + \omega}^{-\Delta} d\epsilon_2 \mathcal{G}_2^{\text{cont}}(\epsilon_2) \mathcal{G}_3^{\text{cont}}(\epsilon_1 + \epsilon_2 - \omega)$$

There are several important remarks on this explicit form. First of all, the contribution denoted (I), i.e. the triple Andreev bound state contribution, seems to add singularities at  $\pm 3\omega^0$  to the self-energy. Yet, both  $\Sigma_{\mathcal{G}}$  and  $\Sigma_{\mathcal{F}}$  are composed by two terms. As shown above, one has

$$\Sigma_{\mathcal{G}}(\tau) = U^2 \mathcal{G}(\tau) \mathcal{G}(\tau) \mathcal{G}(-\tau) - U^2 \mathcal{F}(\tau) \mathcal{F}(\tau) \mathcal{G}(\tau) \quad (\text{I.22})$$

and

$$\Sigma_{\mathcal{F}}(\tau) = -U^2 \mathcal{G}(\tau) \mathcal{G}(\tau) \mathcal{F}(-\tau) + U^2 \mathcal{F}(\tau) \mathcal{F}(\tau) \mathcal{F}(\tau) . \quad (\text{I.23})$$

Note that two contributions to either self-energy have opposite signs. If one considers the total self-energies, the singular contributions of the two parts cancel exactly, because both  $\mathcal{G}$  and  $\mathcal{F}$  have Andreev bound states of same (absolute) weight at frequency  $\pm\omega^0$ . Thus, the total self-energy is a non-singular function.

Because the (I)-term vanishes, the self-energy has only three kinds of contributions. The first ones are processes of energies  $|\omega| \geq \Delta + 2\omega^0$ . They correspond to a sunrise graph with two of the three electrons in an Andreev bound state and one in the continuum. These processes are terms (II) - (IV).

The second kind of contributions have energies  $|\omega| \geq 2\Delta + \omega^0$ . They involve two electrons in the continuum and one electron in an Andreev bound state. They correspond to the terms (V) - (VII).

The third and last processes contributing to the self energies involve only electrons in the continuum of states. Consequently, they start at energies higher than  $3\Delta$ ; they are given by (VIII).

As a concluding remark on these explicit formulas, we want to stress again that the imaginary parts of the self energies have no singular Andreev bound state like contributions and always start at frequencies  $|\omega| > \Delta$ .

# Appendix J

## List of the most important Symbols

Symbol	Comment	Meaning
BCS		Abbreviation for Bardeen, Cooper, Schrieffer. Denotes the microscopic theory for superconductivity proposed by the latter.
ABS		Abbreviation for Andreev bound state.
NRG		Abbreviation for numerical renormalization group.
$\sigma$	$\sigma = \uparrow, \downarrow$	Spin of an electron on the dot or quasiparticle in the leads.
$\vec{k}$		Wave vector of a quasiparticle in the leads.
$\epsilon_{\vec{k},i}$	$i = L, R$	Kinetic energy of a quasiparticle with wave vector $\vec{k}$ in the lead $i$ .
$\epsilon_d$		Level energy of the dot.
$c_{\vec{k},\sigma,i}$		Annihilation operator of a quasiparticle of wave vector $\vec{k}$ and spin $\sigma$ in the lead $i$ .
$d_\sigma$		Annihilation operator of an electron of spin $\sigma$ on the dot.
$n_\sigma$	$n_\sigma = d_\sigma^\dagger d_\sigma$	Spin $\sigma$ population on the dot.
$H$		Total Hamiltonian.
$H_i$	$i = L, R$	Hamiltonian of the lead $i$ (BCS-Hamiltonian).
$H_D$		Hamiltonian of the dot (without Coulomb interaction).
$H_{T_i}$	$i = L, R$	Tunneling between the dot and the lead $i$ .
$U$		Coulomb interaction between two electrons on the dot.
$\xi_d$	$\xi_d = \epsilon_d + U/2$	Energy level of the dot with respect to particle hole symmetry.
$\Delta$		Absolute value of the superconducting gap in the leads.
$\varphi_i$	$i = L, R$	Superconducting phase in the lead $i$ .
$\varphi$	$\varphi = \varphi_L - \varphi_R$	Superconducting phase difference.
$t$		Tunneling amplitude between the dot and the leads.
$D$		Half the electronic bandwidth in the leads.
$\rho_0$	$\rho_0 = 1/(2D)$	Density of states in the leads.

Symbol	Comment	Meaning
$\Gamma$	$\Gamma = 2\pi t^2 \rho_0$	Total hybridization between dot and leads.
$\Gamma_\varphi$		$\Gamma_\varphi = \Gamma \frac{2}{\pi} \arctan\left(\frac{D}{\Delta}\right) \cos\left(\frac{\varphi}{2}\right)$ .
$\widehat{X}$		Operator or Green's function $X$ in Nambu matrix notation.
$\Psi_{\vec{k},i}$		Nambu spinor for the wave vector $\vec{k}$ in the lead $i$ .
$\Psi_D$		Nambu spinor for the dot.
$\tau$		Imaginary time.
$\omega_n$		Matsubara frequency.
$\widehat{G}_{d,d}$		Green's function of the interacting dot.
$\widehat{G}_{d,d}^0$		Green's function of the non-interacting dot.
$\widehat{G}_{\vec{k}i,\vec{k}i}$	$i = L, R$	Green's function of quasiparticles of wave vector $\vec{k}$ in the lead $i$ .
$\widehat{G}_{\vec{k}i,\vec{k}i}^0$	$i = L, R$	Green's function of quasiparticles of wave vector $\vec{k}$ in the lead $i$ decoupled from the dot.
$\widehat{G}_{\vec{k}i,\vec{k}i}^{U=0}$	$i = L, R$	Green's function of quasiparticles of wave vector $\vec{k}$ in the lead $i$ coupled to the non-interacting dot.
$\widehat{G}_i$	$i = L, R$	$\widehat{G}_i = \sum_{\vec{k}} \widehat{G}_{\vec{k}i,\vec{k}i}^0$ .
$G_x^R$		Retarded real time version of the Green's function $G_x$ .
$\mathcal{G}$		Normal, spin-unpolarized Hartree-Fock mean field Green's function.
$\mathcal{F}$		Anomalous, spin-unpolarized Hartree-Fock mean field Green's function.
$g_0^{-1}$		Diagonal element of the inverse Nambu matrix spin-unpolarized Hartree-Fock mean field Green's function.
$f_0^{-1}$		Off-diagonal element of the inverse Nambu matrix spin-unpolarized Hartree-Fock mean field Green's function.
$\Sigma$		Self-energy.
$H_{eff}$		Effective local limit Hamiltonian.
$E_\sigma^0$		Energy of the spin $\sigma$ state on the dot in the effective local limit.
$E_-^0$		Energy of the state $ -\rangle$ in the effective local limit.
$E_+^0$		Energy of the state $ +\rangle$ in the effective local limit.
$a^0$	$a^0 = E_-^0 - E_\sigma^0$	Energy of the low energy ABS in the effective local limit.
$b^0$	$b^0 = E_+^0 - E_\sigma^0$	Energy of the high energy ABS in the effective local limit.

Symbol	Comment	Meaning
$E_\sigma$		Renormalized energy of the spin $\sigma$ state on the dot.
$E_-$		Renormalized energy of the state $ -\rangle$ .
$E_+$		Renormalized energy of the state $ +\rangle$ .
$a$	$a = E_- - E_\sigma$	Renormalized energy of the low energy ABS.
$b$	$b = E_+ - E_\sigma$	Renormalized energy of the high energy ABS.
$u, v$		Coefficients in the BCS-like wave function on the dot.
$E_{\vec{k}}$	$E_{\vec{k}} = \sqrt{\epsilon_{\vec{k},i}^2 + \Delta^2}$	Energy of a quasiparticle of wave vector $\vec{k}$ .
$T_K$		Kondo temperature.
$n_F$		Fermi-Dirac distribution function.
$n_B$		Bose-Einstein distribution function.
$\Phi$		Luttinger-Ward functional.



# Bibliography

- [1] L. I. Glazman and M. Pustilnik, in *Nanophysics: Coherence and Transport*, edited by H. Bouchiat, Y. Gefen, S. Gueron, G. Montambaux, and J. Dalibard (Elsevier Science, 2005), pp. 427–478, arXiv:cond-mat/0501007.
- [2] L. P. Kouwenhoven, D. G. Austing, and S. Tarucha, Rep. Prog. Phys. **64**, 701 (2001).
- [3] W. G. van der Wiel, S. De Franceschi, J. M. Elzerman, T. Fujisawa, S. Tarucha, and L. P. Kouwenhoven, Rev. Mod. Phys. **75**, 1 (2002).
- [4] S. J. Tans, M. H. Devoret, H. Dai, A. Thess, R. E. Smalley, L. J. Geerligs, and C. Dekker, Nature **386**, 474 (1997).
- [5] A. Y. Kasumov, R. Deblock, M. Kociak, B. Reulet, H. Bouchiat, I. I. Khodos, Y. B. Gorbatov, V. T. Volkov, C. Journet, and M. Burghard, Science **284**, 1508 (1999).
- [6] C. W. J. Beenakker and H. van Houten, in *Single-Electron Tunneling and Mesoscopic Devices*, edited by H. Koch and H. Lübbig (Springer Berlin, 1992), arXiv:cond-mat/0111505.
- [7] C. Benjamin, T. Jonckheere, A. Zazunov, and T. Martin, Eur. Phys. J. B **57**, 279 (2007).
- [8] J. Bauer, A. Oguri, and A. C. Hewson, J. Phys.: Condens. Matter **19**, 486211 (2007).
- [9] A. Zazunov, V. S. Shumeiko, E. N. Bratus', J. Lantz, and G. Wendin, Phys. Rev. Lett. **90**, 087003 (2003).
- [10] J. Sköldberg, T. Löfwander, V. S. Shumeiko, and M. Fogelström, Phys. Rev. Lett. **101**, 087002 (2008).
- [11] Private communication with C. Winkelmann.
- [12] I. A. Sadovskyy, G. B. Lesovik, and G. Blatter, Phys. Rev. B **75**, 195334 (2007).
- [13] J. P. Cleuziou, W. Wernsdorfer, V. Bouchiat, T. Ondarçuhu, and M. Monthieux, Nature nanotechnology **1**, 53 (2006).
- [14] A. V. Rozhkov and D. P. Arovas, Phys. Rev. Lett. **82**, 2788 (1999).
- [15] Y. Avishai, A. Golub, and A. D. Zaikin, Phys. Rev. B **63**, 134515 (2001).
- [16] L. Dell'Anna, A. Zazunov, and R. Egger, Phys. Rev. B **77**, 104525 (2008).

- [17] E. Vecino, A. Martín-Rodero, and A. Levy Yeyati, *Phys. Rev. B* **68**, 035105 (2003).
- [18] L. I. Glazman and K. A. Matveev, *JETP Lett.* **49**, 659 (1989).
- [19] A. A. Clerk and V. Ambegaokar, *Phys. Rev. B* **61**, 9109 (2000).
- [20] S. Ishizaka, J. Sone, and T. Ando, *Phys. Rev. B* **52**, 8358 (1995).
- [21] A. Oguri, Y. Tanaka, and A. C. Hewson, *J. Phys. Soc. Jpn.* **73**, 2494 (2004).
- [22] M.-S. Choi, M. Lee, K. Kang, and W. Belzig, *Phys. Rev. B* **70**, 020502 (2004).
- [23] T. Yoshioka and Y. Ohashi, *J. Phys. Soc. Jpn.* **69**, 1812 (1999).
- [24] C. Karrasch, A. Oguri, and V. Meden, *Phys. Rev. B* **77**, 024517 (2008).
- [25] T. Hecht, A. Weichselbaum, J. von Delft, and R. Bulla, *J. Phys.: Condens. Matter* **20**, 275213 (2008).
- [26] F. Siano and R. Egger, *Phys. Rev. Lett.* **93**, 047002 (2004).
- [27] K. Kusakabe, Y. Tanaka, and Y. Tanuma, *Physica E* **18**, 50 (2003).
- [28] Y. Tanaka, N. Kawakami, and A. Oguri, *Phys. Rev. B* **78**, 035444 (2008).
- [29] M.-S. Choi, C. Bruder, and D. Loss, *Phys. Rev. B* **62**, 13569 (2000).
- [30] M. Lee, T. Jonckheere, and T. Martin, *Phys. Rev. Lett.* **101**, 146804 (2008).
- [31] F. Bergeret, A. Levy Yeyati, and A. Martín-Rodero, *Phys. Rev. B* **74**, 132505 (2006).
- [32] J. Bardeen, L. N. Cooper, and J. R. Schrieffer, *Phys. Rev.* **108**, 1175 (1957).
- [33] J. Nygård, D. H. Cobden, and P. E. Lindelof, *Nature* **417**, 722 (2002).
- [34] C. Buizert, A. Oiwa, K. Shibata, K. Hirakawa, and S. Tarucha, *Phys. Rev. Lett.* **99**, 136806 (2007).
- [35] M. R. Buitelaar, T. Nussbaumer, and C. Schönenberger, *Phys. Rev. Lett.* **89**, 256801 (2002).
- [36] H. I. Jørgensen, K. Grove-Rasmussen, T. Novotný, K. Flensberg, and P. E. Lindelof, *Phys. Rev. Lett.* **96**, 207003 (2006).
- [37] P. Jarillo-Herrero, J. A. van Dam, and L. P. Kouwenhoven, *Nature* **439**, 953 (2006).
- [38] M. R. Buitelaar, W. Belzig, T. Nussbaumer, B. Babić, C. Bruder, and C. Schönenberger, *Phys. Rev. Lett.* **91**, 057005 (2003).
- [39] J. J. A. Baselmans, A. F. Morpurgo, B. J. van Wees, and T. M. Klapwijk, *Nature* **397**, 43 (1998).
- [40] J. A. van Dam, Y. V. Nazarov, E. P. A. M. Bakkers, S. De Franceschi, and L. P. Kouwenhoven, *Nature* **442**, 667 (2006).

- [41] A. Eichler, R. Deblock, M. Weiss, C. Karrasch, V. Meden, C. Schönenberger, and H. Bouchiat (2008), arXiv:0810.1671v1.
- [42] J. M. Rowell, Phys. Rev. Lett. **30**, 167 (1973).
- [43] M. Governale, M. G. Pala, and J. König, Phys. Rev. B **77**, 134513 (2008).
- [44] I. Affleck, J.-S. Caux, and A. M. Zagoskin, Phys. Rev. B **62**, 1433 (2000).
- [45] Y. Tanaka, A. Oguri, and A. C. Hewson, New J. Phys. **9**, 115 (2007).
- [46] E. Vecino, A. Martín-Rodero, and A. Levy Yeyati, Phys. Rev. B **68**, 035105 (2003).
- [47] B. D. Josephson, Physics Letters **1**, 251 (1962).
- [48] V. Ambegaokar and A. Baratoff, Phys. Rev. Lett. **10**, 486 (1963).
- [49] M. Tinkham, *Introduction to Superconductivity* (Dover Publications, 2004).
- [50] H. I. Jørgensen, T. Novotný, K. Grove-Rasmussen, K. Flensberg, and P. E. Lindelof, Nano Letters **7**, 2441 (2007).
- [51] J. Kondo, Prog. Theor. Phys. **32**, 37 (1964).
- [52] J. Park, A. N. Pasupathy, J. I. Goldsmith, C. Chang, Y. Yaish, J. R. Petta, M. Rinkoski, J. P. Sethna, H. D. Abruña, P. L. McEuen, et al., Nature **417**, 722 (2002).
- [53] H. Bruus and K. Flensberg, *Many-Body Quantum Theory in Condensed Matter Physics* (Oxford University Press, 2004).
- [54] G. Sellier, T. Kopp, J. Kroha, and Y. S. Barash, Phys. Rev. B **72**, 174502 (2005).
- [55] A. Krichevsky, M. Schechter, Y. Imry, and Y. Levinson, Phys. Rev. B **61**, 3723 (2000).
- [56] T. Novotný, A. Rossini, and K. Flensberg, Phys. Rev. B **72**, 224502 (2005).
- [57] B. I. Spivak and S. A. Kivelson, Phys. Rev. B **43**, 3740 (1991).
- [58] E. Vecino, A. Martín-Rodero, and A. Levy Yeyati, Phys. Rev. B **68**, 035105 (2003).
- [59] F. D. M. Haldane, Phys. Rev. Lett. **40**, 416 (1978).
- [60] M. G. Pala, M. Governale, and J. König, New J. Phys. **9**, 278 (2007).
- [61] A. V. Rozhkov and D. P. Arovas, Phys. Rev. B **62**, 6687 (2000).
- [62] A. Zazunov, D. Feinberg, and T. Martin, Phys. Rev. Lett. **97**, 196801 (2006).
- [63] A. Zazunov, A. Schulz, and R. Egger, Phys. Rev. Lett. **102**, 047002 (2009).
- [64] D. Futterer, M. Governale, M. G. Pala, and J. König, Phys. Rev. B **79**, 054505 (2009).

- [65] K. G. Wilson, *Rev. Mod. Phys.* **47**, 773 (1975).
- [66] T. V. Ramakrishnan and K. Sur, *Phys. Rev. B* **26**, 1798 (1982).
- [67] K. Haule, S. Kirchner, J. Kroha, and P. Wölfle, *Phys. Rev. B* **64**, 155111 (2001).
- [68] A. T. Alastalo, R. J. Joynt, and M. M. Salomaa, *J. Phys.: Condens. Matter* **10**, L63 (1998).
- [69] A. Martín-Rodero, F. J. García-Vidal, and A. Levy Yeyati, *Phys. Rev. Lett.* **72**, 554 (1994).
- [70] A. Levy Yeyati, A. Martín-Rodero, and F. J. García-Vidal, *Phys. Rev. B* **51**, 3743 (1995).
- [71] J. C. Cuevas, A. Martín-Rodero, and A. L. Yeyati, *Phys. Rev. B* **54**, 7366 (1996).
- [72] A. Eichler, M. Weiss, S. Oberholzer, C. Schönenberger, A. Levy Yeyati, J. C. Cuevas, and A. Martín-Rodero, *Phys. Rev. Lett.* **99**, 126602 (2007).
- [73] E. Müller-Hartmann, *Z. Phys. B* **76**, 211 (1989).
- [74] G. Baym and L. P. Kadanoff, *Phys. Rev.* **124**, 287 (1961).
- [75] G. Baym, *Phys. Rev.* **127**, 1391 (1962).
- [76] J. M. Luttinger and J. C. Ward, *Phys. Rev.* **118**, 1417 (1960).
- [77] J. S. Langer and V. Ambegaokar, *Phys. Rev.* **121**, 1090 (1961).
- [78] D. C. Langreth, *Phys. Rev.* **150**, 516 (1966).
- [79] A. C. Hewson, *The Kondo Problem to Heavy Fermions* (Cambridge University Press, 1993).
- [80] A. A. Abrikosov, L. P. Gorkov, and I. E. Dzyalshinski, *Methods of quantum field theory in statistical physics* (Dover Publications, Inc., 1975).
- [81] I. Dzyaloshinskii, *Phys. Rev. B* **68**, 085113 (2003).
- [82] A. Rosch, *Eur. Phys. J. B* **59**, 495 (2007).
- [83] M. R. Galpin and D. E. Logan, *Phys. Rev. B* **77**, 195108 (2008).
- [84] D. E. Logan, M. P. Eastwood, and M. A. Tusch, *J. Phys.: Condens. Matter* **10**, 2673 (1998).
- [85] M. T. Glossop and D. E. Logan, *J. Phys.: Condens. Matter* **15**, 7519 (2003).
- [86] R. P. Feynman, *Rev. Mod. Phys.* **20**, 367 (1948).
- [87] A. Altland and B. Simons, *Condensed Matter Field Theory* (Cambridge University Press, 2006).
- [88] R. Shankar, *Rev. Mod. Phys.* **66**, 129 (1994).

## **Erklärung**

Hiermit versichere ich, die vorliegende Arbeit selbstständig und ohne fremde Hilfe angefertigt zu haben. Verwendete Literatur und andere Unterlagen sind jeweils im Text vermerkt und im Anhang aufgelistet.

Grenoble, den 03. März 2009

Tobias Meng